ABSTRACT

PERFORMANCE AND POWER OPTIMIZATION OF
MULTICARRIER COMMUNICATION SYSTEMS
IN THE PRESENCE OF NONLINEAR DISTORTION

by

Je-hong Jong

Chair: Wayne E. Stark

Multicarrier modulation is of considerable interest for high speed mobile communications, due to its effectiveness in a multipath fading environment. The major drawback of this technique is its performance degradation in the presence of nonlinear amplification. Linear amplification of multicarrier signals, however, would impose a substantial reduction in power efficiency, which is especially undesirable for mobile applications. The goal of this thesis is, therefore, to quantify the nonlinear amplification effects on multicarrier system performance and to optimize overall power consumption of the system.

In this thesis, a general objective function for the power optimization of communication systems with nonlinear power amplifiers is derived. This derivation reveals the shortcomings of the conventionally used objective function. In order to demonstrate the methodology for power optimization based on the objective function, we present optimization procedures for multicarrier systems with various amplifiers, including dc bias controlled amplifiers. In the process of optimization, we are able to demonstrate a significant power reduction using dc bias control schemes for highly nonconstant envelope signals, such as multicarrier signals.

The effect of amplifier nonlinearities on the performance of multicarrier spread spectrum systems in both single-user and multi-user environments is analyzed. For the multi-user case, single-cell multicarrier code division multiple access systems are considered and perfect power control is assumed. A memoryless polynomial model is used to represent the amplifier amplitude nonlinearities, and a slow frequency nonselective independent Rayleigh fading channel is assumed for each modulated carrier.

We derive bit error probability for uncoded systems and upper bounds on the bit error probability for convolutionally coded systems in both single and multi-user systems. In multi-user systems, the effect of other users' nonlinearities on the performance of a desired user is analytically derived and the total power consumption of users is optimized. Finally, we identify the inherent power consumption problem for conventional amplifiers used in power controlled cellular systems. We provide an effective solution to this problem and quantify realizable power savings.

PERFORMANCE AND POWER OPTIMIZATION OF MULTICARRIER COMMUNICATION SYSTEMS IN THE PRESENCE OF NONLINEAR DISTORTION

by

Je-hong Jong

A dissertation submitted in partial fulfillment
of the requirements for the degree of
Doctor of Philosophy
(Electrical Engineering: Systems)
in The University of Michigan
2000

Doctoral Committee:
Professor Wayne E. Stark, Chair
Associate Professor John T. Coffey
Research Scientist Jack R. East
Professor George I. Haddad
Assistant Professor Kimberly M. Wasserman

Dedicated to my parents, my sister, my wife, and to our new son Bryan.

ACKNOWLEDGEMENTS

I would like to thank my thesis advisor Wayne Stark for his support and guidance of my graduate study. His insights and advice have enlightened my knowledge in communication theory. I would also like to thank my committee members, Dr. Jack East, Professors George Haddad, John Coffey, and Kimberly Wasserman for their time and energy spent on improving my thesis.

I wish to express my appreciation to my internship supervisor Dr. Wonjin Sung at Hughes Network Systems, Germantown, MD for sharing his time for valuable discussion. I also benefited greatly from informal discussion with a former research scientist, Kyounghoon Yang, at the University of Michigan, who is now a professor in Korea.

I am deeply indebted to my parents, to my sister, and to my lovely wife, Soo Jung. This work would not have been possible without their support and encouragement. Most of all, the patience and constant understanding of my wife has helped me greatly in concentrating on my graduate studies. I also like to give my gratitude to my parents-in-law. My new son Bryan would not be as healthy as he is now without their help.

I am very grateful to all my colleagues and teachers at the University of Michigan for sharing happy moments and also hard times together. I also feel very lucky to have had Ms. Mimi Adam as my teacher of technical writing at the University of Michigan. Her sincere teaching and advice has introduced me to the pleasure of academic writing. Finally, I would like to thank the Army Research Office (grant number DAAH04-96-1-0001) for generous financial support of my graduate studies.

TABLE OF CONTENTS

LIST OF TABLES

Table

LIST OF FIGURES

Figure

LIST OF APPENDICES

APPENDIX

CHAPTER 1

Introduction

1.1 Motivation

The most preeminent demand in current mobile wireless personal communications is to achieve both low power consumption and reliable high speed transmission. Battery life has become one of the most crucial factors determining the size and weight of portables such as mobile phones and notebooks [1]. Moreover, reliable high speed data transmission (e.g. images and videos), over a wireless channel, is needed and will be increasingly important in order to meet future trends such as multi-media communications.

Multicarrer modulation (MCM) is an effective modulation technique for such high speed data applications, especially in a frequency selective multipath fading channel. This is due to the long symbol duration of MCM, relative to the channel delay spread, which greatly simplifies channel equalization complexity [2, 3]. However, MCM signals usually have a high peak-to-mean-envelope-power ratio (PMEPR). This high PMEPR, in the case of linear amplification, requires the mean output power to be much lower than the saturation power level where the amplifier power efficiency is usually the highest.

Linear amplification of the transmitted signal is desired in order to avoid excessive signal distortion which increases signal bandwidth (spectral regrowth) [4] and bit error rate (BER). However, linear amplification of signals with highly varying envelopes usually imposes low power efficiency. In conventional linear amplifiers, power

efficiency is an approximately inverse linear function of the PMEPR [5]. This low power efficiency is undesirable for mobile or portable transmitters and other applications where energy is a limited resource.

The main goal of this thesis is to find trade-offs in MCM systems between the degree of the amplifier nonlinearity and total system power consumption, for a given system performance level. We achieve this goal by investigating nonlinear amplifier effects on the multicarrier system's BER performance, spectral regrowth, and amplifier power consumption. In the following section, we discuss the outstanding issues in MCM and introduce our approach to resolving them.

1.2 Multicarrier Modulation and Nonlinearities

The basic principle behind multicarrier modulation is to split a high-speed data stream into several slower streams by a serial to parallel process. These streams are then modulated onto separate orthogonal carriers and then added together. The orthogonality condition of the carriers ensures no inter-carrier-interference (ICI) before amplification. Inter-symbol-interference (ISI) from the multipath on each carrier is significantly reduced due to a long symbol duration relative to the channel delay spread. From a frequency domain viewpoint, MCM is a parallel transmission of data in different frequency bands, where the signal on each subband occupies a much smaller bandwidth than that of single carrier transmission. The parallel narrowband transmission reduces the channel frequency selectivity on each subband, hence removing the need for a complex equalizer.

The early work of using parallel transmission of data in the frequency domain (multicarrier modulation) can be found in a military system called Kineplex [6]. The practical application of this scheme became possible due to fast Fourier transform (FFT) techniques [7, 8] for modulation and demodulation. The FFT can eliminate the complexity involved in using a large number of oscillators. This scheme is often called orthogonal frequency division multiplexing (OFDM). The name comes from the fact that the modulated carriers are orthogonal to each other, but many other names, such as multicarrier modulation (MCM) and discrete multitone (DMT), are

used interchangeably.

Considering the advantage of the MCM scheme in multipath fading and the low complexity of the FFT, MCM becomes quite an attractive solution for high speed transmission. In addition, thanks to the continuous active research on MCM in the 80's [9, 10, 11, 12] and early 90's [13, 14, 15, 16], this scheme is currently in use by European digital audio broadcasting (DAB) [17], asynchronous digital subscriber lines (ASDL) [18], and European digital terrestrial broadcasting [19]. More recently, in July 1998, the IEEE decided to select MCM as the basis for a new physical layer standard extension to the existing 802.11 MAC [20] standard for wireless local area networks (WLAN) in the 5 GHz band [21, 22].

In the early 90's, research on adopting the MCM scheme for multi-user CDMA (code division multiple access) cellular systems—MC-CDMA or orthogonal multicarrier CDMA—began. These new systems can be roughly categorized into two types of systems [23]: One uses the spreading code sequence in the frequency domain [24]–[25] and the other uses it in the time domain [26]–[27]. In the first system, the spreading code sequence is serial to parallel (S/P) processed and each spreading code bit (often denoted by "chip") is transmitted over a different carrier. This is equivalent to transmitting the same information over different carriers with the spreading sequence multiplied in the frequency domain without any expansion of the bandwidth. Hence, this system requires a larger number of carriers as the "spreading gain factor" (number of chips in one symbol duration before the S/P processor) increases and needs more complex hardware for the receiver, though it does not have a bandwidth expansion. In the second system, each carrier is multiplied by a different spreading code sequence which has a code bit duration shorter than the symbol duration, expanding the bandwidth. Usually, a smaller number of carriers is used in the second type of system, and depending on the application, each modulated subcarrier can be band limited as in Kondo and Milstein's study [23], or overlapped in an orthogonal manner as in Sourour and Nakagawa's study [27]. In this thesis, we adopt the latter for the MC-CDMA system model, because of its generality in mathematical representation and analytical attractiveness.

1.2.1 Practical Difficulties in MCM: Amplifier Nonlinearities

There are two main practical difficulties in implementing MCM systems: carrier synchronization and power efficient linear amplification (i.e., amplifier nonlinearities). A small frequency offset (whether from an imperfect oscillator or from the channel Doppler spread) can disturb the orthogonality condition of the carriers, degrading BER performance due to the resulting ICI. Thus very accurate frequency synchronization is desired. Yet the smaller bandwidth on each carrier complicates synchronization of MCM systems [28, 29, 30, 31, 32]. For this research, we have assumed perfect synchronization, focusing on the amplifier nonlinearities.

The difficulties in both power efficient and linear amplification are mainly due to the high envelope variations caused by the addition of multiple carriers. As the number of carriers, M, increases, the maximum possible peak envelope power becomes M times the mean envelope power. This high PMEPR requires a wide linear region of the amplifier in order to avoid signal waveform distortion. However, all amplifiers have a saturation region where the output power does not increase even though the input power increases substantially. Hence, the simplest amplifier input/output relationship can be modeled as that of an ideal soft limiter that has two distinct regions, namely the perfect linear region and the saturation region (where the output power remains constant). In this case, when perfect linear amplification is required, the mean output power should be M times less than the maximum possible output power (saturation power). The amount (in dB) by which the average output power is backed off (reduced) from the saturation power is commonly denoted by "output backoff (OBO)". Large OBO clearly demonstrates inefficient usage of available output power, which translates into high power consumption for conventional linear amplifiers, where the amplifier efficiency is usually highest in the saturation region. This is why nonlinear amplification, which allows a portion of the input signal envelope to go into the saturation region and thus raises the average output power closer to the saturation power, is used. However, nonlinear amplification should be done only to a *certain extent* in order to avoid too much signal distortion. One of the objectives of this study is, therefore, to determine the optimum degree of nonlinearity which ensures the smallest system power consumption, taking into account signal distortion

as well. This issue will be discussed in more detail in Section 1.2.2.

Two leading proposed approaches to reducing power consumption are reduction of PMEPR of MCM signals, and improvement of power efficiency in conventional linear amplifiers. The techniques for reducing PMPER include digital hard clipping [33], and block channel coding schemes [34, 35, 36, 37, 38, 39]. The former suffers from increased BER and creates out-of-band radiation, and the latter is only applicable for a small number of carriers because of the decreasing code rate and the error correction property that accompanies increasing M [39]. The techniques for improving power efficiency of linear amplifiers include amplifier linearization techniques [40, 41, 42, 43], and dc bias controlling techniques [44, 45, 46, 47, 48]. The power efficiency gain from the former is only minimal for highly varying envelope signals such as MCM signals. It is important to note that the 'linear' region of a practical amplifier is not as perfectly linear as that of the soft limiter. The linearization techniques are usually employed to linearize the weakly nonlinear region of the amplifier. Among dc bias controlling schemes, the dual dc bias scheme by Yang et al. [44], which is an extension of the single dc bias scheme by Saleh and Cox [48], can independently of envelope variations maintain a drain efficiency of 50% (the maximum power efficiency of ideal class A linear amplifiers). However, their amplifier models consists of linear regions only. In this thesis, these amplifier models will be extended to a more general model (which includes the saturation region) which is necessary for more realistic power optimization.

1.2.2 Power Consumption Optimization

The previous subsection discussed the practical difficulties of amplifying MCM signals linearly without consuming too much power. The current approaches to this problem were examined, along with their inherent shortcomings.

As mentioned briefly in the previous section, when power consumption is a major concern, nonlinear amplification is practically difficult to avoid, especially with high PMEPR signals. However, nonlinear amplification should be permitted only to a *certain degree*, since the resulting distortion of the signal waveform creates in-band and out-of-band interference. The in-band interference increases BER and the out-of-band

interference (spectral regrowth) can interfere with systems in the adjacent channel, which is usually prohibited by the Federal Communication Commission (FCC). Furthermore, the increase in BER by nonlinear distortion requires more received power to maintain the desired BER, which might void the power savings from nonlinear amplification. Hence, there is a trade-off between the degree of nonlinear distortion and total system power consumption.

Despite this trade-off, to date no justified methods have been offered to optimize power consumption. Instead the commonly used method is to find an amplifier output backoff—OBO determines the degree of nonlinearity—which gives the minimum value of a particular objective function, namely the so-called Total Degradation (TD) [40, 49, 50, 41, 51, 52]. Although the purpose of finding the OBO which minimizes TD is to minimize power consumption, its optimality has only been stated by intuition. This thesis will demonstrate that the conventional objective function, TD, is only applicable when optimizing power consumption with conventional fixed dc bias amplifiers. Furthermore, a more general objective function, total dc power degradation (TDD), will be derived and its optimality will be proved.

In the next subsection, we will discuss means to quantify the BER performance degradation caused by nonlinearities, which is needed for power optimization, either by TD or TDD.

1.2.3 Performance Evaluation of MC Systems in the Presence of Nonlinearities

"Perhaps, the most difficult part in dealing with nonlinearities in any communication systems is that there is not much analytical means to study the system performance. Furthermore, usual analytical treatment of nonlinear systems are often forbiddingly complex and have too simplified assumptions, as to negate the very purpose of analysis: insight and generality. Therefore, the simulation approach is the most preferred method to evaluate nonlinear system performance [53]."

Although, simulation is a favored method of performance evaluation, it can not provide insight into the underlying mechanism, thus making it impossible to general-

ize. This clearly motivates the need for analytical means to evaluate nonlinear system performance. In addition, the performance (such as BER and spectral regrowth) of MCM systems in the presence of nonlinearities is mostly obtained by time-consuming Monte Carlo simulation [52, 54, 55]. The necessity of waveform simulation requires longer simulation time—a higher sampling rate is needed due to the number of multiple carriers and higher order intermodulation (IMD) products from the nonlinearities.

Semi-analytical methods proposed by Santella and Mazzenga [51] and Schneider and Tranter [56] can reduce the simulation execution time. Yet, both works concentrate primarily on reducing computational time rather than on the analysis itself. Santella and Mazzenga [51] model the effect of nonlinear distortion as Gaussian noise added to the received symbol. The variance of noise from the nonlinear distortion is obtained by simulation and added to the variance of the additive white Gaussian noise (AWGN) channel: Gaussian approximation of IMD. BER is obtained from the known analytical BER expression for the linear AWGN channel, with modified AWGN variance. Hence, their method is confined to only the AWGN channel. Moreover, their results become inaccurate as the number of carriers decreases.

Schneider's technique [56] to alleviate the simulation time, is to reduce the sampling rate by generating IMD products that lie only in a given frequency band. In terms of analytical approach, they derived BER performance of uncoded MCM with 3 carriers in AWGN. A memoryless 3rd order polynomial model is used to represent the amplifier nonlinearities. Unfortunately, this method is neither generalized for higher order nonlinearities nor for larger numbers of carriers. In addition, there is no method shown that can be applied to channels other than AWGN, such as multi-path fading channels.

This technique is implicitly extended in Sourour [57] to obtain the BER performance of uncoded MC-CDMA systems with 3rd order nonlinearities in AWGN. However, the 3rd order polynomial model for the amplifier can be used only when both nonlinearity effects and the number of carriers are very small (less than 4). In addition, his analysis is also based on a Gaussian approximation of IMD, which becomes inaccurate for a smaller number of carriers when the spreading gain is small. Hence, his analysis is not appropriate for studying nonlinear saturation effects on the

performance of MCM systems.

However, both Schneider's [56] and Sourour's [57] studies constituted an important starting point of this research. In this thesis, we extend the rudimentary techniques hinted at in their analyses and generalize them to higher order nonlinearities. In addition, we analyze the BER performance of convolutionally coded and uncoded MC-CDMA systems both in multipath fading and AWGN. Our analysis will provide the ability to answer some of the novel questions raised in the following subsection.

1.2.4 Power Optimization in MC-CDMA Systems

In current CDMA systems, because of the near-far effect, the average power received from each user at the base station is usually required to be the same, and this is achieved by power control [58]. Therefore, all the users can not operate at the same output backoff, unless they are all at the same distance from the base station. Hence, in the case of perfect power control, if User A is operating more nonlinearly than other users, the other users will undergo not only linear interference from User A, but also nonlinear interference. This raises two novel questions. The first question that arises is how user location, which determines the degree of nonlinearity, affects the desired user's BER. The second question is how to find the set of nonlinearities which will ensure minimum power consumption for all users in a given cell. In this thesis, we will tackle these novel questions by our optimization methods and analytical means we developed. In the process of resolving the second question, we also found that there is an inherent power consumption problem for conventional amplifiers when used in current cellular systems.

1.3 Thesis Overview and Contribution

The balance of this thesis is organized as follows. Chapter 2 provides background information on system models, such as MCMs, multipath fading channels, and nonlinear amplifier models. For the reader's convenience, we introduce Chapters 3 to 6, in terms of their contributions.

In Chapter 3, we propose a general objective function for optimizing the power

consumption of communication systems with nonlinear power amplifiers. The shortcomings of the conventionally used objective function are noted, and the general objective function is analytically derived.

In Chapter 4, we present a methodology, based on the proposed objective function, to optimize power consumption of MCM systems with a general class of amplifiers, including adaptive dc bias controlled amplifiers. Optimum amplifier OBOs (degree of nonlinearities) are obtained for different types of amplifiers which will be described later. In addition, we perform a simplified asymptotic analysis on power consumption, with which we demonstrate the potential power savings that can be realized with dc bias controlled amplifiers. This advantage will be emphasized in Chapter 6, when we optimize power consumption of users in CDMA cellular networks.

In Chapter 5, we obtain analytical results for the bit error probability of uncoded systems and bounds on the bit error probability of coded systems, in the presence of nonlinearities. Adjacent channel power ratio (ACPR) is also obtained to assess the effect of out-of-band interference (spectral regrowth). In addition, the optimum amplifier output power backoffs are determined for both coded and uncoded systems, which yield the smallest power consumption of the overall system.

In Chapter 6, based on the analytical techniques developed in Chapter 5, we extend our analysis to a multi-user environment, a CDMA single-cell system in which mobiles only communicate with a single base station. The effect of other users' nonlinearities on the performance of a desired user is analytically derived and system power consumption of the users is optimized. We identify the inherent power consumption problem for conventional amplifiers, used in current cellular systems. Furthermore, we apply the results obtained in Chapter 4, as a simple but effective solution to this problem.

Finally, Chapter 7 constitutes the conclusion of this thesis, summarizing our findings and original work (contributions) as well as reviewing the implications of this study for future work.

CHAPTER 2

System and Channel Models

The ultimate goal of communications is to recover the information sent through the transmission medium which is usually denoted as "channel". One example of such a channel is a power amplifier in a microphone where the amplified output may not have the same shape as the original input. Usually a power amplifier is not perfectly linear, distorting signals to some extent. Another example is multipath fading prevalent in a wireless environment. Multipath fading occurs due to the presence of multiple objects between the transmitter and receiver. The reflected signals from the objects can add in-phase (constructively) or out-of-phase (destructively), resulting in amplitude variations of the received signal, known as fading. These channels can (and usually do) impair the transmitted signal significantly, making information transfer difficult.

In this chapter, we describe mathematical models for nonlinear amplifiers and multipath fading channels as well as review multicarrier modulation as a means to mitigate the effect of multipath fading. The basic operational principles of MC-CDMA systems and MCM systems are described. Finally, we examine the potential problems of power consumption in MC-CDMA systems for the cellular environment.

2.1 Nonlinear Amplifier

The purpose of the power amplifier is to deliver a specific (usually high) amount of power to a load (i.e., antenna) connected at the output. However, any amplifier becomes nonlinear if driven hard. This is because they all have the saturation region

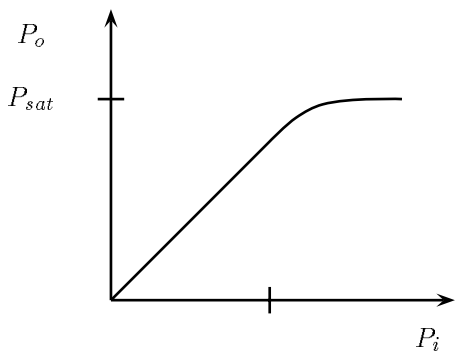

Figure 2.1: Generic relationship of amplifier output power P_o and input power P_i.

where the output power does not increase even though the input power increases substantially, as shown in Figure 2.1. Thus when the modulated envelope—the envelope can be regarded as the square root of instantaneous input power normalized by the impedance—varies, some portion of the output signal may not be as much amplified as others, resulting in signal waveform distortion.

In the following subsection, we first begin our discussion of nonlinear amplifiers with a simple memoryless nonlinear function approximated by a power series (polynomial curve fitting). This simple approximation is very useful in understanding the analytical approaches to modeling the bandpass nonlinear model that we present in the subsequent section. Finally, we discuss the relationship between the instantaneous and envelope characteristics of nonlinear devices along with widely used nonlinear amplifier models.

2.1.1 Nonlinear Systems

Since a nonlinear system does not hold the principle of superposition, it can not be completely described by its transfer function as a linear system. Instead, one common way to characterize input and output of a nonlinear system is by its curve or memoryless function $y(t) = f(x(t))$. "Memoryless" means that the output is a function of the input at the present time only. To explain the effect of nonlinearity in a frequency domain, we approximate the curve by a polynomial as

$$y(t) \;=\; f(x(t)) \;\approx\; \sum_{n=0}^{N} a_n x^n(t). \tag{2.1}$$

When the input $x(t)$ is the sum of the two sinusoids, $\cos(2\pi f_1 t) + \cos(2\pi f_2 t)$, the $y(t)$ from the trigonometric identity consists of all the harmonics of f_1 and f_2 (signals centered at nf_1 and nf_2), as well as the cross product terms at $n_1 f_1 \pm n_2 f_2$, where n_1 and n_2 are positive integers. These cross product terms are usually denoted as the "intermodulation" (IMD) products. The order of the IMD is defined to be $n_1 + n_2$. For example, the output signals at $2f_1 \pm 1f_2$ and $1f_1 \pm 2f_2$ constitute 3rd order IMD products. Note that the nonlinear components create new frequencies which were not present prior to the nonlinearities.

More generally, by the convolution theorem, the Fourier transform of $y(t)$ in (2.1)

$$Y(f) \approx \sum_{n=0}^{N} a_n \left(X^{n-1}(f) * X(f) \right) \tag{2.2}$$

where $X(f)$ is a Fourier transform of $x(t)$, and $X^{n-1}(f)$ denotes a $(n-1)$-fold convolution of $X(f)$. Even if $X(f)$ is band limited by W, the $Y(f)$ is not band limited by W. The convolutional term $(X^{n-1}(f) * X(f))$ creates the frequency components up to nW. This is why a higher oversampling rate is needed in a discrete time simulation of nonlinear systems. The frequency components of $(X^{n-1}(f) * X(f))$, which lie outside of the desired band W (such as harmonics), can be removed by a filtering operation. However, the components inside and near W can not be removed by filtering, because the $X(f)$ information needs to be preserved. These new components, inside and near the desired band, usually constitute the nonlinear signal distortion. In the next subsection, we discuss current techniques to model the nonlinear amplifier in communication systems.

2.1.2 Amplifier Model: Memoryless Bandpass Nonlinearity

Studies [59, 60, 61, 62] of the nonlinear amplifier effects on communication systems began more than 35 years ago with the advent of global-satellite communication systems. In global-satellite systems, the multiple-access operation is achieved by FDM (frequency division multiplexing) using a common broadband traveling-wave-tube (t.w.t.) amplifier placed in the satellite. The amplifier has to be used in saturation mode to reach sufficient power to signal earth. But, in so doing, the nonlinear distortion increases intermodulation products. This has motivated the study on developing

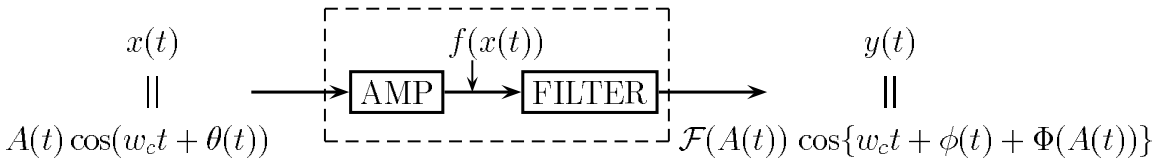

Figure 2.2: Bandpass memoryless model.

analytical models for the amplifiers, in order to assess the nonlinear effect on the communication systems.

Currently available nonlinear models can be divided into two categories—a memoryless model [63, 64, 65] and a model with memory [66, 67, 68]—depending on the frequency selective effects of the amplifier. In this thesis, we focus only on the memoryless model. This model is generally valid for bandpass communication systems, where the signal bandwidth is usually small enough that the amplifier characteristic is almost frequency-independent over the bandwidth of the signal [53].

Perhaps, the most conventionally used memoryless model is a bandpass memoryless model, where the output signal of the amplifier only depends on the envelope of the input to the amplifier. In this model, the relationship between the input and output of the amplifier is described by the two memoryless functions, that is amplitude (AM/AM) and phase (AM/PM) nonlinearities. As shown in Figure 2.2, when the input to the amplifier is the modulated signal

$$x(t) \;=\; A(t)\cos\{w_c t + \phi(t)\} \tag{2.3}$$

the output of the amplifier can be expressed as

$$y(t) \;=\; \mathcal{F}(A(t))\cos\{w_c t + \phi(t) + \Phi(A(t))\} \tag{2.4}$$

where $A(t)$ and $\phi(t)$ are the envelope and the phase of $x(t)$, respectively. The functions $\mathcal{F}(A(t))$ and $\Phi(A(t))$, denote AM/AM and AM/PM, respectively. Usually, $\mathcal{F}(A(t))$ and $\Phi(A(t))$ are obtained by a single sinewave swept tone measurement. In analytic term, this simple single tone measurement method is not truly representative of amplifier behavior with the modulated carriers if we operate on the principles that the modulated signal is the linear combination of the sinusoids around the carrier

frequency and that nonlinear systems do not hold superposition. However, in most cases (from the experiment [69]), the output of the nonlinear amplifier can be modeled as an envelope model as in (2.4) with a single tone measured AM/AM and AM/PM.

The amplifiers commonly used in communication systems can be divided into two types: the traveling wave tube (TWT) and the solid state power amplifier (SSPA). The former is mostly employed for satellite transponders, while the latter is used in a wide variety of applications, including mobile transmitters. The TWT and SSPA have considerably different characteristics in terms of AM/AM and AM/PM. The output in the saturation region of the AM/AM in the TWT decreases with increasing input power but is constant in the SSPA. In addition, the AM/PM effect of the TWT is much larger than that of the SSPA. The measured AM/AM and AM/PM of TWT can be well represented by Saleh's analytical model [67], and AM/AM of SSPA can be well approximated by Cann's model [70].

In this thesis, we primarily concentrate on SSPA type amplifiers and assume no AM/PM effects. This is not only because the SSPA usually has a negligible AM/PM, but also because the effects of AM/AM are found to be much more significant than AM/PM [52, 71].

The AM/AM and AM/PM model are memoryless because the values of the functions at t_1 (i.e., $\mathcal{F}(A(t_1))$ and $\Phi(A(t_1))$) only depend on the value of $A(t)$ at t_1. In addition, it is referred to as a bandpass nonlinearity because the signal in (2.4) has only frequency components around f_c and not around harmonic frequencies, such as $0, 2f_c, 3f_c, \ldots$. The harmonics are implicitly assumed to be rejected by an ideal zonal filter around the carrier frequency. Since $\mathcal{F}(A(t_1))$ and $\Phi(A(t_1))$ do not depend on the carrier frequency, $x(t)$ and $y(t)$ can be represented by the corresponding lowpass equivalent form

$$x_L(t) = A(t)e^{j\phi(t)} \tag{2.5}$$

$$y_L(t) = \mathcal{F}(A(t))e^{\{j\phi(t)+\Phi(A(t))\}}, \tag{2.6}$$

respectively. This form is very attractive for simulation because it can be done in baseband, reducing sampling rate. In the next subsection, we discuss the relationship between the envelope voltage transfer characteristics (AM/AM and AM/PM)

and instantaneous voltage transfer ($f(x(t))$) in Figure 2.2. This is of interest because even though there exist many simple models for instantaneous transfer characteristics of nonlinear devices (such as a soft limiter), the AM/AM and AM/PM representation of the devices is mostly preferred in performance evaluation of the nonlinear communication system.

2.1.3 Instantaneous Voltage and Envelope Voltage

In Subsection 2.1.1, the IMD products from the nonlinear device are explained with instantaneous voltage transfer characteristics ($f(x(t))$) and in Subsection 2.1.2, envelope transfer characteristics (AM/AM and AM/PM) are introduced to represent the nonlinear amplifier in communication systems. In this subsection, we show the general relationship between the instantaneous and the envelope characteristics.

Assume $x(t)$ is the narrow band signal (the envelope varies much slowly than f_c) as in (2.3). By letting

$$\alpha = w_c t + \phi(t)$$

and omitting t for the sake of notational convenience, the output voltage $f(A\cos(\alpha))$, which is a periodic function of α, can be represented by the following Fourier series:

$$\begin{aligned} f(A\cos(\alpha)) &= \frac{1}{2}F_{c,0}(A) \\ &+ \{F_{c,1}(A)\cos(\alpha) + F_{s,1}(A)\sin(\alpha)\} \\ &+ \{F_{c,2}(A)\cos(2\alpha) + F_{s,2}(A)\sin(2\alpha)\} \\ &+ \{F_{c,3}(A)\cos(3\alpha) + F_{s,3}(A)\sin(3\alpha)\} + \cdots \end{aligned}$$

where

$$F_{c,m}(A) = \frac{1}{\pi}\int_0^{2\pi} f(A\cos(\alpha))\cos(m\alpha)d\alpha \tag{2.7}$$

$$F_{s,m}(A) = \frac{1}{\pi}\int_0^{2\pi} f(A\cos(\alpha))\sin(m\alpha)d\alpha. \tag{2.8}$$

The first zone output (around the carrier frequency f_c) of the bandpass filter can be expressed as

$$\begin{aligned} y(t) &= F_{c,1}(A(t))\cos(w_c t + \phi(t)) + F_{s,1}(A(t))\sin(w_c t + \phi(t)) \\ &= \mathcal{F}(A(t))\cos\{w_c t + \phi(t) + \Phi(A(t))\}. \end{aligned} \tag{2.9}$$

This is the same expression as in (2.4) with

$$\begin{aligned} \mathcal{F}(A) &= \sqrt{F_{c,1}^2(A) + F_{s,1}^2(A)} \\ \Phi(A) &= -\tan(F_{s,1}(A)/F_{c,1}(A)) \end{aligned}$$

The complex function $(F_{c,1}(A) + jF_{s,1}(A))/A$ is known as a describing function in control theory or Chebyshev transform of $f(x)$ [64]. Note that when $f(A\cos(\alpha))$ is an even function, $\mathcal{F}(A) = F_{c,1}(A)$ and $\Phi(A) = 0$. In the next subsections, we consider, simple but widely used, nonlinear device characteristics.

Simple Nonlinear Models

In terms of the instantaneous and envelope characteristics, we consider three representative nonlinear device models: the power series model, the ideal soft limiter, and the Cann's model. As noted from Subsection 2.1.1, the power series model is very useful for analysis since the amplifier characteristics are represented by the linear summation of the signal term powers. However, the power series model can well approximate the amplifier curve for a limited range. Hence, it is difficult to test strong nonlinearities in simulation when there is a very large envelope variation in input signal.

On the other hand, the ideal soft limiter and Cann's model can support wide input range for the amplifier. The importance of the ideal soft limiter is that it physically represents the ideal SSPA amplifier characteristics. However, the drawback of the ideal soft limiter is that it can not fully represent the real amplifier characteristics. This drawback can be overcome by the Cann's model, where simple parameters are used to better approximate (represent) the real measured SSPA characteristics.

Ideal Soft Limiter

The ideal soft limiter has the following instantaneous voltage characteristics

$$f(x(t)) = \begin{cases} \frac{L}{l}x(t) & \text{for } |x(t)| \le l \\ L & \text{for } |x(t)| > l, \end{cases} . \tag{2.10}$$

which is usually used to model an ideal amplifier characteristics. In this case, since $f(A\cos(\alpha))$ is an even function its corresponding AM/AM and AM/PM are $\mathcal{F}(A) =$

$F_{c,1}(A)$ and $\Phi(A) = 0$, respectively. $\mathcal{F}(A)$ can be obtained by considering two cases: $A \leq l$ and $A > l$.

When $A \leq l$, the input signal $x = A\cos(\alpha) \leq l$. Thus

$$\begin{aligned}\mathcal{F}(A) &= \frac{1}{\pi}\int_0^{2\pi} f(A\cos(\alpha))\cos(\alpha)d\alpha = \frac{1}{\pi}\int_0^{2\pi}\frac{L}{l}A\cos^2(\alpha)d\alpha \\ &= \frac{L}{l}A. \end{aligned} \tag{2.11}$$

When $A > l$, some of the input signal are clipped and

$$\begin{aligned}\mathcal{F}(A) &= \frac{1}{\pi}\left\{\int_0^{\theta_1} L\cos(\alpha)d\alpha + \int_{\theta_1}^{\theta_2}\frac{L}{l}A\cos^2(\alpha)d\alpha - \int_{\theta_2}^{\theta_3} L\cos^2(\alpha)d\alpha \right. \\ &\quad \left. + \int_{\theta_3}^{\theta_4}\frac{L}{l}A\cos^2(\alpha)d\alpha + \int_{\theta_4}^{2\pi} L\cos(\alpha)d\alpha.\right\}.\end{aligned}$$

Using symmetric property of the integrand,

$$\mathcal{F}(A) = \frac{4}{\pi}\left\{\int_0^{\theta_1} L\cos(\alpha)d\alpha + \int_{\theta_1}^{\pi/2}\frac{L}{l}A\cos^2(\alpha)d\alpha\right\} \tag{2.12}$$

where $\theta_1 = \text{acos}(u)$ and $u = l/A$. Hence

$$\begin{aligned}\mathcal{F}(A) &= \frac{4L}{\pi}\left\{\sin(\theta_1) + \frac{A}{2l}\int_{\theta_1}^{\pi/2}\{1+\cos(2\alpha)\}d\alpha\right\} \\ &= \frac{4L}{\pi}\left\{\sqrt{1-u^2} + \frac{1}{2u}[(\frac{\pi}{2}-\theta_1) + \frac{1}{2}\sin(\pi) - \frac{1}{2}\sin(2\theta_1)]\right\} \\ &= \frac{4L}{\pi}\left\{\sqrt{1-u^2} + \frac{1}{2u}[\text{asin}(u) - u\sqrt{1-u^2}]\right\} \\ &= \frac{2L}{\pi}\frac{A}{l}\left(\frac{l}{A}\sqrt{1-(\frac{l}{A})^2} + \text{asin}(\frac{l}{A})\right)\end{aligned} \tag{2.13}$$

where we use the fact that $\sin(\theta_1) = \sqrt{1-u^2}$ and $\cos(\theta_1) = u$.

In summary,

$$\mathcal{F}(A) = \begin{cases} \frac{L}{l}A & \text{for } A \leq l \\ \frac{2LA}{\pi l}[\text{asin}(\frac{l}{A}) + \frac{l}{A}(1-\frac{l^2}{A^2})^{\frac{1}{2}}] & \text{for } A > l, \end{cases} \tag{2.14}$$

$$\Phi(A) = 0. \tag{2.15}$$

These results are used again in Chapter 4, when we extend the amplifier model used in [48, 44].

Power Series Model

The power series representation is one of the most commonly used methods to represent nonlinear devices because it identifies the contribution of different power terms. This is especially useful in determining the parameters of predistortion since predistortion is often realized by compensating low order power terms (usually 3rd and 5th) [53]. Furthermore, this polynomial model is used, in Chapter 5 and 6, to analyze nonlinear distortion effects on communication systems.

The AM/AM and AM/PM of the following instantaneous characteristics

$$y(t) \;=\; f(x(t)) \;=\; \sum_{n=0}^{N} \alpha_n x^n(t) \tag{2.16}$$

are

$$\mathcal{F}(A) \;=\; \sum_{m=0}^{(N-1)/2} \frac{\alpha_{2m+1}}{2^{2m}} \binom{2m+1}{m+1} A^{2m+1} \tag{2.17}$$

$$\Phi(A) \;=\; 0. \tag{2.18}$$

This can be easily derived by the binomial expansion of $x(t)$, and the complete derivation can be found in [53, pages 160–161]. Note that only odd terms in (2.16) contribute to AM/AM as in (2.17). This is why only odd order terms are considered in bandpass nonlinear model.

Cann's Model

Perhaps, the most widely used SSPA amplifier model in simulation is Cann's model which has the instantaneous voltage characteristics [53, 70]

$$f(x(t)) = \frac{L \,\mathrm{sgn}(x(t))}{[1 + (\frac{l}{|x(t)|})^s]^{1/s}} \tag{2.19}$$

where s controls the smoothness of the transition from the linear region to saturation region and where l and L denote the maximum linear instantaneous input and maximum output voltage, respectively. Figure 2.3(a) shows $f(x(t))$ with $l = 0.7$ and $L = 1$ for different s'. As $s \to \infty$, the characteristics become that of the ideal soft limiter given in (2.10). The AM-AM of the Cann's model can be obtained from the above equation (2.19) using (2.7), or from (2.17) with the α's obtained by curve fitting the voltage characteristics in (2.19). Figure 2.3(b) shows the AM-AM of $f(x(t))$

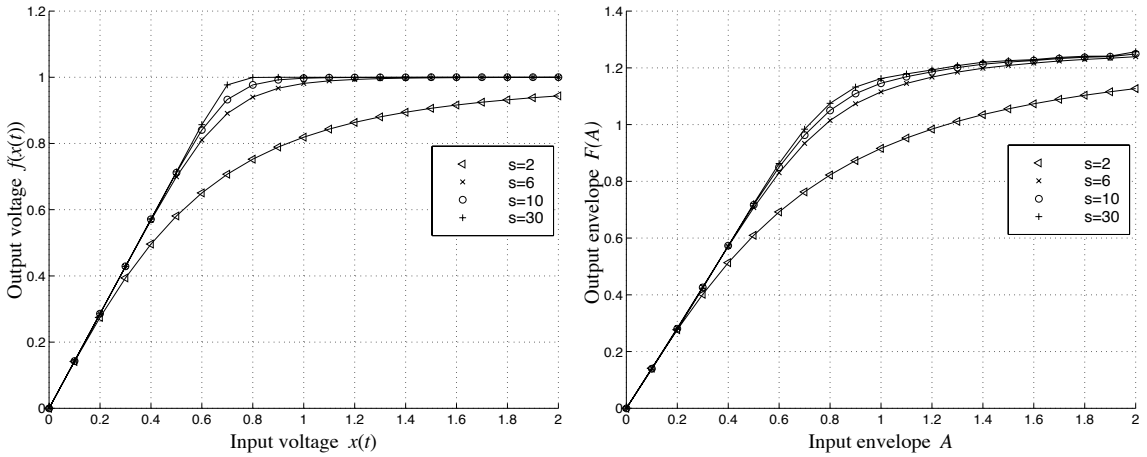

(a) (b)

Figure 2.3: Cann's model: (a) instantaneous voltage and (b) envelope voltage characteristics.

in Figure 2.3(a). This figure is obtained by first curve fitting $f(x(t))$ in (2.19) by the polynomial model in (2.16) with $N = 19$. Then it is plotted according to (2.17). However, when the AM-AM data (from the real measurement) is available, the following modified Cann's AM-AM [51]

$$\mathcal{F}(A) = \frac{LA}{[1 + (\frac{l}{A})^s]^{1/s}} \tag{2.20}$$

can be simply used as a curve-fitting function, which is especially convenient for simulation.

2.2 Multipath Fading Channel

In a wireless channel environment, multiple objects (such as cars, trees, buildings) between the transmitter and receiver can reflect the transmitted signal. These reflected signals can be received with different delays. In addition, the channel can be time-varying due to the movement of the environment or due to the motion of the transmitter and receiver. Given this phenomenon, the multipath channel is usually modeled as a linear time-varying filter. This model was developed by Bello [72] and is called the 'wide-sense stationary, uncorrelated scattering' (WSUSS) fading. The

detailed treatment of this statistical model can be found in the research of Bello [72], Proakis [73], and Biglieri [74]. In this section, we give an overview of the WSSUS multipath fading model and highlight the main parameters, which will be used in the rest of the thesis.

2.2.1 WSUSS Model

In WSUSS, the fading process is modeled as a linear time-varying filter with a low pass equivalent impulse response $h_L(t;\tau)$, where $h_L(t;\tau)$ is a complex Gaussian random process. This is known as a Rayleigh fading channel when the mean of the process is zero. For the cases where there is a strong direct path, the process has a nonzero mean and is called Rician fading [73]. In this thesis, we only focus on the Rayleigh fading channel.

The impulse response $h_L(t;\tau)$ is the response at time t due to an impulse at time $t-\tau$. Hence, if $x_L(t)$ is the low pass equivalent input signal to the channel, the low pass equivalent output signal $r_L(t)$ is given by

$$r_L(t) = \int_{-\infty}^{\infty} h_L(t;\tau)x_L(t-\tau)d\tau. \tag{2.21}$$

The assumption for WSSUS is that the correlation between the channel outputs at two different times only depends on the time difference, and that the channel outputs at different path delays are uncorrelated. This can be mathematically described by

$$E[h_L(t;\tau_1)h_L^*(t+\Delta t;\tau_2)] = \phi(\tau_1;\Delta t)\delta(\tau_2-\tau_1) \tag{2.22}$$

where $\delta(t)$ is the Dirac delta function; $E[X]$ denotes the expectation of random variable X; $\phi(\tau;0)$ denotes the amount of power received at a given delay τ and is called 'multipath intensity profile'. The range of τ at which $\phi(\tau;0)$ is nonzero, is called the 'multipath delay spread', T_m [73].

The channel frequency response $H_L(f;t)$ is the Fourier transformation of the impulse response $h_L(t;\tau)$. The correlation between the frequency responses at two different frequencies is given by

$$\begin{aligned}\Phi(f_1,f_2;\Delta t) &= E[H_L(f_1;t)H_L^*(f_2;t+\Delta t)] \\ &= \int_{-\infty}^{\infty} \phi(\tau;\Delta t)\exp(-j2\pi(f_2-f_1)\tau)d\tau. \end{aligned}\tag{2.23}$$

The correlation depends only on the frequency separation $(f_2 - f_1)$ for a given Δt. The minimum frequency separation needed to have the frequency responses uncorrelated is called the 'coherence bandwidth', B_c, and it is defined as the inverse of multipath delay spread by

$$B_c = 1/T_m. \tag{2.24}$$

If the signal bandwidth is much smaller than the coherence bandwidth B_c, the signal spectrum undergoes the same attenuation; this channel is a frequency nonselective fading channel (or flat fading). On the contrary, when the signal bandwidth is larger than the coherence bandwidth B_c, the channel is a frequency selective fading channel, and the signal spectrum will undergo different attenuation.

The time-varying nature of the channel impulse response can also be described by $\Phi(f_1, f_2; \Delta t)$ by fixing the values of f_1 and f_2. In particular, $\Phi(0; \Delta t)$ measures the time correlation of the received tone. The Fourier transform of $\Phi(0; \Delta t)$ is the 'Doppler power spectral density',

$$S(\lambda) \;=\; \int_{-\infty}^{\infty} \Phi(0;\tau) \exp(-j2\pi\lambda\tau) d\tau. \tag{2.25}$$

The range of λ at which $S(\lambda)$ is nonzero, denotes the 'Doppler spread', B_d. It is defined as the inverse of 'coherence time', T_d by

$$B_d = 1/T_d. \tag{2.26}$$

The coherence time T_d denotes the largest time difference for which the responses are correlated. The smaller the value of T_d, the more rapidly the channel response changes with time. If T_d is much larger than the symbol duration T_s, the fading is said to be slowly varying. Throughout this thesis, we consider the slow fading channel in which the channel responses are constant over the symbol duration, T_s. In the next subsection, we describe this WSSUS model more explicitly with a channel impulse response.

2.2.2 Channel Response

We can obtain the mathematical model for the time varying impulse response of the channel, by noting the Doppler effect and the time resolution of the filter. The

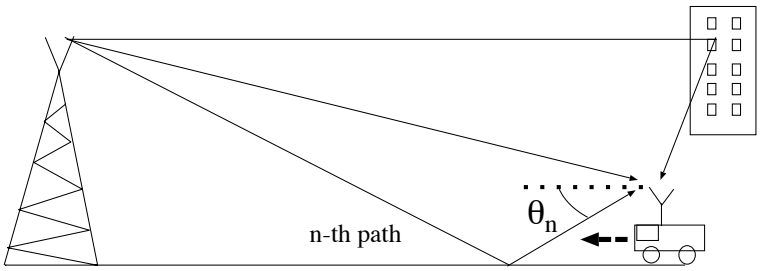

Figure 2.4: Multipath channel.

Doppler effect is the phenomena of variation in frequency of any transmitted wave as the source and observer approach or move away. Hence, if the n-th arriving path to the moving vehicle has an angle θ_n with respect to moving direction (as in Figure 2.4), the frequency of the arriving path is shifted by

$$f_n^s = f_d \cos\theta_n \tag{2.27}$$

$$f_d = f_c v/c \tag{2.28}$$

where v is the vehicular speed and c is the speed of light, and f_c is the carrier frequency [75]. The filter with bandwidth W can resolve (or distinguish) two distinct pulses with separation of τ if $\tau > W^{-1}$ [73]. Hence, the channel impulse response can be modeled as

$$h_L(t;\tau) \;=\; \sum_{n=1}^{N} \beta_n(t)\delta(\tau - \tau_n) \tag{2.29}$$

where N is the number of resolvable path groups, and the complex coefficient for the n-th path group

$$\beta_n(t) \;=\; \sum_{i=1}^{I_n} \beta_{n,i} \exp\{j(2\pi f_{n,i}^s t + \phi_{n,i})\} \tag{2.30}$$

where I_n is the number of the unresolved paths of n-th group. The amplitude, phase and Doppler shift of i-th path of n-th group are $\beta_{n,i}$, $\phi_{n,i}$, and $f_{n,i}^s$, respectively. The above process $\beta_n(t)$ can be well approximated by the complex Gaussian process (from the central limit theorem), if I_n is a moderately large number (e.g., larger than 5) and $\phi_{n,i}$ is uniformly distributed. In this case, the magnitude $|\beta_n(t)|$ becomes Rayleigh and the phase $\angle\beta_n(t)$ becomes a uniform random variable.

Frequency Selectivity

When $N = 1$ (i.e., all the delays are less than W^{-1}), the channel simplifies to the multiplicative channel with the received signal

$$\begin{aligned} r(t) &= \int_{-\infty}^{\infty} h_L(t;\tau) x_L(t-\tau) d\tau. \\ &= \beta(t) x_L(t-\tau). \end{aligned} \tag{2.31}$$

In this case, all the path energy is concentrated in one group with maximum delay less than W^{-1}, that is, $T_m < W^{-1}$. From (2.24), the signal bandwidth (receiver filter bandwidth) W, is smaller than the coherence bandwidth B_c, resulting in the same attenuation of all the signal spectrum. This multiplicative channel is usually called the frequency nonselective channel or flat fading. On the other hand, when $N > 1$, the received signal

$$r(t) = \sum_{n=1}^{N} \beta_n(t) x_L(t-\tau_n) \tag{2.32}$$

where $N = \lfloor WT_m \rfloor + 1$ [73]. In this case, the signal bandwidth, W, is larger than the coherence bandwidth B_c, resulting in a different attenuation of the signal spectrum: the frequency selective channel.

Time Selectivity

The time varying nature of the channel can be observed from the variation of the path coefficient $\beta_n(t)$. From the WSSUS assumption, the coefficients for the different path groups are uncorrelated. The time correlation between the same path group $\beta_n(t)$ at time t and $t + \Delta t$ is

$$E[\beta_n(t)\beta_n^*(t+\Delta t)] = \sum_{i=1}^{I_n} \beta_{n,i}^2 E[\exp\{-j(2\pi f_d \cos\theta_{n,i}\Delta t)\}]. \tag{2.33}$$

If we assume the $\theta_{n,i}$ to be a independent, identically distributed (iid) random variable uniformly distributed over $[0, 2\pi]$,

$$\begin{aligned} E[\beta_n(t)\beta_n^*(t+\Delta t)] &= \sum_{i=1}^{I_1} \beta_{n,i}^2 \left\{ \frac{1}{2\pi} \int_o^{2\pi} \exp\{-j(2\pi f_d \cos\theta_{n,i}\Delta t)\} d\theta_{n,j} \right\} \\ &= \{\sum_{i=1}^{I_n} \beta_{n,i}^2\} J_o(2\pi f_d \Delta t) \end{aligned} \tag{2.34}$$

where $J_o(x)$ is the zero-th order Bessel function. The n-th order Bessel function is defined as

$$J_n(x) = \frac{1}{2\pi}\int_o^{2\pi} \exp\{-jx\sin\theta - jn\theta\}d\theta. \tag{2.35}$$

In summary,

$$E[\beta_n(t)\beta_m^*(t+\Delta t)] = \{\sum_{i=1}^{I_n}\beta_{n,i}^2\}J_o(2\pi f_d\Delta t)\delta(n-m). \tag{2.36}$$

In this thesis, however, we mainly consider a slowly varying fading channel so that the fade level is approximately constant over a symbol duration.

Multipath Intensity Profile

When an impulse is applied to the channel, the average received power at the output of a multi-path channel is given by

$$P_r = \sum_{n=1}^{N} E[|\beta_n(t)|^2]. \tag{2.37}$$

Hence, the intensity profile defined in (2.22)

$$\begin{aligned}\phi(\tau;0) &= E[h_L(t;\tau)h_L^*(t;\tau)] \\ &= \sum_{n=1}^{N} E[|\beta_n(t)|^2]\delta(\tau-\tau_n)\end{aligned} \tag{2.38}$$

represents the average power strength distribution as a function of the delay. With the intensity profile, the time dispersion of the channel can be represented by the root mean square (rms) delay spread [76]

$$\tau_{rms} = \sqrt{E[\tau^2] - E^2[\tau]} \tag{2.39}$$

where

$$\begin{aligned}E[\tau^i] &= \frac{\int_0^\infty \tau^i\phi(\tau;0)d\tau}{\int_0^\infty \phi(\tau;0)d\tau} \\ &= \frac{\sum_{n=1}^N \tau^i E[|\beta_n(t)|^2]}{\sum_{n=1}^N E[|\beta_n(t)|^2]}.\end{aligned} \tag{2.40}$$

This gives time dispersion of the channel in the average sense, compared to the multipath delay spread T_m. This is because channels that have the same T_m can

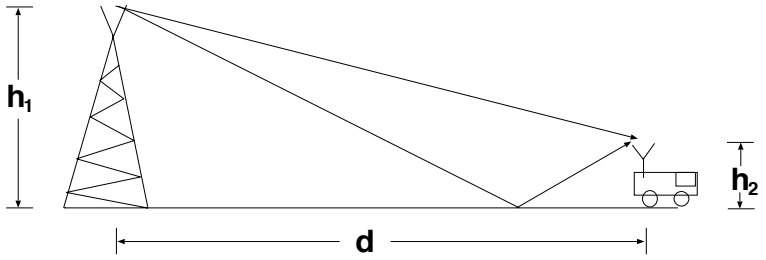

Figure 2.5: Mobile radio channel.

have very different intensity profiles, thus affecting system performance. The typical value of τ_{rms} is on the order of nanoseconds for indoor channels and on the order of microseconds for outdoor channels.

Channel Propagation Loss

The distance separation (d) between the transmitter and receiver reduces the average received power. In a single-path free-space propagation, if the transmitted power is P_t, the received signal has power

$$P_r = P_t G_t G_r \left(\frac{c}{4 f_c \pi d}\right)^2$$

where G_t and G_r are the transmitter and receiver antenna gains, respectively [76]. Hence, the received power is reduced by a factor of 20 dB for every decade of distance. In a mobile radio channel, as shown in Figure 2.5, where the height of the antennas are h_1 and h_2, respectively, it can be easily shown [76] that the received power

$$P_r \approx P_t G_t G_r \frac{h_1^2 h_2^2}{d^4}. \tag{2.41}$$

In the above derivation, two paths (a direct and a perfectly reflected path) are considered and it is assumed that $d \gg \max(h_1, h_2)$. The received power decreases at a rate of 40 dB/decade compared to 20 dB/decade in free space propagation. The actual received power attenuation varies between 20 dB/decade and 60 dB/decade, depending on the environment (whether in office, house, factory, outdoors, or other situations) [76]. In this thesis, we model the distance power loss to be 40 dB/decade, which is typically the case for cellular radio environments.

2.3 Multicarrier Modulation

As mentioned in Chapter 1, in a multicarrier system a high-speed data stream is split into several slower streams, each of which is transmitted on a separate carrier. Inter-symbol-interference (ISI) from the multipath on each carrier is significantly reduced by a long symbol duration relative to the channel delay spread. Moreover, the residual ISI between MCM symbols can be eliminated by the insertion of a guard interval periodically between MCM symbols. In this section, we review in detail basic operational principles of conventional multicarrier modulation (so called, OFDM). We then describe the multicarrier CDMA system (MC-CDMA) model as well as the basic system assumptions used in the rest of the thesis. And, finally, we discuss the novel problems of MC-CDMA systems which emerged from their application in the context of multi-user communication systems and power consumption.

2.3.1 An MCM System Model

The basic form of MCM signals is

$$x(t) = \sum_{n=-\infty}^{\infty} \mathrm{Re}\{x_L(t-nT_s)e^{j2\pi f_c t}\}. \tag{2.42}$$

In (2.42), the lowpass equivalent signal $x_L(t)$, of $x(t)$ in the time interval $[nT_s,(n+1)T_s]$, is given by

$$x_L(t-nT_s) = \sum_{q=0}^{M-1} X_n(q)e^{j2\pi f_q(t-nT_s)}p_{T_s}(t-nT_s) \tag{2.43}$$

where f_c and $f_q = q/T_s$ are the carrier frequency and frequency separation between the q-th subcarrier and carrier frequency, respectively. $X_n(q)$ denotes the complex data of the q-th subcarrier at the n-th block. The alphabet for $X_n(q)$ is determined by the modulation scheme for each carrier. In this thesis, we restrict our interest to $\mathrm{Re}\{X_n(q)\} \in \{\pm 1\}$ and $\mathrm{Im}\{X_n(q)\} \in \{0, \pm 1\}$ (i.e., BPSK or QPSK modulation for each carrier). A unit rectangular pulse in $[0, T_s]$ is denoted by

$$p_{T_s}(t) = \begin{cases} 1 & 0 \le t < T_s \\ 0 & \text{otherwise.} \end{cases}$$

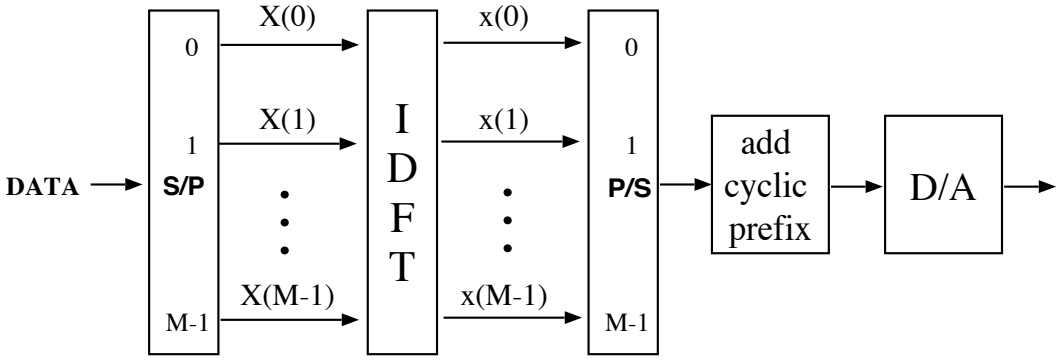

Figure 2.6: OFDM modulation by IDFT.

As a result of rectangular pulse shaping for each carrier, the power spectral density function of each channel is a sinc function, generating large sidelobes. These sidelobes can be reduced by either a filtering or a time window function.

The classic treatment of the window function in MCMs can be found in the papers of Weinstein [8] and Ochiai [36]. Filtered MCMs, on the other hand, will be used in Chapter 4 of this thesis.

In practice, to reduce the large number of oscillators in this modulation/demodulation scheme, the Discrete Fourier transform (DFT) technique is often utilized. In the following, we describe the DFT realization of MCM signals, which is commonly referred to as OFDM.

OFDM: DFT Implementation

The block diagram of an OFDM transmitter is shown in Figure 2.6. This scheme operates block-wise, taking M complex data symbols $(X_n(0), X_n(1), \cdots, X_n(M-1))$, and yielding the following M complex sequence out of the inverse DFT (IDFT)

$$x_n(i) \;=\; \sum_{q=0}^{M-1} X_n(q) e^{\frac{j2\pi iq}{M}},\; i = 0, 1, \ldots, M-1. \tag{2.44}$$

Note that the discrete time sequence $\{x_n(i)\}$ corresponds to the samples of $x_L(t)$ at time $t = nT_s + iT_s/M, 0 \leq i < M$. The sequence is then low pass filtered (D/A) to approximate the n-th block (i.e. n-th OFDM symbol) of $x_L(t)$ in time interval $nT_s \leq t < (n+1)T_s$. The demodulation of MCM signals is in essence an inverse process of modulation, as shown in Figure 2.7.

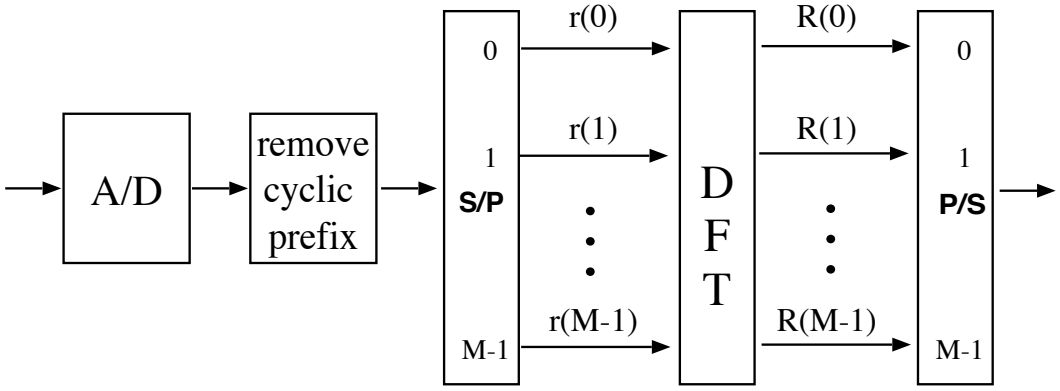

Figure 2.7: OFDM demodulation by DFT.

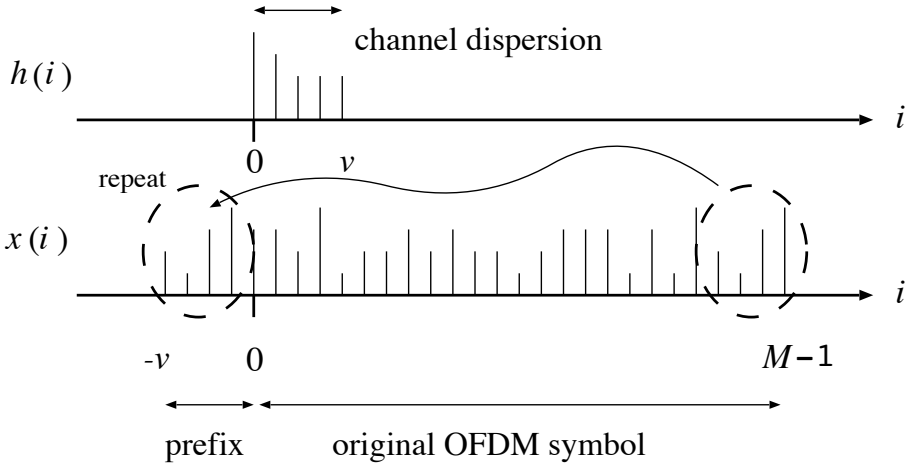

Figure 2.8: Guard interval and cyclic prefix.

Channel Dispersion: Guard Interval and Cyclic Prefix

In order to eliminate the ISI between OFDM symbols (blocks) from the channel delay spread, a guard interval (about the same time duration of multipath delay spread) is inserted at the start of each block periodically. Furthermore, the tail of each block is repeated in the guard interval [73, page 691]. That is, when the channel dispersion spans $v+1$ signal samples, as shown in Figure 2.8, a sequence $\{x_n(-v), \ldots, x_n(-1), x_n(0), \ldots, x_n(M-1)\}$, with $x_n(-i) = x(M-i)$, $1 \leq i \leq v$, is transmitted instead of M samples of sequence. The disadvantage of this guard interval is the loss of data rate by a factor of $(M+v)/M$ for a given T_s. Nonetheless, this repetition is still needed to preserve orthogonality between each carrier after

demodulation with DFT. Although the system model is based on the assumption that a proper length of a guard interval is included, all the results are obtained with the assumption that there is no data rate loss (or effective energy loss for a fixed data rate) by the guard interval. This is because all the results can be easily scaled for a given length of the guard interval, and also when the number of carriers become large, the data rate loss becomes negligible.

Note that the multiplication of the DFT of two sequences is equivalent to the circular convolution of the two sequences in time domain, not to the conventional sliding convolution. However, the output of the multipath channel is the conventional sliding convolution of the transmitted signal and channel impulse response. In more detail, suppose the discrete time channel response for the n-th block is nonzero only for v samples, $\{h_n(i), 0 \leq i \leq v\}$, as shown in Figure 2.8. Then the output sequence of the channel is the sliding convolution of $\{x_n(i)\}$ and $\{h_n(i)\}$ given by

$$\begin{aligned} r_n(i) &= \sum_{j=-\infty}^{\infty} h_n(j)x_n(i-j) \\ &= \sum_{j=0}^{v} h_n(j)x(i-j). \end{aligned} \tag{2.45}$$

With the cyclic prefix in $\{x_n(i)\}$, $\{r_n(i), 1 \leq i < M\}$ becomes

$$\sum_{j=0}^{v} h_n(j)x(i-j) = \sum_{j=0}^{v} h_n(j)x((i-j)_M) \tag{2.46}$$

$$= \sum_{j=0}^{M-1} h_n(j)x((i-j)_M) \tag{2.47}$$

where $(i-j)_M = i-j$ modulo M, and the last equation denotes the circular convolution of $\{x_n(i)\}$ and $\{h_n(i)\}$.

Hence, without noise in the channel, the output sequence of the DFT in the demodulator is just the multiplication of the DFT of $\{x_n(i)\}$ and $\{h_n(i)\}$, given by

$$\text{DFT}(\{r_n(i)\}) = \{R_n(q)\} = \{H_n(q)X_n(q)\} \tag{2.48}$$

where $H_n(q)$ denotes the DFT of $\{h_n(i)\}$,

$$\sum_{i=0}^{v} h_n(i)e^{-j2\pi iq/M} \text{ for } q = 0, \ldots, M-1. \tag{2.49}$$

From (2.48), it is clear that with the cyclic prefix in $\{x_n(i)\}$ the effect of the multipath on the transmitted signals is merely a scaling of the amplitude and phase shift of each subcarrier. The amplitude and phase information of the channel is usually available at the receiver for coherent detection, eliminating the need of a complex equalizer.

Channel Coding and Interleaving

The bit error rate performance of OFDM in a Rayleigh multi-path fading channel without channel coding is the same as that of a single carrier with flat Rayleigh fading, which is only a linear inverse in the signal-to-noise power ratio. Hence, in order to improve performance usually channel coding (error correction coding) is necessary in OFDM system. With channel coding, the structured redundant bits are added to the information bits to protect the information bits from errors.

Usually, most codes are designed to combat random independent errors, whereas channels (such as slowly varying multipath fading) can cause dependent signal impairment. Hence, in order to break the channel memory effects, interleaving and deinterleaving (so called time diversity) is usually adopted in coded systems. Interleaving is a process of reordering symbols in coded streams in such a way that the received code symbols after deinterleaving are merely independent of each other. Throughout the rest of the thesis, perfect interleaving is assumed, that is, all the code symbols are assumed independent of each other.

Envelope Variation of MCM: Peak-to-Mean-Envelope-Power-Ratio

The instantaneous power of $x_L(t)$, assuming a rectangular window, is

$$\begin{aligned}
(x_L(t))(x_L(t))^* &= \sum_{q=0}^{M-1}\sum_{k=0}^{M-1} X_n(q)X_n^*(k)e^{j2\pi(f_q-f_k)t} \\
&= \sum_{k=0}^{M-1}|X(k)|^2 + 2\mathrm{Re}\left\{\sum_{k=0}^{M-1}\sum_{l=k+1}^{M-1} X(k)X^*(l)e^{j2\pi(k-l)t/T_s}\right\} \\
&= M + 2\mathrm{Re}\left\{\sum_{m=1}^{M-1} R_X(m)e^{j2\pi mt/T_s}\right\} \qquad (2.50)
\end{aligned}$$

where we assume $|X_n(q)|^2 = 1$, and $R_X(m)$ denotes an aperiodic autocorrelation function of sequence $\{X_n(q)\}$, given by

$$R_X(m) = \sum_{k=0}^{M-1-m} X_n(k)X_n^*(k+m).$$

The mean envelope power of $x_L(t)$ is defined as

$$\frac{1}{T_s}\int_n^{(n+1)T_s} |x_L(t)|^2 dt = M.$$

and the peak envelope power of $x_L(t)$ is defined as

$$\max_t |x_L(t)|^2.$$

For the sequence $\{X_n(q)\}$ of independent data, the peak envelope power occurs when $\{X_n(q)\}$ are all in-phase at time $t = 0$, yielding

$$\max_t |x_L(t)|^2 = M^2$$

Hence, the peak-to-mean-envelope-power-ratio (PMEPR) of MCM with random data is

$$\max_t |x_L(t)|^2 / \left\{ \frac{1}{T_s}\int_n^{(n+1)T_s} |x_L(t)|^2 dt \right\} = M$$

which increases linearly with the number of carriers. However, this is very undesirable for power efficient and linear amplification, as is explained in Chapter 3. The block channel coding schemes proposed in the work of Ochiai [35, 36] and Davis [39] restrict $\{X_n(q)\}$ as a codeword with which $R_X(m)$ in (2.50) has small values, resulting in smaller PMEPR. Yet, at present, this scheme is only applicable for a small number of carriers because of the decreasing code rate and error correction property that accompanies increasing M [39]. In this thesis, the techniques of reducing PMEPR (including the block coding schemes) are not considered. This is not only because the present block coding schemes is immature, but also to understand, in fundamental, the nonlinear effects on the conventional multicarrier communication systems when no techniques are applied. Nonetheless, we do consider techniques, as introduced in Chapter 4, for reducing power consumption, even operating in a linear region with very high PMEPR signals.

2.3.2 Multi-User Communication Systems: MC-CDMA

Multi-User Communications

In multi-user communications, multiple users access a common channel to transmit information to the receiver. Multiple access can be achieved in several different ways. The most commonly used access schemes are time division multiple access (TDMA), frequency division multiple access (FDMA), and code division multiple access (CDMA). In TDMA each user is exclusively allocated particular time slots (subintervals) and in FDMA each user is allocated frequency slots (subbands), respectively. In CDMA, all the users share the entire bandwidth and can transmit signals at any time, but their signals are distinguished by a signature code (unique code sequence) assigned to each user.

The CDMA is a form of spread spectrum (SS) where the transmission bandwidth (W) is much larger than the data rate (R_b). The signature code (spreading code) is used to both spread the signal bandwidth at the transmitter and despread the signal at the receiver. The despreading process not only helps distinguish user signals but also suppresses interference, such as multipath and jamming.

In SS systems, the data signal of user k, denoted by $d_k(t) = \sum_{j=-\infty}^{\infty} d_k^{(j)} p_{T_s}(t - jT_s)$ where $d_k^{(j)} \in \{\pm 1\}$, is multiplied by a spreading code $a_k(t) = \sum_{j=-\infty}^{\infty} \sum_{i=0}^{N-1} a_k^{(i)} p_{T_c}(t - iT_c - jT_s)$ where the chip sequence $\{a_k^{(i)}\} \in \{\pm 1\}$. The ratio of the data symbol duration T_s to the chip duration T_c is the spreading gain of the system and is denoted by

$$N = T_s/T_c \geq 1. \tag{2.51}$$

It is desirable for a spreading code to appear random to users other than the intended user. In practice, a pseudo-random spreading code is used for the convenience of both generation and synchronization by the receiver: for the intended user the signal is deterministic and periodic, whereas it appears to have the statistical properties of sampled white noise for the unintended user [77, 78]. Pseudo-random codes such as maximal-length, orthogonal, Gold, and Kasami code, exhibit different characteristics in terms of code length, auto and cross correlation properties. Hence, the performance of SS systems will be affected by the choice of code. However, in order to avoid

discrepancies in performance with a specific code, in this thesis we elected to work with the average performance using a random spreading code. In other words, $a_k^{(i)} \in \{\pm 1\}$ is modeled as an iid random variable with equal probabilities.

MC-CDMA System

So far, we have reviewed the fundamental principles of OFDM and SS modulation, as well as CDMA. In this subsection, we describe the basic system model for MC-CDMA considered in this thesis. Different types of MC-CDMA can be found in [79, 80]. The MC-CDMA considered here has M subcarriers, and each subcarrier is binary phase shift keying (BPSK) modulated. The data stream of the q-th carrier of the k-th user is denoted by

$$d_{k,q}(t) = \sum_{j=-\infty}^{\infty} d_{k,q}^{(j)} p_{T_s}(t - jT_s) \tag{2.52}$$

where the data sequence $\{d_{k,q}^{(j)} \in \{\pm 1\}\}_{j=-\infty}^{\infty}$ is a sequence of iid data symbols (perfectly interleaved code symbols for coded systems) with equal probability. The BPSK modulated signal on the q-th carrier is then multiplied by a random spreading code

$$a_{k,q}(t) = \sum_{n=-\infty}^{\infty} \sum_{i=0}^{N-1} a_{k,q}^{(i)} p_{T_c}(t - iT_c - nT_s) \tag{2.53}$$

where the chip sequence $\{a_{k,q}^{(i)} \in \{\pm 1\}\}_{i=0}^{N-1}$ is a sequence of iid random variables with equal probabilities. Each spreading code has a chip duration of

$$T_c = T_s/N = MT_bR_c/N \tag{2.54}$$

where N is the spreading gain of the system, R_c is the code rate in information bits per coded bit, and $T_b = R_b^{-1}$ is the information bit duration before channel encoding. Hence, (coded) MC-CDMA signals have the form

$$x_k(t) = \sqrt{2P_k} \sum_{n=-\infty}^{\infty} \sum_{q=0}^{M-1} d_{k,q}(t) a_{k,q}(t) \cos\{(w_c + w_q)t + \theta_{k,q}\} \tag{2.55}$$

where P_k is the power per carrier of the k-th user, w_c is the carrier frequency and $\theta_{k,q}$ is an iid random variable uniformly distributed over $[0, 2\pi)$. The separation between

q-th carrier frequency and center frequency w_c is denoted by $w_q = 2\pi q/T_c$. Note that the carrier separation is a multiple of $1/T_c$ (not $1/T_s$) in order to maintain the orthogonality between each carrier.

System Bandwidth and Design Consideration of MC-CDMA.

If we define the signal bandwidth as a null-to-null bandwidth, each subcarrier of the MC-CDMA system has a bandwidth of $2/T_c$. Thus, the overall system bandwidth with M carriers becomes

$$W = \frac{M+1}{2}\frac{2}{T_c} = \frac{M+1}{T_c}. \tag{2.56}$$

For a given bandwidth W, code rate R_c, and data rate R_b, the spreading gain factor

$$N = \frac{T_s}{T_c} = \frac{MT_bR_c}{T_c} = \frac{M}{M+1}\frac{WR_c}{R_b}. \tag{2.57}$$

With a multi-carrier system, the chip duration T_c is longer than the chip duration ($T_{c,1}$) of a single carrier systems by a factor of

$$\frac{T_c}{T_{c,1}} = \frac{M+1}{2} \tag{2.58}$$

from the following relationship

$$W = \frac{2}{T_{c,1}} = \frac{M+1}{2}\frac{2}{T_c}.$$

In addition, the spreading gain of a multicarrier signal is approximately double that (N_1) of a single carrier system when M is large, since

$$N_1 = \frac{1}{2}\frac{WR_c}{R_b} = \frac{M+1}{2M}N. \tag{2.59}$$

Since we want the multipath fading for each modulated carrier to be flat, the bandwidth of each carrier needs to be smaller than the coherence bandwidth B_c. Thus,

$$\frac{2}{T_c} \leq B_c = \frac{1}{T_m}.$$

Multiplying the above equation by $(M+1)/2$ yields,

$$W = \frac{M+1}{2}\frac{2}{T_c} \leq \frac{M+1}{2}\frac{1}{T_m}.$$

Table 2.1: The minimum required M for flat fading

GSM Model (W Hz)	Rural	Urban	Hilly
T_m (μ sec)	0.5	5	17
min$\{M\}$ (1MHz, 4MHz)	1, 3	9, 39	33, 135

As a result, for a given bandwidth W and delay spread T_m, the required M to insure flat fading for each carrier is

$$M \geq \lceil 2WT_m \rceil - 1. \tag{2.60}$$

where $\lceil x \rceil$ denotes the largest integer smaller than $x+1$. Table 2.1 lists the minimum M, required when W is 1 Mhz and 4 Mhz, with the GSM-recommended multipath model [81]. In the GSM-recommended model, the delay spread is obtained for typical rural, urban, and hilly areas. In the hilly areas, the delay spread is relatively large, requiring larger M than other areas.

Cellular Radio Systems

The typical cellular radio systems consist of a collection of nearly disjointed cells with a base station located at the center of each cell as shown in Figure 2.9. In this thesis, however, we confine our research to a single cell system, only one base station supporting multiple users as shown in Figure 2.10. In addition, we only consider the communication link from mobile user to base station, which is commonly named as a reverse link. The reverse link is not only generally considered a performance limiting link but also a power limited link because of the power consumption of the handsets.

Unlike the forward link (communication from base to mobiles), in the reverse link it is a difficult task for a base station to control (synchronize) the received data bit starting time of all the users. Even in those cases where all users transmit signals simultaneously, the received signals have different delays when the distance of the users to the base station differs. Due to this condition, the reverse link is usually asynchronous. Therefore, in this thesis, a random delay is added to the starting bit time of each user. Each delay is modeled as an iid uniform random variable distributed

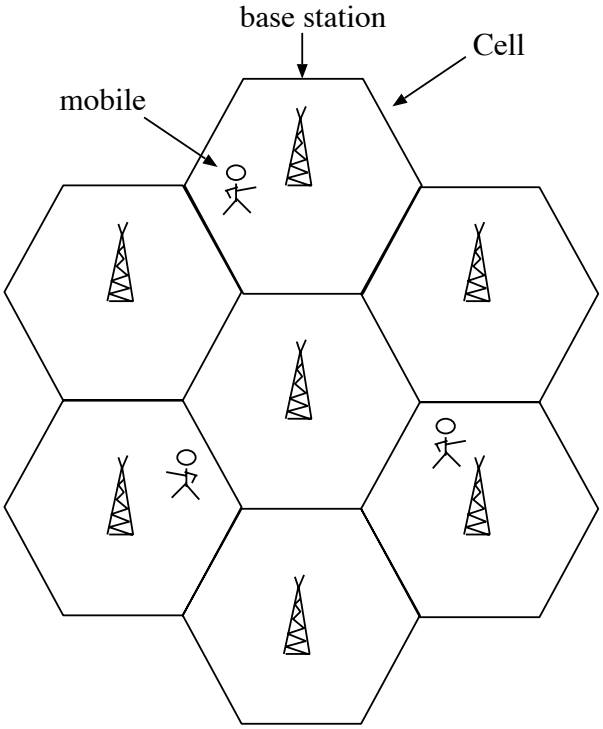

Figure 2.9: Cellular radio environments.

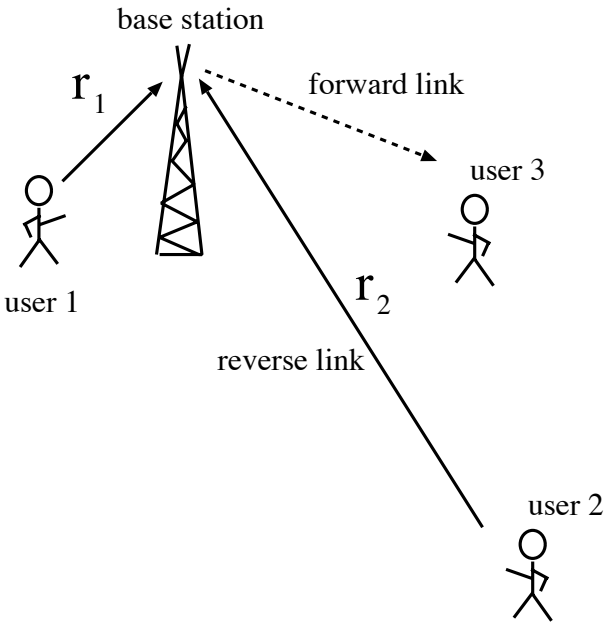

Figure 2.10: Single cell systems.

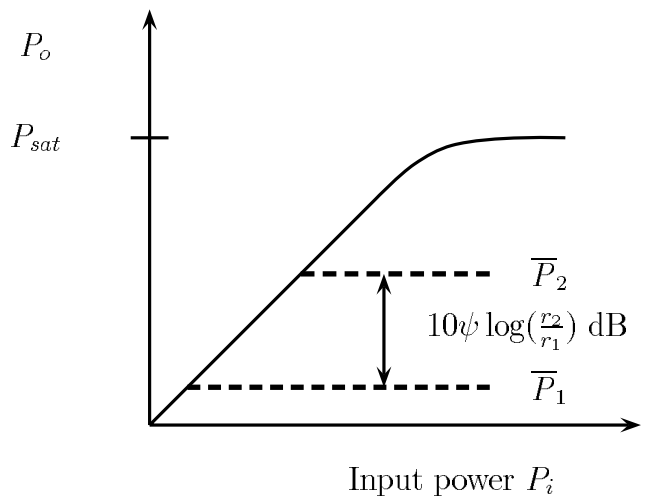

Figure 2.11: Amplifier output power of users.

over one symbol duration ($[0, T_s]$).

The variations in distances of the users from the base can provide quite different multipath fading environments to the users. In this thesis, it is assumed that each user undergoes independent fading. Also, the propagation loss causes variations of the average received power depending on user distances. The signal power of users near the base can interfere significantly with signals from more distant users, degrading overall cell performance. This is known as 'near-far effect'. Power control mitigates 'near-far effect' by keeping all the average received power at the base station at the same level regardless of their locations [58]. In this thesis, we assume perfect power control, that is, the average received signal powers from users are the same. Nonetheless, note that instantaneous received powers may vary because of the multipath fading.

The conventional use of power control in a multi-user system raises very important novel issues regarding amplifier power consumption and nonlinear effects. In the case of perfect power control with a propagation loss proportional to the distance to the ψ-th power, if user 2 (at distance r_2 from the base), in Figure 2.10, is transmitting the average output power $\overline{P}_2$, the average output power $\overline{P}_1$ of user 1 (r_1 from the base) should be smaller than $\overline{P}_2$ by a factor of

$$\frac{\overline{P}_2}{\overline{P}_1} = \left(\frac{r_2}{r_1}\right)^{\psi}$$

as shown in Figure 2.11. In other words, user 2 is operating closer to saturation than user 1. Also, if nonconstant envelope modulated signals are used, then user 1 will undergo not only linear interference from user 2, but also nonlinear interference (IMD products). As mentioned in Chapter 1, this raises two important questions. The first question is how user location, which determines the degree of nonlinearity, affects the desired user's BER. The second question is how we find the sets of nonlinearities which will ensure minimum power consumption for all users in a given cell. Chapter 6 will develop optimization and analytical methods to understand these issues.

CHAPTER 3

Performance Measures for Power Optimization of Communication Systems

3.1 Introduction

The need for low power consumption is well recognized in current and future mobile personal communications. Battery life now becomes one of the most important factors determining the size and weight of portable terminals. Hence, prolonging battery life or efficient usage of a battery becomes an important goal in wireless communications.

Conventionally, this goal of minimizing power consumption has been achieved by using power efficient transmitter amplifiers and by reducing the required average transmitted power for a given transmission reliability. The latter is achieved by using powerful channel coding schemes [82] whereas the former is accomplished by using power efficient nonlinear amplifiers with constant envelope modulation schemes, such as quadrature phase shift keying (QPSK) and minimum shift keying (MSK). With constant envelope modulation schemes, a transmitter power amplifier can operate in the nonlinear saturation region, where the efficiency of the power amplifier is largest, without distorting the modulated signal waveform.

Now, nonconstant envelope modulation schemes, which provide greater bandwidth efficiency, are preferred: such as pulse shaped QPSK, quadrature amplitude modulation (QAM) and OFDM. The larger bandwidth efficiency can support higher data

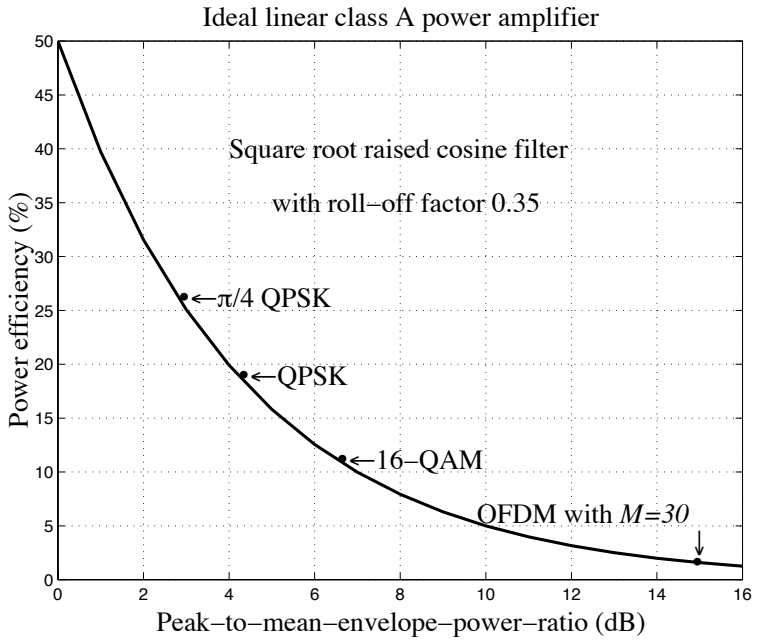

Figure 3.1: Power efficiency versus PMEPR for different modulation schemes.

transmission with less adjacent channel interference.

However, when a nonconstant envelope modulation is passed through a nonlinearity, in-band and adjacent channel interference is created. For linear amplification, the power efficiency of conventional amplifier (class A) is an inverse linear function of the peak-to-mean-envelope-power ratio (PMEPR) as shown in Figure 3.1 (see Appendix A). As a result, high PMEPR modulation schemes waste a great amount of available power for linear amplification, thus allowing a certain degree of nonlinear amplification, even for nonconstant envelope signals.

To quantify nonlinear effects or optimize power consumption, several performance measures are currently being used. To quantify the out-of-band interference from the nonlinearity, adjacent channel power ratio (ACPR) is often employed. It will also be employed in this thesis as well. When the in-band interference from the nonlinearity is a major concern, authors of recent papers [40, 49, 50, 41, 51, 52] use total degradation (TD) as an objective function for finding an optimum driving level (or optimum output backoff) of the amplifier. However, the justification for this function has remained intuitive, and, as shown in this chapter, the conventional objective function, TD, is only applicable when quantifying system power consumption with fixed dc bias

amplifiers where the dc power is constant[1].

In this chapter, we introduce a more general objective function, total dc power degradation (TDD), to quantify and optimize power consumption of the systems employing nonlinear amplifiers.

3.2 Performance Measures

The intuitive justification used in conventional TD can not tell us the underlying mechanism of the optimization process, nor the type of the amplifier that can be optimized. In short, it is not clear what is really being optimized. In this section, after a brief review of the intuitive justification behind TD, we will derive a more general objective function, TDD, which can accommodate non-fixed dc bias amplifiers. It will be shown that TD is in essence a special case of TDD when the amplifier dc power is constant.

Second, we review the validity of the assumptions made for the proposed function TDD. In doing so, we introduce generalized TDD (GTDD), which is a modified TDD, to obtain more accurate results when the assumptions are not practical or when system power consumption with different amplifiers needs to be compared. It is very important to note that the main role of TD or TDD is to find an optimum driving level for a given amplifier, and can not be used alone to compare system power consumption with different amplifiers.

Finally, we close this section with a discussion of the performance measure for out-of-band interference, ACPR.

3.2.1 Conventional Objective Function, TD

The conventional definition of TD is as follows:

$$TD \;=\; OBO\ (\text{dB}) + \Delta_{E_b/N_0}(OBO)\ (\text{dB}) \tag{3.1}$$

[1]Technically, the fixed dc bias does not imply that dc power is constant for all input power range. However, throughout this thesis it is implicitly assumed that the dc power is constant for a fixed bias scheme, which is usually true for class A amplifiers.

where the amplifier outback off (OBO) is a ratio of the amplifier output saturation power to the average output power given by

$$OBO \;=\; P_{sat}/\overline{P_o}. \tag{3.2}$$

The smaller the OBO, the closer the average output power to the maximum available output power. In turn, the amplifier becomes more power efficient, but with drawback of more signal distortion for nonconstant envelope signals. This degradation, so called E_b/N_0 degradation, is denoted by

$$\Delta_{E_b/N_0}(OBO) \;=\; E_b/N_0(OBO)\ (\text{dB}) - E_b/N_0(linear)\ (\text{dB}) \tag{3.3}$$

where $E_b/N_0(OBO)$ is the required average received signal energy-per-bit-to-noise density ratio to meet a target BER (e.g., 10^{-4}) at a given OBO. This $E_b/N_0(OBO)$ is always greater than or equal to that with a linear amplifier ($E_b/N_0(linear)$).

The E_b/N_0 degradation can be reduced by operating the amplifier with a large backoff (linear region). However, operations with a large backoff increase the power consumption of the amplifier, and this loss is described by the OBO term in (3.1). Thus, we can expect an optimum OBO which yields the smallest loss from the sum of the two opposing terms in dB: signal distortion ($\Delta_{E_b/N_0}(OBO)$) and power loss of the amplifier (OBO). This is the intuitive justification of the concept of TD. However, in the next subsection, we indeed derive a more general objective function TDD.

3.2.2 Proposed Objective Function, TDD

The assumptions behind TDD with the amplifier setup in Figure 3.2 are as follows:

1) Amplifier gain (G = output power/input power) is high.

2) The dc power, $P_{dc}(t)$, has a maximum value of $P_{dc,m}$.

3) Saturation power is related to the maximum dc power,
by $P_{sat} = \alpha P_{dc,m}$, $(0 < \alpha \leq 1)$.

Assumption 1 comes from the fact that a transmitter power amplifier is usually a high gain amplifier. Since the amplifier gain is high, the input signal power is negligible, compared to the output power (which is less than dc power). We will re-examine this assumption in the next subsection.

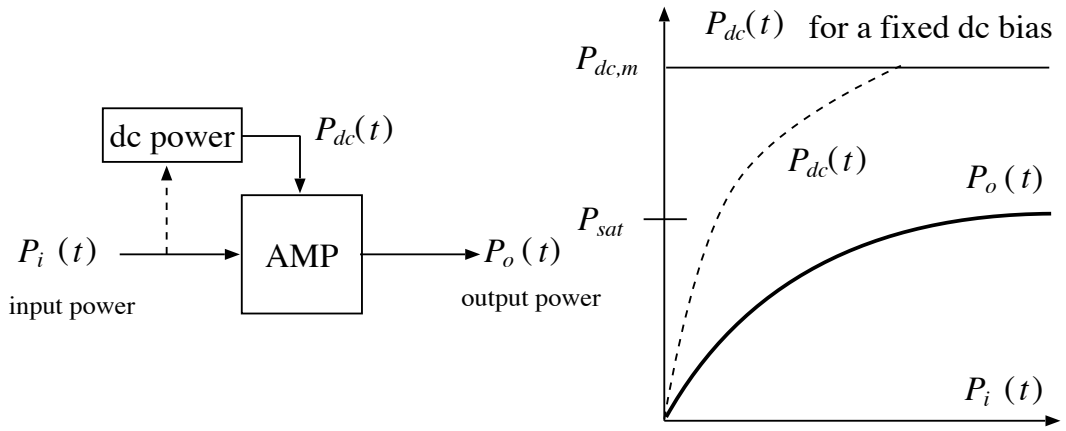

Figure 3.2: Amplifier characteristics.

Neglecting the input power, the only available power source is dc power $P_{dc}(t)$. Hence, the optimum system needs the smallest average dc power $\overline{P_{dc}}$ to meet the target BER. The digital signal processing power in the transmitter and receiver is not considered, because power consumption in digital circuits are determined by different factors, such as a clock speed and switching activity. Assumptions 2 and 3 come from the physics of the amplifier.

Now, we will show that minimizing TDD is equivalent to minimizing average dc power needed to meet target BER. In addition, we will show that TD is only valid for a fixed bias scheme, which will presented in the following derivation of TDD.

We first define the function

$$S(OBO) = P_{dc,m}/\overline{P_{dc}} \tag{3.4}$$

where $S(OBO) \geq 1$, and the equality holds for the fixed bias scheme for all OBOs. This quantity denotes either a dc power saving that can be achieved by using a dc bias controlled amplifier, or a power calculation correction term that is needed for any amplifier which has a non-fixed dc power.

Writing (3.4) in dB gives

$$P_{dc,m}(\text{dB}) \;\; = \;\; \overline{P_{dc}}\ (\text{dB}) + S(OBO)\ (\text{dB}). \tag{3.5}$$

If the channel propagation gain is g, the average received power, $\overline{P_r}$, equals g times the average output power of the amplifier, $\overline{P_o}$. Then, from the definition of OBO in

(3.2),

$$P_{sat} = OBO\overline{P_o}(OBO) = OBO\overline{P_r}(OBO)/g. \tag{3.6}$$

From assumption 3 ($P_{sat} = \alpha P_{dc,m}$), the above equation can be rewritten as

$$P_{dc,m}\ (\text{dB}) = \overline{P_r}(OBO)\ (\text{dB}) + OBO\ (\text{dB}) - \alpha g\ (\text{dB}). \tag{3.7}$$

From (3.5) and (3.7),

$$\overline{P_{dc}}(\text{dB}) = \overline{P_r}(OBO)\ (\text{dB}) + OBO\ (\text{dB}) - S(OBO)\ (\text{dB}) - \alpha g\ (\text{dB}). \tag{3.8}$$

Since α and g do not depend on OBO, the OBO which minimizes the term

$$\overline{P_r}(OBO)\ (\text{dB}) + OBO\ (\text{dB}) - S(OBO)\ (\text{dB}) \tag{3.9}$$

minimizes the required average dc power for a given required BER. This is equivalent to minimizing the following term,

$$\begin{aligned} TDD\ (\text{dB}) &= \overline{P_r}(OBO)\ (\text{dB}) + OBO\ (\text{dB}) - S(OBO)\ (\text{dB}) && (3.10)\\ &+ T_b/N_0\ (\text{dB}) - E_b/N_0(linear)\ (\text{dB}) \\ &= OBO\ (\text{dB}) - S(OBO)\ (\text{dB}) + \Delta_{E_b/N_0}(OBO)\ (\text{dB}) && (3.11) \end{aligned}$$

where $E_b/N_0(OBO) = \overline{P_r}(OBO)T_b/N_0$. This is because the information bit duration T_b, noise spectral density level N_0, and $E_b/N_0(linear)$ are independent of the amplifier nonlinearities (OBOs).

In summary,

$$TDD\ (\text{dB}) = OBO\ (\text{dB}) - S(OBO)\ (\text{dB}) + \Delta_{E_b/N_0}(OBO)\ (\text{dB}). \tag{3.12}$$

An optimum OBO to minimize $\overline{P}_{dc}$ also gives the minimum value of TDD. The first two terms in (3.12) represent the amplifier inefficiency and the last term denotes the receiver performance degradation from the nonlinear signal distortion. Only for fixed bias does TDD equal TD, since S(OBO) = 0 dB in this case. As can be seen, TD can not account for the dc power consumption accurately when dc power is not constant. Thus, TD should be used only with fixed dc bias amplifiers.

3.2.3 Notes on TDD and Its Generalization

In this subsection, we briefly discuss ways to modify TDD to consider input power and α in (3.8). The total available power source includes not only dc power also input power. Input power consumption can not be ignored when the amplifier gain (G) is small. Even when the gain of the amplifier is high in the linear region (high OBOs), the gain decreases as OBO becomes smaller. This is because the output power remains almost constant in the saturation region even with increased input power. Hence, when the G is small, the following quantity, fractional input power FI (dB), needs to be added to TDD (dB) in (3.12):

$$\begin{aligned} FI(OBO)\ (\text{dB}) &= 10\log\left(1+\frac{\overline{P_{in}}(OBO)}{\overline{P_{dc}}(OBO)}\right) \\ &= 10\log\left(1+(\frac{\alpha}{\overline{G}(OBO)})(\frac{S(OBO)}{OBO})\right) \end{aligned} \tag{3.13}$$

and the average amplifier gain is denoted by $\overline{G}(OBO) = \overline{P_o}(OBO)/\overline{P_i}(OBO)$ for a given OBO. In Chapter 4, we will show quantitatively when this fractional input power has to be added. Moreover, it will be shown in Chapter 4 that the term FI can be safely ignored when the G in linear region is larger than 20 dB (which is usually true in practice) even for low OBOs.

In order to quantify power consumption with different amplifiers, α should be included, since different amplifiers have different α's.

Thus, when more accurate device level system optimization is needed, a more general objective function, generalized TDD (GTDD),

$$GTDD\ (\text{dB}) = TDD(OBO)\ (\text{dB}) + FI(OBO)\ (\text{dB}) - \alpha\ (\text{dB}) \tag{3.14}$$

can be used. For a higher level system optimization, TDD has some advantages over GTDD in its simple expression and in its independence of absolute amplifier parameters such as α or $\overline{G}$.

3.2.4 Out-of-Band Interference

The out-of-band interference power is usually quantified by the ACPR, which is defined as a ratio of the out-of-band signal power in the adjacent channel to the

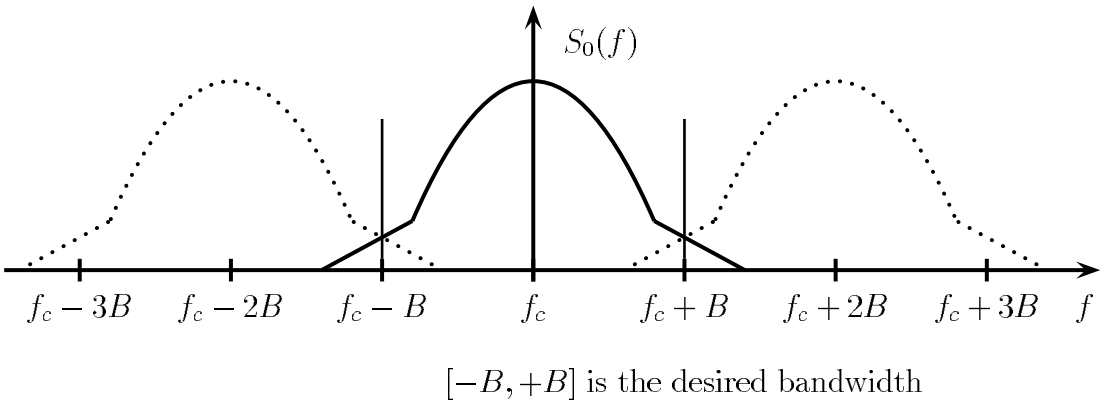

Figure 3.3: PSD of the desired signal and adjacent channel signals.

in-band signal power, given as

$$\text{ACPR}(B) = \frac{\int_{f_c-3B}^{f_c-B} S_o(f)\,df \;+ \int_{f_c+B}^{f_c+3B} S_o(f)\,df}{\int_{f_c-B}^{f_c+B} S_o(f)\,df} \tag{3.15}$$

where $[-B, B]$ is the desired in-band, and $S_o(f)$ is the power spectral density of the amplified signal $s_o(t)$. A slightly different version of ACPR can be found in the works of Kenney [4] and Sevic [83]. However, all the definitions of ACPR share the fact that they indicate more spectral regrowth for large ACPR.

3.3 Conclusion

In this chapter, we have proposed a more general objective function TDD for optimizing communication system power consumption with nonlinear amplifiers. We have shown that the conventional objective function TD is only useful when optimizing system power consumption with fixed dc bias amplifiers. We also carefully re-examined the basic assumptions behind TDD, and provided GTDD to accommodate input power and α which are neglected in TDD. Finally, we presented the ACPR that will be used in the rest of the thesis. In the following chapter, with the proposed measure TDD, a methodology is presented to optimize power consumption for a general class of amplifiers, including the adaptive dc bias controlled amplifier.

CHAPTER 4

Power Optimization of OFDM with dc Bias Controlled Amplifiers

4.1 Introduction

In the last chapter, an objective function for optimizing power consumption of communication systems with nonlinear power amplifiers was proposed. In this chapter, with this objective function, a methodology is presented to optimize power consumption with a general class of amplifiers, including recently proposed adaptive dc bias controlled amplifiers [44]. These techniques [44, 45, 46, 47, 48] for adaptively controlling the dc bias of a power amplifier are of considerable interest because of their high efficiency and linearity. For communication systems, single carrier pulse shaped quadrature phase shift keying (QPSK) and orthogonal frequency division multiplexing (OFDM) modulation schemes are considered because of the difference in their envelope variations: QPSK has relatively smaller envelope variations whereas OFDM has large variations.

This chapter is organized as follows. Section 4.2 presents the communication system model. In addition, this section discusses the basic principles and main parameters of dc bias controlled amplifiers. In particular, we consider three different types of dc bias controlled amplifiers: (1) fixed, (2) single, and (3) dual dc bias controlled amplifiers. Section 4.3 provides a simplified asymptotic analysis of the amplifier inefficiency term to demonstrate potential power reduction from the bias controlled

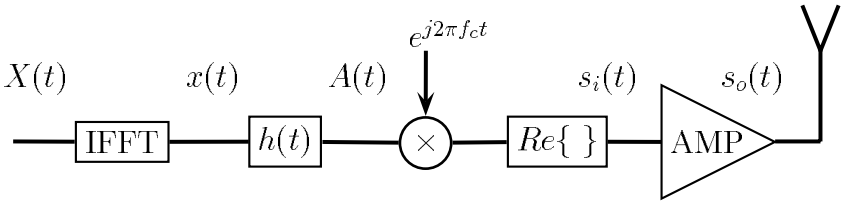

Figure 4.1: OFDM transmitter.

schemes. Section 4.4 shows the bit error rate (BER) and adjacent channel power ratio (ACPR) obtained through computer simulation, which quantify the nonlinear effects of the amplifier. We then quantify and compare power consumption with the bias schemes. Section 4.5 summarizes the main results.

4.2 System Model

4.2.1 Modulation

A block diagram of the transmitter is shown in Figure 4.1. As explained in Section 2.3.1, the data stream $X(t)$ is spilt into M streams (serial to parallel process), each of which is transmitted on a separate carrier. Each carrier is modulated with QPSK. This modulation scheme is implemented by the inverse fast Fourier transform technique (IFFT) and operates block-wise every $T_s = MT$ seconds. That is M symbols are transmitted every T_s, and each symbol constitutes 2 information bits.

The output of the IFFT is then parallel to serial processed to yield

$$x(t) = \sum_{l=0}^{M-1} x_{c,l}\, \delta(t - lT) \text{ for } t \in [0, MT] \tag{4.1}$$

where $\delta(t)$ is the Dirac delta function, and

$$x_{c,l} = \frac{1}{\sqrt{M}} \sum_{k=0}^{M-1} \{X_i(k) + jX_q(k)\} e^{\frac{j2\pi lk}{M}} \tag{4.2}$$

where $X_i(k) \in \{-1, 1\}$ and $X_q(k) \in \{-1, 1\}$ are information bits. In a single carrier QPSK transmitter, M is simply set to 1 in (4.1) and (4.2). As can be seen in (4.2), the signal distribution becomes complex Gaussian (from the central limit theorem) as M increases, resulting in higher envelope variations.

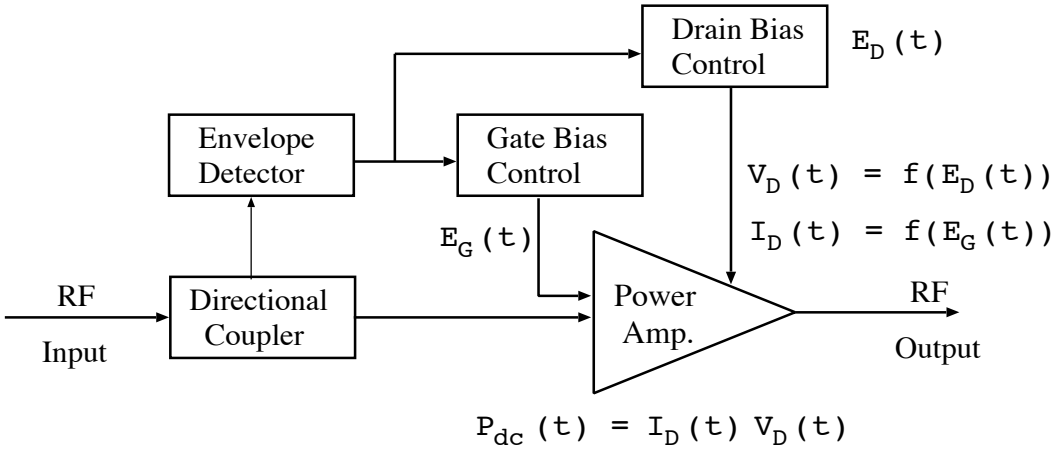

Figure 4.2: dc bias controlled amplifier.

Finally, the complex data stream $x(t)$ is low pass filtered by the square root raised cosine with roll-off factor β

$$h(t) = 8\beta \frac{\cos[(1/T + 2\beta)\pi t] + \sin[(1/T - 2\beta)\pi t](8\beta t)^{-1}}{(\pi\sqrt{T})[1 - (8\beta t)^2]} \tag{4.3}$$

generating the modulated signal

$$\begin{aligned} s_i(t) &= \mathrm{Re}\{A(t)e^{j2\pi f_c t}\} \\ &= V_i(t)\cos(2\pi f_c t + \theta(t)) \end{aligned} \tag{4.4}$$

where $A(t) = x(t) * h(t)$, $V_i(t) = |A(t)|$ is the envelope voltage of the signal, $\theta(t) = \angle A(t)$ is the phase, and f_c is the carrier frequency.

4.2.2 dc Bias Controlled Amplifiers

A dc bias controlled amplifier with time varying envelope signal is illustrated in Figure 4.2. The envelope of a sample of the input RF signal is detected, and is used to control the gate "dc" bias voltage $E_G(t)$ and the drain "dc" bias voltage $E_D(t)$. In a conventional fixed dc bias amplifier, bias voltages are all constant regardless of the input RF signal envelope. In a single dc bias control, $E_G(t)$ is dynamically controlled such that the "dc" bias current $I_D(t)$ is forced to be proportional to the signal envelope [48]. In dual, both $E_G(t)$ and $E_D(t)$ are controlled such that each "dc" bias current $I_D(t)$ and bias voltage $V_D(t)$ is forced to be proportional to the

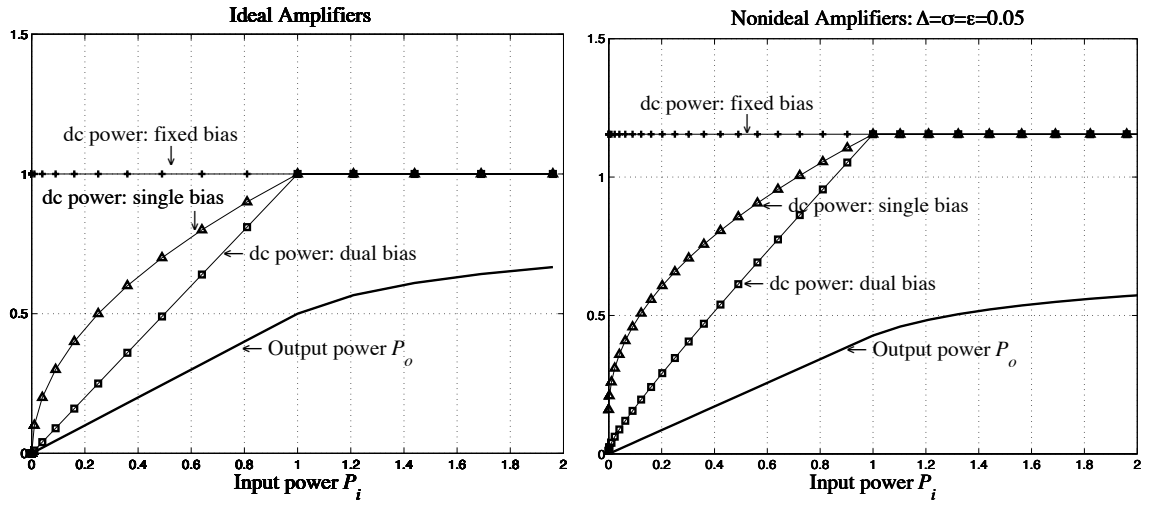

(a) (b)

Figure 4.3: Amplifier characteristics: (a) ideal, and (b) nonideal: $\Delta = \sigma = \epsilon = 0.05$.

signal envelope [44]. Hence, dc power $P_{dc}(t) = I_D(t)\,V_D(t)$ changes according to the envelope in both single and dual bias controlled amplifiers, whereas it is constant in the fixed bias controlled amplifiers. However, the considered bias schemes all have the same output power characteristics. It should be noted that output power $P_o(t)$ only depends on the input power and amplifier parameters, not on the bias schemes.

In the following subsection, analytical expression for the amplifier characteristics are listed. Also, transistor parameters, such as output knee voltage Δ, output conductance ϵ, and soft cut-off/pinch-off σ, are included in the amplifier model. The detailed physical meaning of the parameters are explained in Appendix A. But, essentially when the parameter values are not zeros, the result is that dc power consumption increases with a reduction of output power than in the ideal case (when all parameter values are zeros) as depicted in Figure 4.3.

We have included these nonideal parameters not only to make the amplifier model more realistic, but also to show how power consumption of different nonlinear amplifiers can be compared in terms of the modified TDD (i.e. GTDD). Again, we should note that the main role of TDD is to find an optimum driving level for a given amplifier. Moreover, the TDD should be modified to compare power consumption in

systems with different amplifiers. For example, different amplifiers can have different values for the nonideal parameters.

Amplifier Characteristics

As mentioned in Section 2.1.2, the amplifier model is a bandpass memoryless nonlinear model with no AM/PM. In this model, if the input to the amplifier is the modulated signal in (4.4), the output of the amplifier is expressed as

$$s_o(t) = V_o(t)\cos\{2\pi f_c t + \theta(t)\} \tag{4.5}$$

where the output envelope $V_o(t)$, which is a function of the input envelope $V_i(t)$, denotes AM/AM. The AM/AM, considered in this chapter, can be divided into two regions according to whether $V_i(t)$ being greater than $V_{i,m}$ or not. The value $V_{i,m}$ denotes the maximum sinusoid input envelope voltage that can be amplified linearly. For AM/AM of the linear region (i.e., $V_i(t) \le V_{i,m}$), we adopt the same AM/AM of Yang's model in Appendix A. The AM/AM of the saturation region (i.e., $V_i(t) \ge V_{i,m}$) is obtained by the Fourier series expansion (see (2.14) in Section 2.1.3) of the instantaneous voltage which is assumed to be constant as in the case of a soft limiter. Hence, the AM/AM considered in this chapter is

$$V_o(t) = \begin{cases} V_{o,m}\,\frac{V_i(t)}{V_{i,m}} & \text{for } V_i(t) \le V_{i,m} \\ \frac{2V_{o,m}}{\pi}[\frac{V_i(t)}{V_{i,m}}\,\text{asin}(\frac{V_{i,m}}{V_i(t)}) + \sqrt{1-(\frac{V_{i,m}}{V_i(t)})^2}] & \text{for } V_i(t) \ge V_{i,m}. \end{cases} \tag{4.6}$$

The value $V_{o,m}$ is the maximum sinusoid output envelope voltage that can be amplified linearly, given by

$$V_{o,m} = \sqrt{(1-\Delta)(1-\epsilon-\sigma+\epsilon\sigma\Delta)} \tag{4.7}$$

which depends on the transistor parameters.

The input and output signal power is related to the envelope voltage by

$$P_i(t) = V_i^2(t)/2 \qquad \text{and} \qquad P_o(t) = V_o^2(t)/2, \tag{4.8}$$

respectively. The amplifier gain (output power/input power) in the linear region, i.e., the linear amplifier gain, is denoted by

$$G_l = V_{o,m}^2/V_{i,m}^2. \tag{4.9}$$

Table 4.1: Parameters for different dc bias schemes

Bias scheme	$C_{V,0}$	$C_{I,0}$	$C_{V,1}$	$C_{I,1}$
Fixed bias	$1+\Delta$	$1+\epsilon+\sigma-\epsilon\sigma\Delta$	0	0
Single bias	$1+\Delta$	$\epsilon(1+\Delta)+2\sigma(1-\epsilon\Delta)$	0	$(1-\epsilon)(1-\epsilon\Delta)$
Dual bias	2Δ	$2\{\epsilon\Delta+\sigma(1-\epsilon\Delta)\}$	$1-\Delta$	$1+\epsilon-\sigma-2\epsilon\Delta+\epsilon\sigma\Delta$

For example, Figure 4.3 (a) is plotted with $V_{i,m}=\sqrt{2}$, $V_{o,m}=1$, and $G_l=1/2$.

The relationship between normalized dc power $P_{dc}(t)$ and normalized input voltage envelope

$$e(t) \;=\; V_i(t)/V_{i,m} \tag{4.10}$$

is as follows:

$$P_{dc}(t) \;=\; \begin{cases} (C_{V,0}+C_{V,1}e(t))(C_{I,0}+C_{I,1}e(t)) & \text{for } e(t)\le 1 \\ P_{dc,m} & \text{for } e(t)\ge 1 \end{cases} \tag{4.11}$$

$$P_{dc,m} \;=\; (1+\Delta)(1+\epsilon+\sigma-\epsilon\sigma\Delta). \tag{4.12}$$

The parameters $C_{V,0}$, $C_{V,1}$, $C_{I,0}$, and $C_{I,1}$ depend on the configuration of dc bias controlled schemes, and are listed in Table 4.1. The derivations of Table 4.1 are given in Appendix A. The dc power is a linear function of normalized input $e(t)$ for the single bias scheme and a quadratic function for the dual bias scheme. If we rewrite the output power as a function of $e(t)$, we obtain

$$P_o(t) \;=\; \begin{cases} \frac{V_{o,m}^2}{2}\,e^2(t) & \text{for } e(t)\le 1 \\ \frac{2V_{o,m}^2}{\pi^2}[e(t)\,\mathrm{asin}(e(t))+\sqrt{1-e^2(t)}]^2 & \text{for } e(t)\ge 1. \end{cases} \tag{4.13}$$

The power output backoff (OBO) of the amplifier is defined as

$$\mathrm{OBO}=\frac{P_{sat}}{\overline{P_o}}=\frac{V_{sat}^2}{\overline{V_o^2}} \tag{4.14}$$

which is the ratio of saturation power P_{sat} to the average output power $\overline{P_o}$. The averagings (over-bars) are done over the input envelope variations, i.e., over $e(t)$. The saturation voltage (V_{sat}) is set to be the asymptotic output voltage, i.e., $\max V_o(t)=$

$\lim_{e(t)\to\infty} V_o(t) = \frac{4}{\pi}V_{o,m}$. For a given saturation power, smaller OBO gives larger average output power (resulting in more power efficiency); however, it gives more signal distortion (resulting in more required received power for a given BER) for nonconstant envelope signals. The optimum OBO which minimizes overall power consumption is obtained, with the proposed measure TDD, for each bias scheme in Section 4.4.

4.3 Asymptotic Analysis of Amplifier Inefficiency Term OBO (dB) - S(OBO) (dB)

In this subsection, we discuss the asymptotic behavior of OBO (dB) − S(OBO) (dB) when OBO is large, with the three ideal bias schemes ($\epsilon = \Delta = \sigma = 0$). From this simplified asymptotic analysis, we will gain some insight into TDD and show the potential power saving that can be realized with dc bias controlled amplifiers.

Since the output power increases monotonically with the input power in our amplifier model, a larger OBO means a smaller normalized input power, i.e., $\overline{e^2} \ll 1$. In this case, the probability that $e(t)$ is greater than one is small. Let's assume

$$\overline{e} \approx \int_0^1 e f_e(e)\, de \quad \text{and} \quad \overline{e^2} \approx \int_0^1 e^2 f_e(e)\, de \tag{4.15}$$

where $f_e(e)$ is the probability density function of $e(t)$. From this, when OBO is large,

$$\text{OBO} = \frac{V_{sat}^2}{\overline{V_o^2}} = \frac{(4/\pi)^2 V_{o,m}^2}{V_{o,m}^2 \int_0^1 e^2 f_e(e)\, de + \int_1^\infty V_o^2(e) f_e(e)\, de} \approx \frac{(4/\pi)^2}{\overline{e^2}} \tag{4.16}$$

and, similarly,

$$\text{S(OBO)} = P_{dc,m}/\overline{P_{dc}} \approx \begin{cases} 1 & \text{for fixed bias} \\ 1/\overline{e} & \text{for single bias} \\ 1/\overline{e^2} & \text{for dual bias.} \end{cases} \tag{4.17}$$

Hence, when OBO is large, the power amplifier inefficiency term,

$$\text{OBO (dB)} - \text{S(OBO) (dB)} \approx \begin{cases} \text{OBO (dB)} & \text{for fixed bias} \\ 20\log(4/\pi) + 10\log(\overline{e}/\overline{e^2}) & \text{for single bias} \\ 20\log(4/\pi) \approx 2.1 \text{ (dB)} & \text{for dual bias.} \end{cases} \tag{4.18}$$

If we assume that $\Delta_{E_b/N_0}(\text{OBO}) \approx 0$ dB for large OBO, the above results imply that the TDD can be finite even for an infinite OBO in the ideal dual bias scheme, whereas it can be infinite for the fixed bias amplifier. For the ideal dual bias, when OBO is large, OBO (dB) $-$ S(OBO) (dB) has a constant value of 2.1 dB, regardless of the statistics of the modulated signal envelope. The OBO (dB) $-$ S(OBO) term with the ideal single bias scheme depends on the envelope statistics.

Since the envelope of the OFDM signal (assuming the number of subcarriers is larger than 10) can be well approximated by the Rayleigh random variable, $\overline{e} = \sqrt{\pi\overline{e^2}}/2$ in this case. Thus, from (4.16) and (4.18), for the ideal single bias with OFDM,

$$\text{OBO (dB)} - \text{S(OBO) (dB)} \approx 5\log(4/\pi) + 1/2 \text{ OBO (dB)}. \tag{4.19}$$

The ideal single bias scheme reduces the slope of OBO (dB) by a factor of half. These observations can help designing power efficient amplifiers jointly with modulation schemes, since different modulation schemes have different envelope statistics. In addition, these results are verified with simulation in the following section.

4.4 Simulation Results and Discussions

A Monte Carlo method is used in the simulation. The signals are oversampled at a rate of 16 (16 samples are taken in each T seconds) for the BER calculation and with a rate of 32 for the ACPR calculation. For accurate results, a higher sampling rate is needed for the ACPR calculation than for the BER. The square root raised cosine filter with roll-off factor β of 0.35 is used for the transmitter and receiver filters (currently standard for North American TDMA Digital Cellular (IS-54/136) [71]). The considered filter has a finite impulse length of $96T_s$, which is enough for ACPR calculation down to -50 dB at $BT = 2.0$. For the OFDM systems to be considered in this chapter, the number of carriers, $M = 64$.

The modulated signal, $s_i(t)$, is first amplified and then corrupted by additive white Gaussian noise (AWGN) with two sided power spectral density $N_0/2$. The received signal is filtered with square root raised cosine filter (a filter matched to the signal before the nonlinearities). Due to the nonlinearity, however, the matched

filter receiver is not anymore the optimum receiver. The decision on the data is made after DFT of the output samples of the matched filter, where the demodulated data sequence is compared with the transmitted data sequence to calculate BER.

4.4.1 In-band distortion: TDD

Figures 4.4(a) and (b), show the BER of OFDM and QPSK, respectively, for different OBOs. As expected, the BER increases as the OBO becomes smaller, and for a BER of 10^{-4} for OFDM, the E_b/N_0 degradation is about 6.2 dB when OBO = 2 dB. However, E_b/N_0 degradation is very small for QPSK, due to its small envelope variations. It is important to note that the bias schemes and parameters of the amplifiers do not affect BER, since the bias schemes do not affect the output power and the nonideal parameters are normalized in the OBO.

Figure 4.5 shows the TDD for the three different ideal dc bias controlled amplifiers, when the target BER is 10^{-4} and the parameters ϵ, Δ, and σ are all set to zero. The solid lines in the plots are the power amplifier inefficiency terms OBO (dB) $-$ S(OBO) (dB) for each scheme, and the difference between the solid line and the curve for a given scheme is the E_b/N_0 degradation. Optimum OBOs of OFDM in Figure 4.5(a), which give the minimum values of the TDDs, are found to be 4, 5, and 8 dB for the ideal fixed, single, and dual dc bias scheme, respectively. For the ideal dual bias scheme, the increase in the TDD for OBO $>$ 8 dB is too small to be seen in the plot.

Optimum OBOs for QPSK in Figure 4.5(b) are all no larger than 0.5 dB for all three bias schemes. Hence, in terms of reducing dc power consumption, it is desirable to drive the amplifier hard for single carrier QPSK signal. However, there are two facts should be considered to taking this action. First, these low output backoffs increase spectral regrowth. When the out-of-band interference is a major concern, OBO must be increased. This issue will be discussed again at the end of this section, when we examine ACPR. Second, input power consumption, in these low OBOs, may not be negligible compared to TDD when an amplifier gain is not high enough.

This input power consumption of OFDM and QPSK is quantified in Table 4.2 and 4.3, respectively, by the fractional input power (FI) defined in (3.13). In order to illustrate worst case scenario, we consider the dual bias scheme (rather than the

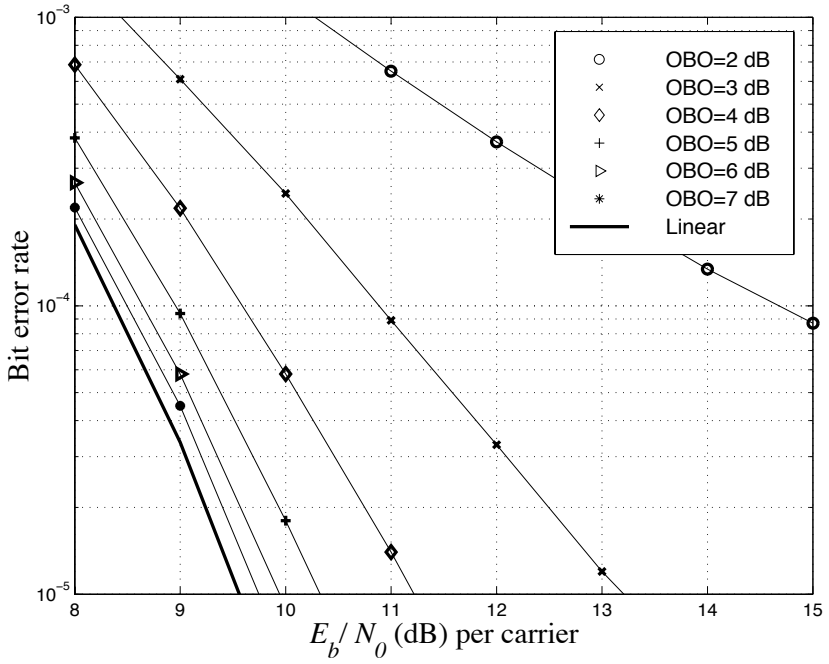

(a)

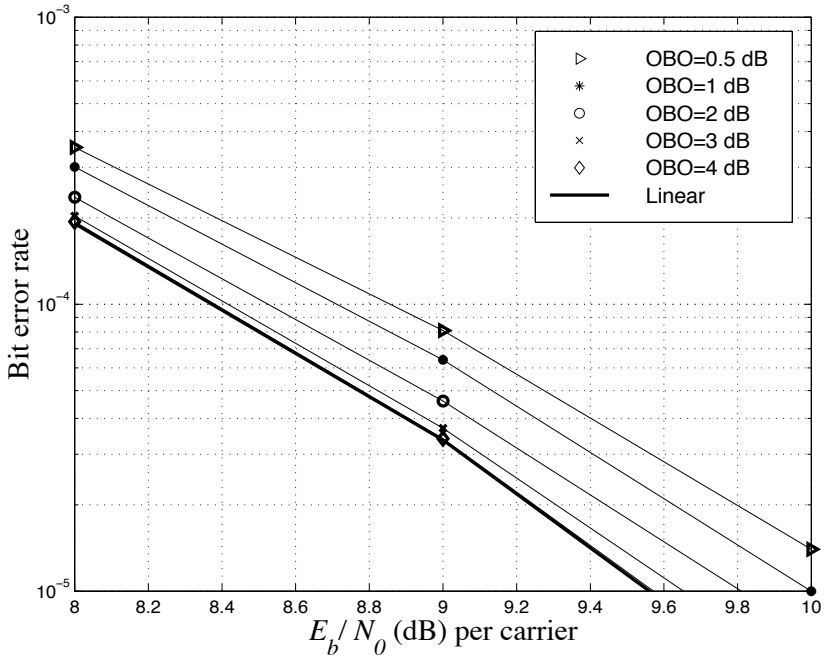

(b)

Figure 4.4: BER for different OBOs (dB): (a) OFDM and (b) QPSK.

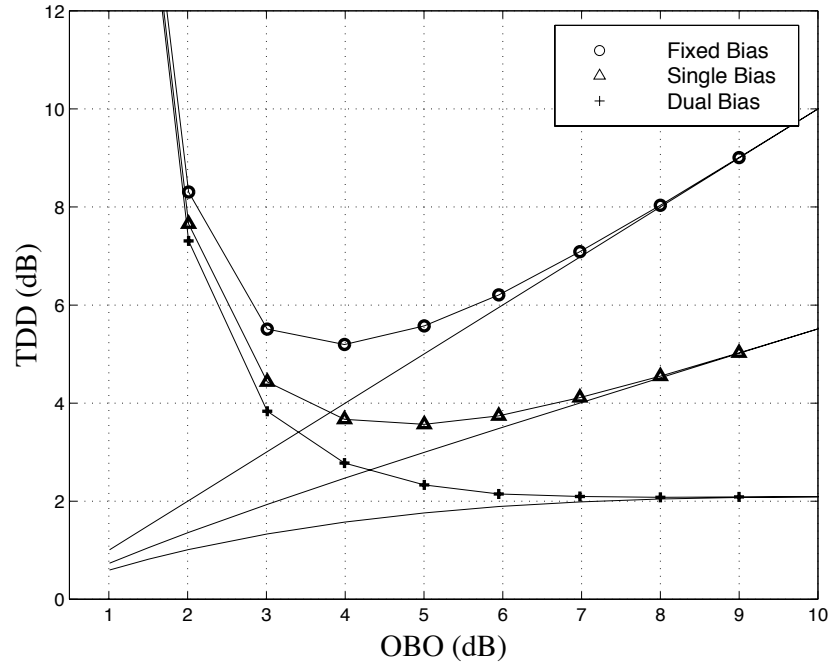

(a)

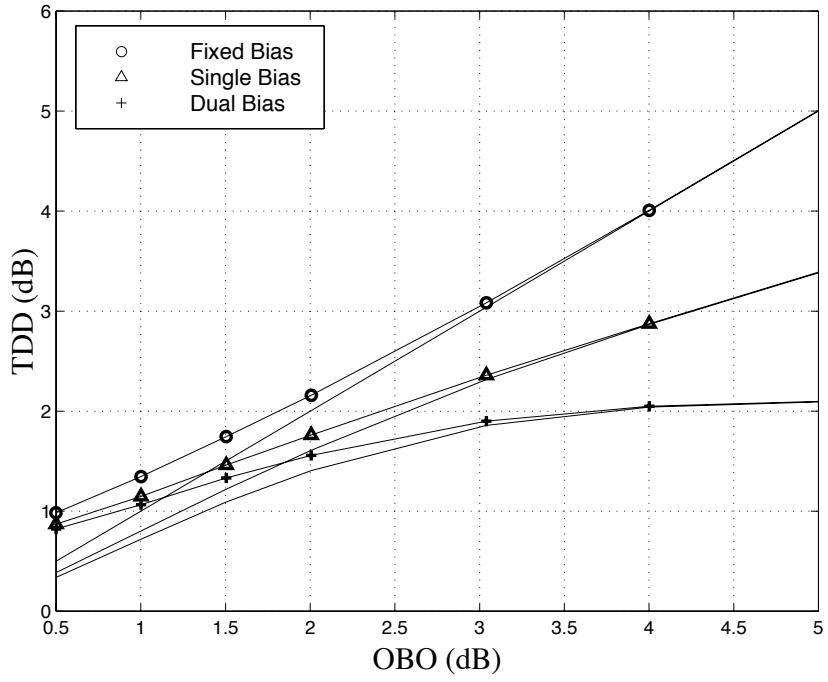

(b)

Figure 4.5: TDD (dB) for three different ideal dc bias schemes: (a) OFDM (b) QPSK.

fixed and single scheme) because for a given input power the FI of the dual bias is the largest among the dc bias schemes.

Table 4.2: Fractional input power, FI (dB) for different values of the OBO and G_l: OFDM with ideal dual bias

	OBO (dB)						
G_l (dB)	0.5	1	1.5	2	3	5	7
10	2.18	1.10	0.73	0.54	0.37	0.26	0.24
14	1.00	0.47	0.31	0.22	0.15	0.10	0.09
18	0.43	0.19	0.12	0.09	0.06	0.04	0.04
20	0.27	0.12	0.08	0.06	0.04	0.03	0.02
22	0.17	0.08	0.05	0.04	0.02	0.02	0.01

Table 4.3: Fractional input power, FI (dB) for different values of the OBO and G_l: QPSK with ideal dual bias

	OBO (dB)						
G_l (dB)	0.5	1	1.5	2	3	5	7
10	1.17	0.55	0.37	0.30	0.23	0.21	0.21
14	0.50	0.23	0.15	0.12	0.10	0.09	0.09
18	0.21	0.09	0.06	0.05	0.04	0.03	0.03
20	0.13	0.06	0.04	0.03	0.02	0.02	0.02
22	0.08	0.04	0.02	0.02	0.02	0.01	0.01

In Table 4.2, the values of FI with OFDM are relatively large compared to OBO when $G_l = 10$ dB and OBO is small. However, in these small OBO regions, since Δ_{E_b/N_0} degradation is large, the increase in FI (dB) does not affect the decision of the optimum OBO significantly. However, with QPSK in Table 4.3, the values of FI are not negligible compared to both OBO and Δ_{E_b/N_0} degradation when $G_l = 10$ dB and OBO is small. Hence, in this case, FI (dB) has to be added to TDD (dB) for finding the right optimum OBO, as shown in Figure 4.6. As G_l and OBO become

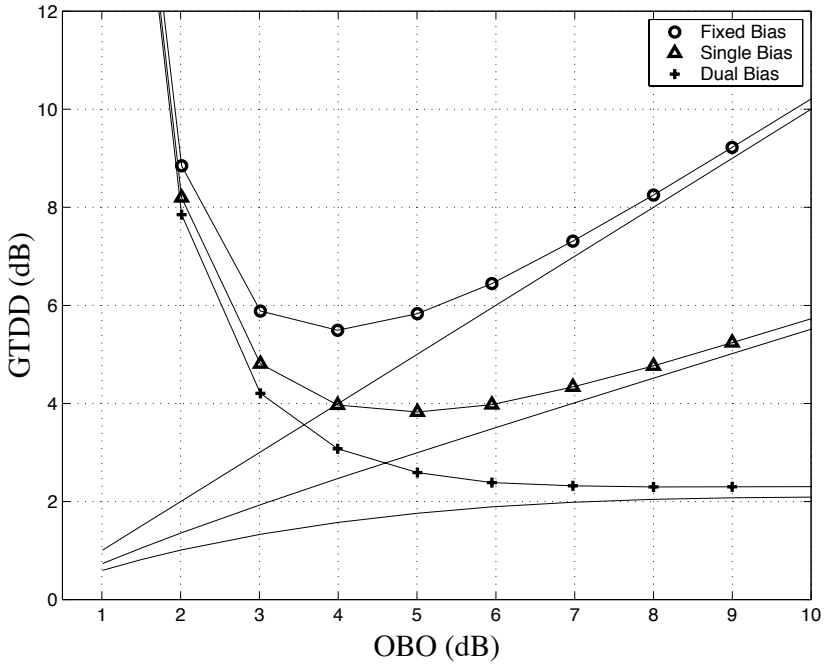

(a)

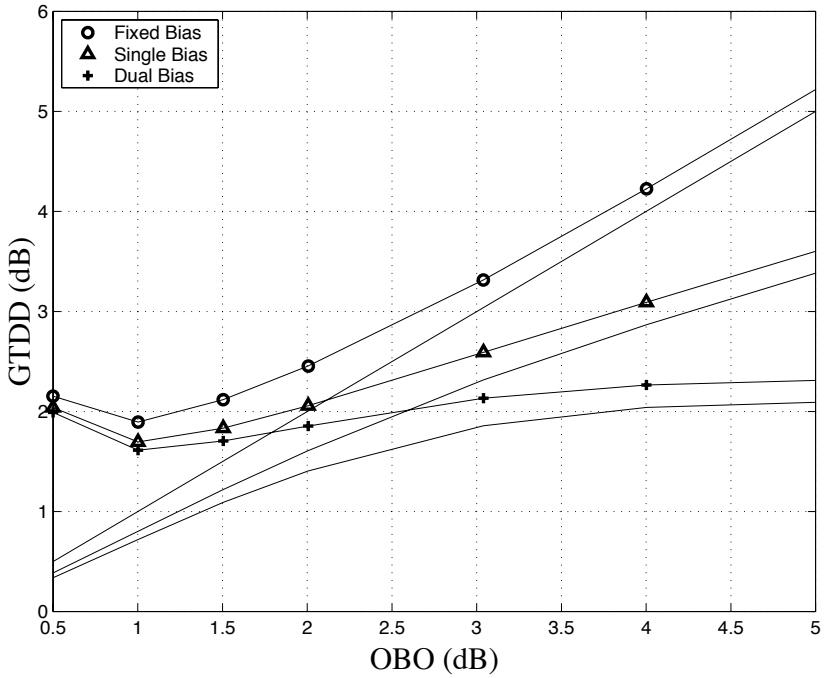

(b)

Figure 4.6: GTDD (dB) (including input power consumption) for three different ideal dc bias schemes: (a) OFDM (b) QPSK.

large, the magnitude and variation of FI become small in both OFDM and QPSK. When the linear gain G_l is more than 20 dB, the effects of the input power can be safely ignored even for low OBOs.

Figures 4.7(a) and (b), show plots of the power amplifier inefficiency term OBO (dB) − S(OBO) (dB) for OFDM and QPSK, respectively, for 3 different parameters: $\epsilon = \Delta = \sigma = 0$, $\epsilon = \Delta = \sigma = 5\%$, and $\epsilon = \Delta = \sigma = 10\%$. The power loss increases as the parameter values increase. In the OBO range of 2 dB – 4 dB, the power inefficiency term OBO (dB) − S(OBO) (dB) of QPSK is about 0.5 dB higher than that of OFDM. This difference becomes smaller as OBO increases. The inefficiency term in QPSK and OFDM both have about 2.1 dB as given in (4.18) for the ideal dual bias scheme.

It is important to note that, to compare power consumption of these nine different amplifiers (three different bias schemes and three different parameters) for each modulation, α must be included in the TDD, as mentioned in Chapter 3, before the power consumption comparison. The α's (dB) are -0.92, -1.37, and -3.57 for $\epsilon = \Delta = \sigma = 0$, 5%, and 10%, respectively. These values are calculated from

$$\alpha = \frac{P_{sat}}{P_{dc,m}} = \frac{8}{\pi^2} \frac{C_p}{(1+\Delta)(1+\epsilon+\sigma-\epsilon\sigma\Delta)}.$$

As can be seen from the larger $-\alpha$ (dB) with the nonideal parameters, power consumption increases as the amplifiers deviate from the ideal condition. The power consumption with six different amplifiers (omitting the cases when $\epsilon = \Delta = \sigma = 5\%$) are plotted in Figure 4.8.

4.4.2 Out-of-band interference: ACPR

Figure 4.9(a) shows ACPR (dB) at $BT_s = 1.35/2$ of OFDM and QPSK. The ACPR of OFDM decays slowly (approximately piece-wise inverse linear) with OBO, and is about -15 dB when OBO = 1 dB. The ACPR of QPSK is smaller than that of OFDM, and the slope is sharper than that of OFDM. Above OBO = 5 dB, QPSK is almost linearly amplified, resulting in constant residual ACPR. In theory it should be zero. This residual ACPR is from the truncation of filter time response in simulation. Figures. 4.9(b) and (c), each shows ACPR versus B in OFDM and QPSK, respectively. The ACPR still decays slowly with B.

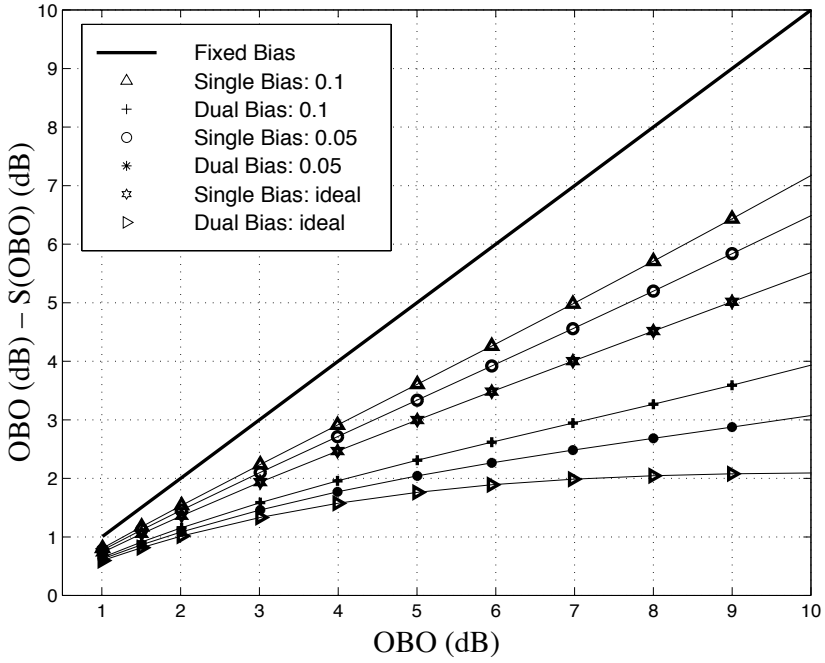

(a)

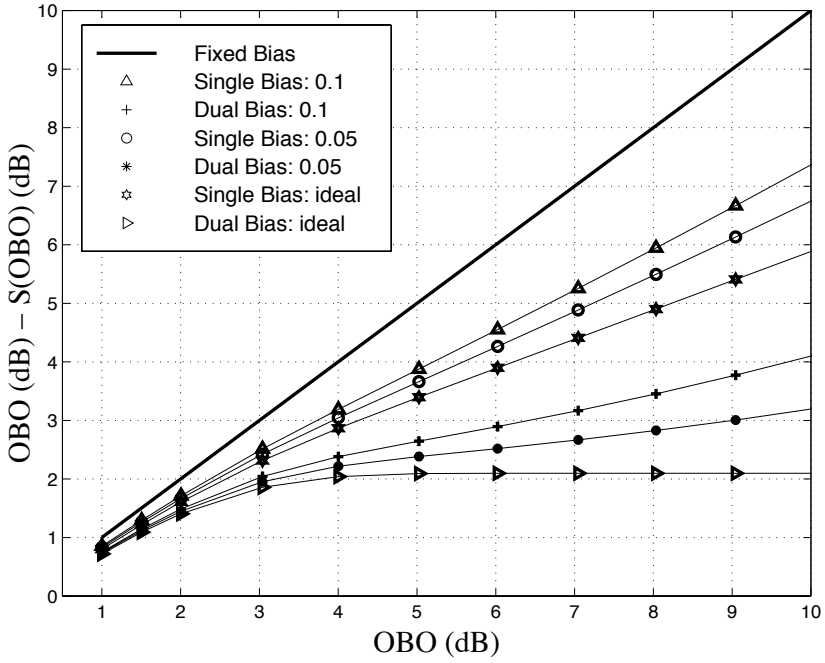

(b)

Figure 4.7: OBO (dB) - S(OBO) (dB) for different values of parameters: (a) OFDM and (b) QPSK.

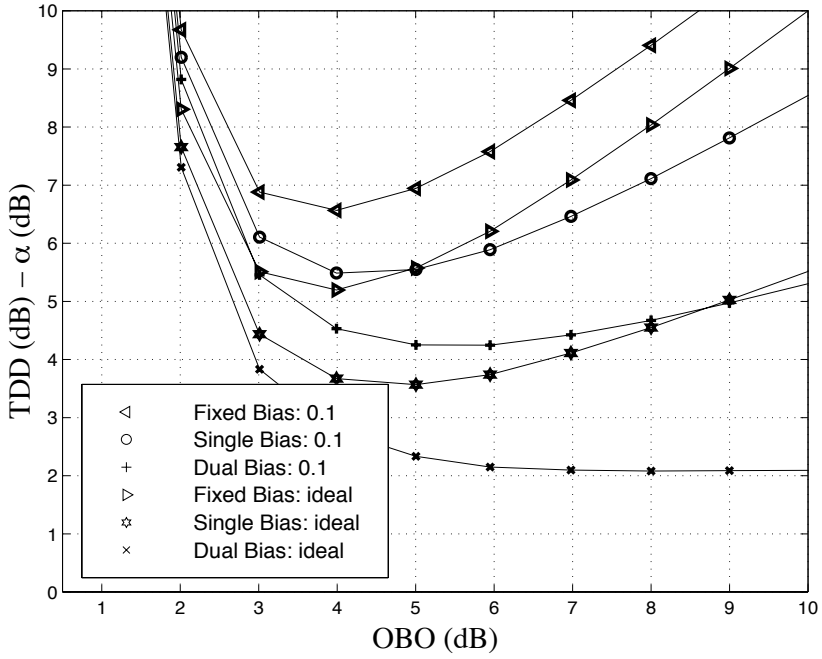

(a)

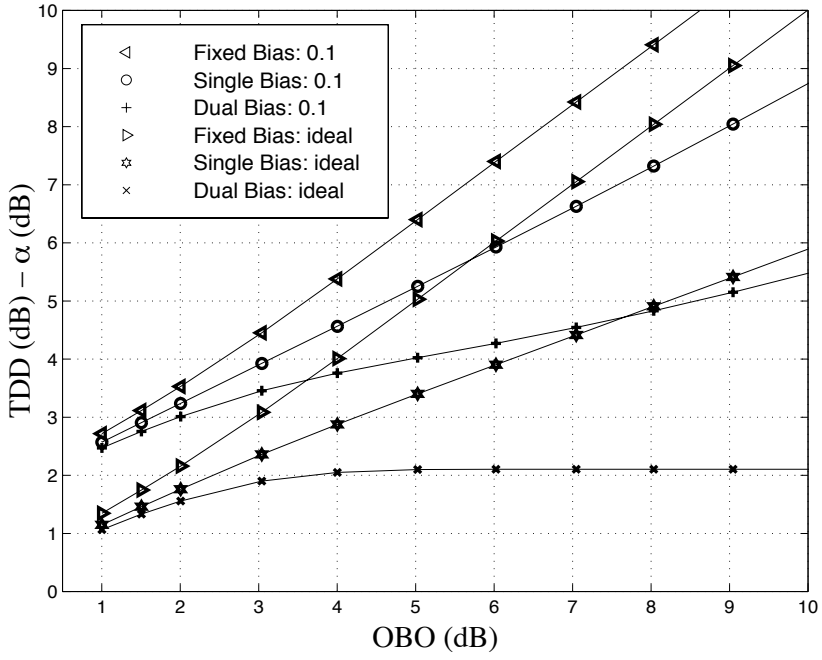

(b)

Figure 4.8: TDD (dB) $-$ α (dB) of different amplifiers with: (a) OFDM and (b) QPSK.

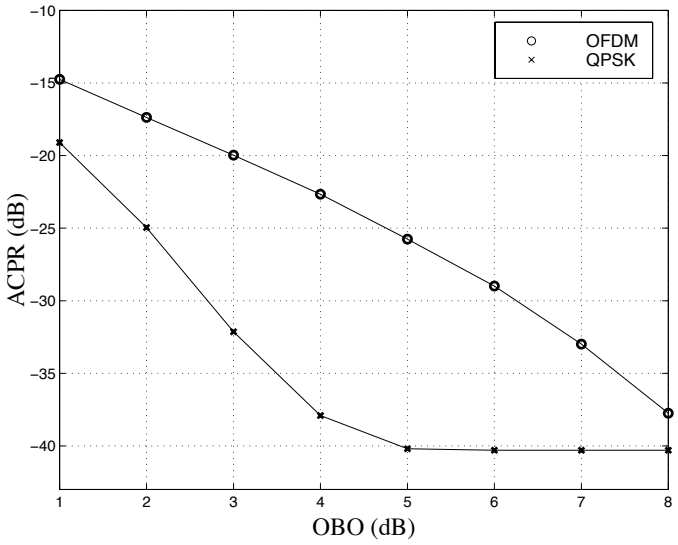

(a)

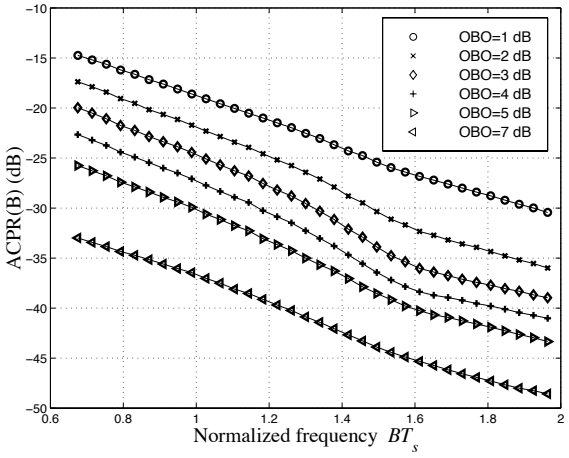

(b)

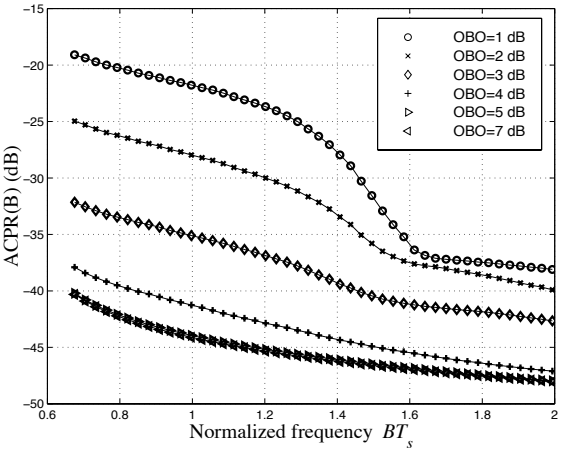

(c)

Figure 4.9: (a) ACPR at BT_s=1.35/2; ACPR vs. normalized frequency BT_s: (b) OFDM and (c) QPSK.

As can be seen in Figure 4.4, the E_b/N_0 degradation decays relatively fast with OBOs. This degradation can be further reduced by channel coding and spread spectrum techniques, whereas the ACPR can not be reduced with these techniques, unless envelope variation becomes very small. As a result, although the optimum OBO for QPSK, in terms of minimizing dc consumption, is found to be less than 0.5 dB according to Figure 4.5(b), the OBO, required to meet ACPR of -38 dB (for example) or less at $BT_s = 1.35/2$, is found to be at least 4 dB (8 dB for OFDM) from Figure 4.9(a). In this case, the ideal dual scheme has TDD of 2 dB less than that of the ideal fixed bias scheme; furthermore, this saving with OFDM is more than 2.3 dB for the ideal single and than 6 dB for the ideal dual bias scheme. A dc bias control scheme provides a solution for using a linear amplifier (less ACPR) without sacrificing power consumption, especially with highly nonconstant envelope modulated signals.

4.5 Conclusion

In this chapter, we have quantified and optimized system power consumption with the objective function TDD, proposed in Chapter 3. The obtained results suggest that a significant power reduction can be achieved by using the dc bias controlled amplifiers, especially for highly nonconstant envelope modulated signals. When the dual bias control scheme is used, even with linear amplification (high OBOs) the power loss from the inefficiency of the amplifier, compared to the power loss at the amplifier's operating saturation region (low OBOs), is minimal.

This low power consumption with high OBO is especially desirable when the adjacent channel interference from nonlinear amplification is a major concern. It is also a major advantage for the even constant envelope signals in current CDMA cellular systems, where power control is required. This advantage of dc bias control schemes in the cellular systems will be quantified and further discussed in Chapter 6.

Acknowledgments

The authors would like to thank Riten Gupta for his helpful comments on this chapter.

CHAPTER 5

Performance Analysis and Power Optimization of Single-User MCSS Systems

5.1 Introduction

In Chapters 3 and 4, we discussed power optimization objective functions and methodology, along with advanced amplifier techniques, such as dc bias controlled amplifiers. In this and the following chapters, we conduct system performance (BER and ACPR) analysis as well as power optimization of the MC system. Particularly in this chapter, we analyze the performance of convolutionally coded single-user MCSS systems in the presence of both multipath fading and nonlinear distortion. The analytical approach used in this chapter is extended to multi-user MC-CDMA systems in the following chapter.

This chapter is organized as follows. In Section 5.2, the coded MCSS system and the channel model are given. A conventional fixed dc bias amplifier is considered. Section 5.3 presents the analysis of BER and ACPR of the system. In the performance analysis, the interference terms from the nonlinearities are modeled as Gaussian random variables. In Section 5.4, we discuss numerical results, including the performance trade-off between the amplifier output backoff (OBO) and the BER sensitivity (E_b/N_o degradation), used in power optimization. The effect of the nonlinearity on the ACPR is also examined at the end of this section. In Section 5.5, we summarize our main conclusion of this chapter.

5.2 System and Channel Model

5.2.1 Transmitter

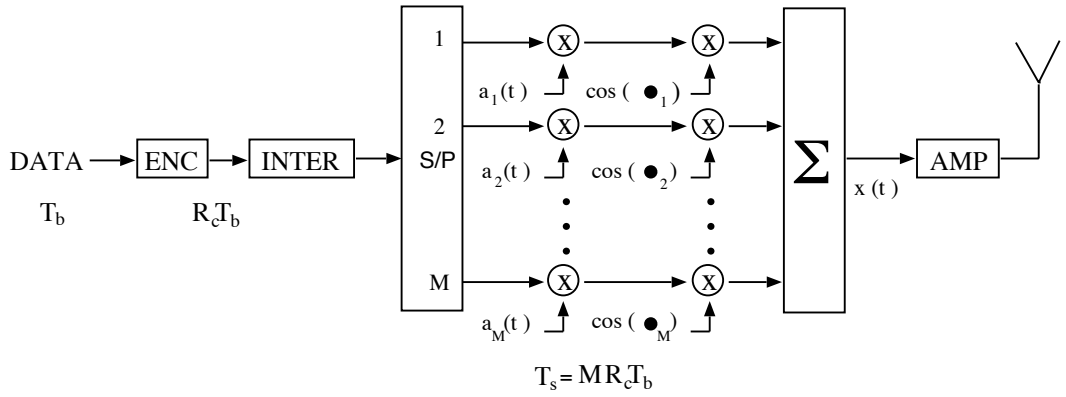

Figure 5.1: MCSS transmitter.

The MCSS transmitter model we employed is shown in Figure 5.1. For the sake of clarity, the basic system parameters, as outlined in Chapter 2, are as follows. The convolutionally encoded information sequence is interleaved and converted from a serial stream to M parallel streams. The code symbol stream for the q-th carrier is denoted by $\{d_q^{(j)}\}$ where $d_q^{(j)} \in \{\pm 1\}$. The signal on the q-th carrier is given by $d_q(t) = \sum_{j=-\infty}^{\infty} d_q^{(j)} p_{T_s}(t - jT_s)$, where $T_s = MT_bR_c$ is the symbol duration, R_c being the code rate and T_b the information bit duration before encoding. The signal on the q-th carrier is then multiplied by a random spreading code $a_q(t)$, where $a_q(t) = \sum_{j=-\infty}^{\infty} \sum_{i=0}^{N-1} a_q^{(i)} p_{T_c}(t - iT_c - jT_s)$ and the chip sequence $\{a_q^{(i)}\} \in \{\pm 1\}$ is a sequence of iid random variables with equal probabilities. Each spreading code has a chip duration of $T_c = T_s/N$ where N is the spreading gain of the system. Finally, the signals on all the carriers are added together before amplification. The output signal $x(t)$ of the modulator is then given by

$$x(t) = \sqrt{2P} \sum_{q=1}^{M} a_q(t) d_q(t) \cos\{(w_c + w_q)t + \theta_q\} \tag{5.1}$$

where P is the power per carrier, w_c is the carrier frequency and the θ_q is an iid random variable uniformly distributed over $[0, 2\pi)$. The separation between the q-th carrier frequency and center frequency w_c is denoted by $w_q = 2\pi q/T_c$.

The modulated signal is first nonlinearly amplified, then distorted by multipath fading and, finally, corrupted by AWGN with two-sided spectral density $N_0/2$.

5.2.2 Channel Model

This subsection is devoted to the analysis of the received signal after the channel, including the derivation of the output signal of the nonlinear amplifiers. In order to do so, we discuss the nonlinear amplifier and multipath fading model.

Amplifier Model

The amplifier model considered in this chapter is a bandpass memoryless nonlinear model as described in Chapter 2. The AM/AM and AM/PM are given by

$$\mathcal{F}(A(t)) = \alpha_1 A(t) + \alpha_3 A^3(t) + \alpha_5 A^5(t) + \ldots + \alpha_n A^n(t) \tag{5.2}$$

$$\Phi(A(t)) = 0 \tag{5.3}$$

where n is odd and the α_i's, which are the coefficients of the polynomial, determine the degree of nonlinearity. The coefficients of the polynomial are obtained from curve fitting Cann's SSPA model, which will be discussed in Section 5.4.

Amplifier Output Signal

The amplifier input signal $x(t)$ in (5.1) can be expressed in terms of its envelope $A(t)$ and phase $\phi(t)$ as $x(t) = A(t)\cos\{w_c t + \phi(t)\}$. The expressions for $A(t)$ and $\phi(t)$ are given in Appendix B. With this form of an input, the amplifier output signal can be represented as

$$\begin{aligned} y(t) &= \mathcal{F}(A(t))\cos\{w_c t + \phi(t)\} \\ &= \{\alpha_1 A(t) + \alpha_3 A^3(t) + \alpha_5 A^5(t) + \cdots + \alpha_n A^n(t)\}\cos\{w_c t + \phi(t)\} \\ &= \{\alpha_1 + \alpha_3 A^2(t) + \alpha_5 A^4(t) + \cdots + \alpha_n A^{n-1}(t)\}\, x(t) \\ &= x^{(1)}(t) + x^{(3)}(t) + x^{(5)}(t) + \cdots + x^{(n)}(t) \end{aligned} \tag{5.4}$$

where $x^{(1)}(t) = \alpha_1 x(t)$ denotes the linearly amplified signal term, and $x^{(n)}(t)$ (for $n \geq 3$) denotes the amplified signal term from the n-th order nonlinearity, the explicit

expressions for which are as follows:

$$x^{(3)}(t) = \alpha_3(\sqrt{2P})^3 \sum_{l_1=1}^{M}\sum_{l_2=1}^{M}\sum_{l_3=1}^{M} \widetilde{a}_3(t)\widetilde{d}_3(t)\cos\{(w_c + w_{\jmath_3})t + \theta_{\hat{\jmath}_3}\} \tag{5.5}$$

$$x^{(5)}(t) = \alpha_5(\sqrt{2P})^5 \sum_{l_1=1}^{M}\sum_{l_2=1}^{M}\cdots\sum_{l_5=1}^{M} \widetilde{a}_5(t)\widetilde{d}_5(t)\cos\{(w_c + w_{\jmath_5})t + \theta_{\hat{\jmath}_5}\} \tag{5.6}$$

$$\vdots$$

$$x^{(n)}(t) = \alpha_n(\sqrt{2P})^n \sum_{l_1=1}^{M}\sum_{l_2=1}^{M}\cdots\sum_{l_n=1}^{M} \widetilde{a}_n(t)\widetilde{d}_n(t)\cos\{(w_c + w_{\jmath_n})t + \theta_{\hat{\jmath}_n}\} \tag{5.7}$$

where the index $\jmath_n = l_1 + l_2 - l_3 + \cdots + l_{n-1} - l_n$, (i.e., $w_{\jmath_n} = 2\pi\jmath_n/T_c = w_{l_1} + w_{l_2} - w_{l_3} + \cdots + w_{l_{n-1}} - w_{l_n}$), the phase $\theta_{\hat{\jmath}_n} = \theta_{l_1} + \theta_{l_2} - \theta_{l_3} + \cdots + \theta_{l_{n-1}} - \theta_{l_n}$, and

$$\widetilde{a}_n(t) = a_{l_1}(t)\, a_{l_2}(t)\cdots a_{l_n}(t) \tag{5.8}$$

$$\widetilde{d}_n(t) = d_{l_1}(t)\, d_{l_2}(t)\cdots d_{l_n}(t). \tag{5.9}$$

The derivation of (5.7) is given in Appendix B.

We note that each output signal generated from the 3rd, 5th, ..., n-th order nonlinearity can be divided into two signal components: the deterministic in-phase signal and the random interference signal. The in-phase signal refers to the output signal of the amplifier which becomes a scaled replica of the input signal $x(t)$ in a deterministic way. This in-phase signal adds to the linearly amplified signal $\alpha_1 x(t)$, modifying the magnitude of the linearly amplified signal. On the other hand, the interference signal refers to the output signal that can possibly interfere with $x_1(t)$, and is not deterministic.

For example, when the index vector (l_1, l_2, l_3) in $x^{(3)}(t)$ belongs to set

$$\mathcal{A}_3 = \{(l_1, l_2, l_3) : (l_1 = l_3) \vee (l_2 = l_3)\}$$

the corresponding signal terms in $x_3(t)$ constitutes $\alpha_3(\sqrt{2P})^2 x(t)$. Note that the sets $\{(l_1, l_2, l_3) : (l_1 = l_3)\}$ and $\{(l_1, l_2, l_3) : (l_2 = l_3)\}$ each constitutes M copies of $\alpha_3(\sqrt{2P})^2 x(t)$ to $x^{(3)}(t)$, but one copy is constituted by both sets. Hence, the sets $\mathcal{A}_3$ constitutes exactly $\Lambda_3(M) = 2M - 1$ copies of $\alpha_3(\sqrt{2P})^2 x(t)$ to $x_3(t)$. As a result, $x^{(3)}(t)$ can be represented as the sum of a scaled version of the original signal, which

we call the desired signal, and the interfering signal, as shown below:

$$\begin{aligned} x^{(3)}(t) &= \alpha_3(\sqrt{2P})^2\Lambda_3(M)x(t) + \\ &\quad \alpha_3(\sqrt{2P})^3 \underbrace{\sum_{l_1=1}^{M}\sum_{l_2=1}^{M}\sum_{l_3=1}^{M}}_{\mathcal{A}_3^c} \widetilde{a}_3(t)\widetilde{d}_3(t)\cos\{(w_c + w_{j_3})t + \theta_{\hat{j}_3}\}. \end{aligned} \tag{5.10}$$

Similarly, when the index vector $(l_1, l_2, l_3, l_4, l_5)$ in $x^{(5)}(t)$ belongs to the set

$$\begin{aligned} \mathcal{A}_5 = \{(l_1,l_2,l_3,l_4,l_5) \;:\; &((l_2 = l_3) \wedge (l_4 = l_5)) \vee ((l_4 = l_3) \wedge (l_2 = l_5)) \\ \vee\; &((l_1 = l_3) \wedge (l_4 = l_5)) \vee ((l_4 = l_3) \wedge (l_1 = l_5)) \\ \vee\; &((l_1 = l_3) \wedge (l_2 = l_5)) \vee ((l_2 = l_3) \wedge (l_1 = l_5))\} \end{aligned}$$

the corresponding terms in $x^{(5)}(t)$ constitute $\alpha_5(\sqrt{2P})^4 x(t)$. There are $\Lambda_5(M) = 6M^2 - 9M + 4$ such terms contributed by the set $\mathcal{A}_5$.

In general, when the index vector $(l_1, l_2, \ldots, l_n)$ in the summation defining $x^{(n)}(t)$ belongs to the set $\mathcal{A}_n$ defined below, the corresponding terms in $x^{(n)}(t)$ constitute the in-phase signal.

$$\mathcal{A}_n = \{(l_1, l_2, \ldots, l_n) : \bigvee_{\pi} ((l_{\pi_1} = l_3) \wedge (l_{\pi_2} = l_5) \wedge \cdots \wedge (l_{\pi_r} = l_n))\} \tag{5.11}$$

where the 'OR' ($\bigvee$) operation runs over all possible permutations of π of every combination of $r = \frac{n-1}{2}$ distinct integers from the set {1, 2, 4, ... , $n-1$}, resulting in $\binom{r+1}{r} r! - 1$ 'OR's. The number of in-phase signal terms in the $x^{(n)}(t)$, $\Lambda_n(M)$ can be obtained using a well known equation for the size of the union of a finite number of sets [84, page 37], which is also given in Appendix C. It should be noted that as n gets larger, the labor necessary to calculate $\Lambda_n(M)$ exactly would be quite considerable (and tedious) without some systematic grouping, selection, and recursive methods. However, in most cases, $n \leq 9$ is enough to represent amplifier nonlinearities, and so we list $\Lambda_n(M)$ for $n = 3, 5, 7, 9$ in Appendix C.

In summary, the nonlinearly amplified signal terms $x^{(n)}(t)$ can be decomposed into a scaled version of the original signal (which is deterministic) and the interfering

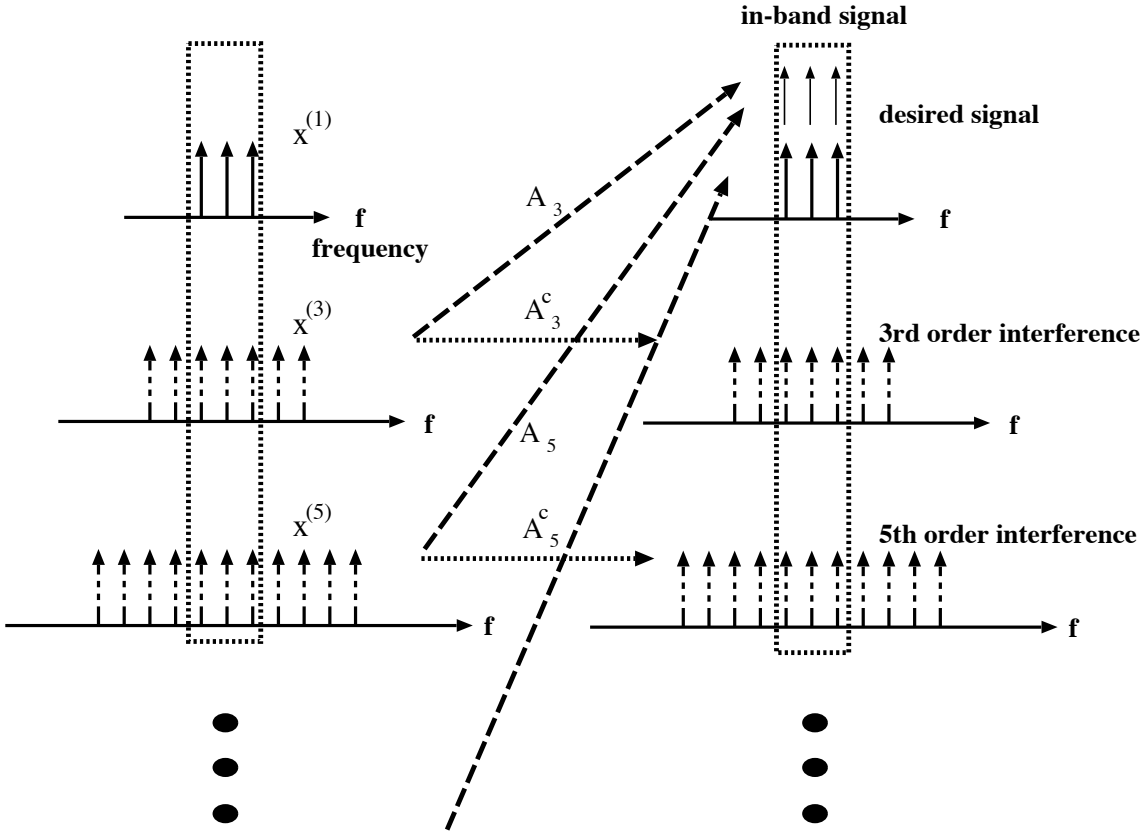

Figure 5.2: The decomposition of the output signal of the nonlinear amplifier.

signal (which is random) as

$$\begin{aligned} x^{(n)}(t) &= \alpha_n(\sqrt{2P})^{n-1}\Lambda_n(M)x(t) + \\ &\quad \alpha_n(\sqrt{2P})^n \underbrace{\sum_{l_1=1}^{M}\sum_{l_2=1}^{M}\cdots\sum_{l_n=1}^{M}}_{\mathcal{A}_n^c} \widetilde{a}_n(t)\widetilde{d}_n(t)\cos\{(w_c + w_{j_n})t + \theta_{\hat{j}_n}\} \end{aligned} \quad (5.12)$$

where $\mathcal{A}_n^c$ is the complement of the set $\mathcal{A}_n$ defined in (5.11). This decomposition of the amplifier output signal is schematically illustrated in Figure 5.2, considering $M = 3$ carriers for the input signal. The desired signal carriers, as well as the interference signal carriers are plotted in the frequency domain. Note that new frequency components are generated by the higher order polynomials which lie outside the box. These out-of-band signals cause interference to the adjacent channels, which will be quantified by ACPR in Section 5.3.3.

Multipath Fading Model

We consider frequency selective channel in the transmitted bandwidth but flat (frequency non-selective) fading for each carrier, assuming the bandwidth for each carrier is smaller than the coherence bandwidth defined in Chapter 2. Hence, the low-pass equivalent channel response for the q-th carrier

$$h_{L,q}(t) \;=\; \beta_q(t)\exp(j\varphi_q(t))\delta(t) \tag{5.13}$$

where $\beta_q(t)$ is an iid Rayleigh distributed random variable with $E[\beta_q^2(t)]= 1$. The phase $\varphi_q(t)$ is an iid random variable uniformly distributed over $[0, 2\pi)$. In this model, we assume a slowly varying Rayleigh fading for each carrier so that the fades ($\beta_q(t)$ and $\varphi_q(t)$) are constant over the symbol duration. In the rest of this chapter, we omit t in $\beta_q(t)$ and $\varphi_q(t)$. The independence of β_q and φ_q on transmitted symbols can be justified by the use of sufficient interleaving. The random variables β_q and φ_q are constant over the symbol duration but are independent from the symbol to symbol. The received signal after multipath fading and AWGN channel is

$$r(t) \;=\; n(t) + H^{(1)}\sqrt{2P}\sum_{q=1}^{M}\beta_q a_q(t)d_q(t)\cos\{(w_c+w_q)t+\widehat{\theta}_q\} + I(t) \tag{5.14}$$

where $\widehat{\theta}_{\jmath_n} = \theta_{\hat{\jmath}_n} + \varphi_{\jmath_n}$, and

$$H^{(1)} = \{\alpha_1 + \alpha_3(\sqrt{2P})^2\Lambda_3(M) + \alpha_5(\sqrt{2P})^4\Lambda_5(M) + \cdots + \alpha_n(\sqrt{2P})^{n-1}\Lambda_n(M)\}. \tag{5.15}$$

The interference signal from the nonlinearities is

$$\begin{aligned} I(t) \;=\;& \alpha_3(\sqrt{2P})^3\sum_{l_1=1}^{M}\sum_{l_2=1}^{M}\sum_{l_3=1}^{M}\mathrm{I}_{\{\mathcal{A}_3^c\}}\beta_{\jmath_3}\widetilde{a}_3(t)\widetilde{d}_3(t)\cos\{(w_c+w_{\jmath_3})t+\widehat{\theta}_{\jmath_3}\} + \\ & \alpha_5(\sqrt{2P})^5\sum_{l_1=1}^{M}\sum_{l_2=1}^{M}\cdots\sum_{l_5=1}^{M}\mathrm{I}_{\{\mathcal{A}_5^c\}}\beta_{\jmath_5}\widetilde{a}_5(t)\widetilde{d}_5(t)\cos\{(w_c+w_{\jmath_5})t+\widehat{\theta}_{\jmath_5}\} + \cdots \\ +\;& \alpha_n(\sqrt{2P})^n\sum_{l_1=1}^{M}\sum_{l_2=1}^{M}\cdots\sum_{l_n=1}^{M}\mathrm{I}_{\{\mathcal{A}_n^c\}}\beta_{\jmath_n}\widetilde{a}_n(t)\widetilde{d}_n(t)\cos\{(w_c+w_{\jmath_n})t+\widehat{\theta}_{\jmath_n}\} \end{aligned} \tag{5.16}$$

where $\widehat{\theta}_q = \theta_q + \varphi_q$, and the indicator function, $\mathrm{I}_{\{\zeta\}}$, equals one if the indices in the summation belong to set ζ, and, zero if not.

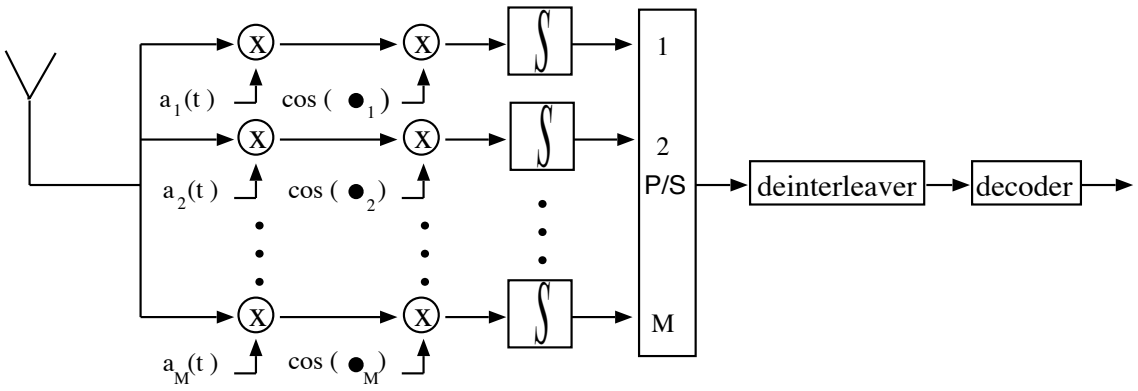

Figure 5.3: MCSS receiver structure.

5.3 Performance Analysis

In this section, we first analyze the demodulator output statistics and then derive the average BER for the uncoded systems. For the coded systems, we obtain an upper bound on the average BER. Finally, the ACPR is defined to characterize the spectral regrowth (out-of-band signals) of the nonlinearly amplified signal.

5.3.1 Demodulator and its output statistics

We consider a conventional matched filter receiver (a filter matched to the signal before the nonlinearities). The receiver is shown in Figure 5.3. The coherently demodulated symbol, after the integrate-and-dump filter of the q-th subcarrier for time $t \in [0, T_s]$, is

$$\begin{aligned} Z_q &= \int_0^{T_s} r(t) a_q(t) \cos\{(w_c + w_q)t + \widehat{\theta}_q\} dt \\ &= \eta + D_q + J_{non,q} \end{aligned} \tag{5.17}$$

where η is Gaussian random variable with mean 0 and variance $N_0 T_s/4$. The desired term for the q-th channel is

$$D_q = H^{(1)} \sqrt{2P} \beta_q d_q^{(0)} T_s/2 \tag{5.18}$$

and the interference term to the q-th carrier from the 3rd, 5th, ... , and n-th order nonlinearity is

$$J_{non,q} = J_{non,q}^{(3)} + J_{non,q}^{(5)} + \cdots + J_{non,q}^{(n)} \tag{5.19}$$

where the interference term from the n-th order nonlinearity which falls on the q-th channel is given by

$$J_{non,q}^{(n)} = \alpha_n \frac{(\sqrt{2P})^n}{2} \beta_q \sum_{l_1=1}^{M} \sum_{l_2=1}^{M} \cdots \sum_{l_n=1}^{M} \mathrm{I}_{\{A'_{n,q}\}} d_{l_1}^{(0)} d_{l_2}^{(0)} \cdots d_{l_n}^{(0)} \cos(\theta_{\hat{\jmath}_n} - \theta_q) \int_0^{T_s} \widetilde{a}_n(t) a_q(t)\, dt \tag{5.20}$$

where set $\mathcal{A}'_{n,q}$ is defined as $\{(l_1, l_2, \ldots, l_n) : (\jmath_n = q)\} \cap \mathcal{A}_n^c$, with $\mathcal{A}_n$ as defined in (5.11). Note that $\jmath_n = l_1 + l_2 - l_3 + \cdots + l_{n-1} - l_n$ and $\theta_{\hat{\jmath}_n} = \theta_{l_1} + \theta_{l_2} - \theta_{l_3} + \cdots + \theta_{l_{n-1}} - \theta_{l_n}$.

Conditional Variance

The conditional variance of $I_{non,q}$, given the fade level β_q, can be calculated by adding the individual conditional variances of $J_{non,q}^{(3)}, J_{non,q}^{(5)}, \ldots, J_{non,q}^{(n)}$, since these terms are uncorrelated and each conditional mean is zero. However, special care has to be taken for calculating the conditional variance of $J_{non,q}^{(\bullet)}$, since some of the signal terms in the expression for $J_{non,q}^{(\bullet)}$ are not independent (in fact, some terms are identical).

Observe that, for $J_{non,q}^{(3)}$, the signal terms contributed by the index vector (l_1, l_2, l_3) and (l'_1, l'_2, l'_3) are the same if (l_1, l_2) is a permutation of (l'_1, l'_2). As a result, the corresponding signal terms can be added deterministically. Similarly, for $J_{non,q}^{(5)}$, the terms contributed by the index vectors $(l_1, l_2, l_3, l_4, l_5)$ are identical if (l_1, l_2, l_4) and (l_3, l_5) are permutations of (l'_1, l'_2, l'_4) and (l'_3, l'_5), respectively. In general, the terms in $J_{non,q}^{(n)}$ contributed by $(l_1, l_2, l_3 \ldots, l_{n-1})$ and $(l'_1, l'_2, l'_3 \ldots, l'_{n-1})$ are the same when $(l_1, l_2, \ldots, l_{n-1})$ and $(l_3, l_5, \ldots, l_n)$ are permutations of $(l'_1, l'_2, \ldots, l'_{n-1})$ and $(l'_3, l'_5, \ldots, l'_n)$, respectively.

Based on the above, we can divide $\mathcal{A}'_{n,q}$ into groups as follows. $(l_1, l_2, l_3 \ldots, l_{n-1}) \in \mathcal{A}'_{n,q}$ and $(l'_1, l'_2, l'_3 \ldots, l'_{n-1}) \in \mathcal{A}'_{n,q}$ belong to the same group if and only if they contribute identical terms to $J_{non,q}^{(n)}$. Let $\{G_{i,q}(n) : i \in \mathcal{I}\}$ be the set of all such groups, where $\mathcal{I}$ is the some (finite) index set. For example, $(l_1 = 1, l_2 = 3, l_3 = 2)$ and $(l_1 = 3, l_2 = 1, l_3 = 2)$ belong to $G_{i,2}(3)$; $(l_1 = 2, l_2 = 2, l_3 = 2, l_4 = 2, l_5 = 3)$, and $(l_1 = 2, l_2 = 2, l_3 = 3, l_4 = 2, l_5 = 2)$ belong to $G_{j,1}(5)$. Note that $(l_1 = 2, l_2 = 2, l_3 = 3)$ itself constitutes a group $G_{k,1}(3)$, and i,j,k are arbitrary indices to denote

different groups.

Then, the conditional variance of $J_{non,q}^{(n)}$

$$\begin{aligned} \mathrm{Var}[J_{non,q}^{(n)}|\beta_q] &= \frac{P\beta_q^2 T_s^2}{4N}\{(H_q^{(n)})^2\} && (5.21) \\ (H_q^{(n)})^2 &= \alpha_n^2 (2P)^{n-1} \sum_i |G_{i,q}(n)|^2. && (5.22) \end{aligned}$$

The summation in (5.22) runs over the set of groups, and $|G_{i,q}(n)|$ denotes the size of each group, equivalently, the number of index vector $(l_1, l_2, l_3, \ldots, l_n)$ which belong to the group $G_{i,q}(n)$. We note that even though the calculation of $\sum_i |G_{i,q}(n)|^2$ in (5.22) is straight forward by computer, the closed form expression is difficult to obtain for arbitrary n. The closed form expression for $\sum_i |G_{i,q}(n)|^2$ for $n = 3$ and $1 \le q \le M$ is as follows:

$$\sum_i |G_{i,q}(3)|^2 = \begin{cases} \frac{M-2}{2} + (M-2)^2 + 2(q-1)(M-q) & \text{if } M \text{ is even} \\ \frac{M-2+(-1)^q}{2} + (M-2)^2 + 2(q-1)(M-q) & \text{if } M \text{ is odd} \end{cases} \quad (5.23)$$

and the derivation is shown in Appendix D.

As a result, the conditional mean and variance of $J_{non,q}$ are $E[J_{non,q}|\beta_q] = 0$ and $\mathrm{Var}[J_{non,q}|\beta_q] = P\beta_q^2 T_s^2 \{(\widetilde{H}_q^{(n)})^2\}/4N$, respectively. And, finally, the conditional mean and variance of Z_q

$$\begin{aligned} E[Z_q|\beta_q] &= \sqrt{2P}\beta_q d_q^{(0)} \frac{T_s}{2} H^{(1)} && (5.24) \\ \mathrm{Var}[Z_q|\beta_q] &= \frac{N_0 T_s}{4} + \frac{P\beta_q^2 T_s^2}{4N}\{(\widetilde{H}_q^{(n)})^2\}, && (5.25) \end{aligned}$$

respectively, where

$$(\widetilde{H}_q^{(n)})^2 = (H_q^{(3)})^2 + (H_q^{(5)})^2 + \cdots + (H_q^{(n)})^2. \quad (5.26)$$

5.3.2 Bit Error Rate Performance

Uncoded System Performance

Since $J_{non,q}$ in (5.19), after grouping, is a linear combination of uncorrelated random variables, providing that M or N is sufficiently large ($MN > 5$), the conditional probability density function (pdf) of $J_{non,q}$ becomes Gaussian by the central limit theorem. Hence, if we approximate the nonlinear interference term ($J_{non,q}$) by a Gaussian

random variable, the conditional BER of the q-th subcarrier is

$$P_{b,q|\beta_q} = Q\left(\sqrt{\mathrm{SNR}(\beta_q)}\right) \tag{5.27}$$

where $Q(x) = (1/\sqrt{2\pi})\int_x^\infty \exp(-u^2/2)du$. The conditional $\mathrm{SNR}(\beta_q)$ given β_q,

$$\mathrm{SNR}(\beta_q) = \frac{E^2[Z_q|\beta_q]}{\mathrm{Var}[Z_q|\beta_q]} = \frac{2\bar{\gamma}\beta_q^2}{1+\bar{\varrho}+\beta_q^2\bar{\gamma}\frac{\varrho_q}{N}} \tag{5.28}$$

where

- $\bar{\gamma}_q = [(H^{(1)})^2+(\widetilde{H}_q^{(n)})^2]PT_s/N_0$: average received symbol-energy-to-noise power density ratio (E_s/N_0) on the q-th carrier.
- $\bar{\gamma} = \frac{1}{M}\sum_{q=1}^{M}\bar{\gamma}_q$: E_s/N_0 per carrier.
- $\varrho_q = [(\widetilde{H}_q^{(n)})^2]/(H^{(1)})^2$: normalized nonlinear interference variance on a q-th carrier.
- $\bar{\varrho} = \frac{1}{M}\sum_{q=1}^{M}\varrho_q$: normalized nonlinear interference variance per carrier.

Note that $\bar{\gamma}_q = (H^{(1)})^2(1+\varrho_q)PT_s/N_0$, and the out-of-band signal power is not included in the calculation of $\bar{\gamma}$. Instead, the out-of-band power is effectively included in the amplifier output backoff (OBO) term. This issue will be explained in detail when we discuss OBO in Section 5.4.1 and ACPR in Section 5.3.3. The proof of the second equality in (5.28) is given in Appendix E.

Hence, the unconditional BER of the q-th subcarrier

$$P_{b,q} = \int_0^\infty f(\beta_q)Q\left(\sqrt{\mathrm{SNR}(\beta_q)}\right)\,d\beta_q \tag{5.29}$$

$$= \frac{1}{2} - \frac{1}{\sqrt{2\pi}}\int_{u=0}^{\sqrt{\frac{2N}{\varrho_q}}}\exp\{-\frac{u^2}{2}[1+\frac{1+\bar{\varrho}}{\bar{\gamma}(1-\frac{\varrho_q u^2}{2N})}]\}du \tag{5.30}$$

and the average bit error rate is then

$$P_b = \frac{1}{M}\sum_{q=1}^{M}P_{b,q}. \tag{5.31}$$

Upper Bounds on the Bit Error Rate for Coded Systems

For the coded system, we consider a convolutional code of rate $R_c = 1/2$ with constraint length 7 with maximum likelihood decoding. We assume that a perfect channel estimate is available so that we can weigh the output of the integrate-and-dump filter by the factor

$$g_i = E[Z_i|\beta_i, d^{(i)} = 1]/\mathrm{Var}[Z_i|\beta_i]. \tag{5.32}$$

We also assume that we have a sufficiently large sized interleaver so that the code symbols after the deinterleaving are independent of each other. The upper bounds on the BER can be obtained from the union bound [85, page 327] as

$$P_b \leq \sum_{d=d_{free}}^{\infty} w_d P_2(d) \tag{5.33}$$

where w_d is the total number of nonzero information bits on a path with hamming distance d, the pairwise error probability $P_2(d)$ is the error probability between two codewords which differ in d symbols, and d_{free} is the free distance of the code. We use truncated w_d up to approximately $d = 30$ which are tabulated in [86]. Note that the pairwise error probability $P_2(d)$ is just the error probability of a repetition code of length d.

Assuming we send the all-zero message (i.e., a codeword with all ones), $P_2(d)$ is given by,

$$P_2(d) = P\{\sum_{i=1}^{d} g_i Z_i \leq 0\} = P\{Z(d) \leq 0\} \tag{5.34}$$

where $Z(d) = \sum_{i=1}^{d} g_i Z_i$. Since, given β_i, the demodulator output values are Gaussian random variables, the statistics of $Z(d)$ given β_i's is also Gaussian with the conditional mean

$$E[Z(d)|\beta_1, \beta_2, \ldots, \beta_d] = \sum_{i=1}^{d} E^2[Z_i|\beta_i]/\mathrm{Var}[Z_i|\beta_i]$$

and the conditional variance

$$\mathrm{Var}[Z(d)|\beta_1, \beta_2, \ldots, \beta_d] = \sum_{i=1}^{d} E^2[Z_i|\beta_i]/\mathrm{Var}[Z_i|\beta_i].$$

Hence, the conditional pairwise error probability,

$$P\{Z(d) \leq 0 | \beta_1, \beta_2, \ldots, \beta_d\} \;=\; Q\left(\sqrt{\sum_{i=1}^{d} \mathrm{SNR}(\beta_i)}\right) \tag{5.35}$$

where

$$\mathrm{SNR}(\beta_i) = \frac{E^2[Z_i|\beta_i]}{\mathrm{Var}[Z_i|\beta_i]} \geq \mathrm{SNR}_{min}(\beta_i) = \frac{2\bar{\gamma}\beta_i^2}{1+\bar{\varrho}+\beta_i^2\bar{\gamma}\frac{\varrho}{N}}. \tag{5.36}$$

The ϱ in the above equation is taken from the maximum value of ϱ_q among the M carriers, i.e., from the center carrier ($\varrho = \varrho_q$, for $q = \lfloor (M+1)/2 \rfloor$). $\lfloor X \rfloor$ denotes the smallest integer greater than $X-1$. In addition, since the $Q(x)$ function is monotonically decreasing with x, we obtain the following inequality

$$Q\left(\sqrt{\sum_{i=1}^{d} \mathrm{SNR}(\beta_i)}\right) \;\leq\; Q\left(\sqrt{\sum_{i=1}^{d} \mathrm{SNR}_{min}(\beta_i)}\right). \tag{5.37}$$

Now, we need to average the above equation over the random parameters, $\{\beta_i\}$'s. For the numerical convenience, we use the alternative representation of $Q(x)$ [87, 88], which is given by

$$Q(x) \;=\; \frac{1}{\pi}\int_0^{\pi/2} \exp\left(-\frac{x^2}{2\sin^2\theta}\right) d\theta. \tag{5.38}$$

With this representation, (5.34) is upper bounded by

$$P_2(d) \;\leq\; \frac{1}{\pi}\int_0^{\pi/2} I_{in}^d(\theta)\; d\theta \tag{5.39}$$

where

$$I_{in}(\theta) \;=\; \int_0^{\infty} \exp\{-\frac{1}{2\sin^2\theta}\mathrm{SNR}_{min}(\beta_i)\} f_{\beta_i}(\beta_i) d\beta_i \tag{5.40}$$

and $f_{\beta_i}(\beta_i)$ is a pdf of the Rayleigh random variable. By a change of variable (letting $\mathrm{SNR}_{min}(\beta_i) = y$), (5.40) becomes

$$I_{in}(\theta) \;=\; \int_0^{\frac{1}{v}} \exp\{-\frac{y}{2\sin^2\theta}\}\left(\frac{u}{(1-vy)^2}\exp\{-\frac{uy}{1-vy}\}\right) dy \tag{5.41}$$

where $u = (1+\bar{\varrho})/2\bar{\gamma}$ and $v = \varrho/2N$.

5.3.3 Adjacent Channel Power Ratio

In order to quantify the out-of-band interference from nonlinear amplification, we define the adjacent channel power ratio (ACPR) as the ratio of the total out-of-band carrier power to the in-band (main channel) carrier power

$$\begin{aligned} \text{ACPR} &= \{\text{Out-of-band carrier power}\} \,/\, \{\text{Main channel carrier power}\} \\ &= \frac{\sum_{q=l_{min}}^{q=l_{max}} \{(\widetilde{H}_q^{(n)})^2 P\} + \sum_{q=r_{min}}^{q=r_{max}} \{(\widetilde{H}_q^{(n)})^2 P\}}{\sum_{q=1}^{M} \{(H^{(1)})^2 P + (\widetilde{H}_q^{(n)})^2 P\}} \end{aligned} \tag{5.42}$$

where the indices $l_{min} = \{n{+}1{-}(n{-}1)M\}/2$ and $l_{max} = 0$ denote the carrier frequency indices for the left side of the main channel. Similarly, the indices $r_{min} = M + 1$ and $r_{max} = \{(n+1)M - n + 1\}/2$ denote the carrier frequency indices for the right side of the main channel. Since the spectral regrowth is symmetric, the numerator of the above expression becomes $2\sum_{q=l_{min}}^{q=l_{max}} \{(\widetilde{H}_q^{(n)})^2 P\}$; thus ACPR can be written as

$$\text{ACPR} = \frac{2\sum_{q=l_{min}}^{q=l_{max}} \{(\widetilde{H}_q^{(n)})^2\}}{\{M(H^{(1)})^2(1+\bar{\varrho})\}}. \tag{5.43}$$

These out-of-band signals, intermodulation products falling out-of-band, interfere with existing systems in adjacent channels. Moreover, in the asynchronous multi-user systems, the out-of-band signals can interfere with the in-band signals of other users, as will be seen in Chapter 6. it should be noted that in the considered single user case, the out-of-band signals do not interfere with the in-band signals, since the out-of-band signals are still orthogonal to the in-band signals.

Besides, ACPR denoting the interference power, it also denotes the loss of the available output power of the amplifier: the out-of-band signal power cannot be incorporated into the desired received power, resulting in a waste of available source power. This loss can be quantified by the ratio of the out-of-band carrier power to the total output signal power of the amplifier

$$\begin{aligned} \Upsilon &= \frac{\{\text{Out-of-band carrier power}\}}{\{\text{Output signal power of the amplifier}\}} \\ &= \frac{\{\text{Out-of-band carrier power}\}}{\{\text{Out-of-band carrier power+ Main channel carrier power}\}} \\ &= \frac{1}{1+\text{ACPR}^{-1}} \approx \text{ACPR} \quad (\text{ACPR}^{-1} >> 1). \end{aligned} \tag{5.44}$$

From (5.44), it is clear that the ACPR can also be interpreted as an available in-band power loss from the nonlinear amplifier as well as interference power to the adjacent channel. Even though this power loss is usually small compared to the E_b/N_0 degradation, this power loss can be reintroduced into equation by either simply replacing $\bar{\gamma}$ in (5.28) with $(1-\Upsilon)\bar{\gamma}$ or by using a modified OBO which takes into account this loss. In this thesis, the latter is adopted and the modified OBO is explained in the following section.

5.4 Numerical Results and Discussion

In this section, we first briefly review the performance trade-off measures to be used. Then, we describe basic system parameters, considered in the performance evaluation. In particular, we explain how we set the amplifier operation point (i.e., OBO). We also discuss the amplifier model used in this chapter, along with some of limitation imposed from using a polynomial model. Finally, we numerically evaluate and quantify BER, TD, and ACPR as well as we examine and discuss the results.

5.4.1 Performance Tradeoff

To quantify the trade-off between the power saving from operating in the saturation and the loss caused by the nonlinear distortion, we use the objective function TD, introduced in Chapter 3. This is based on the assumption that the amplifier dc power is constant.

If we reiterate the TD,

$$\text{TD (dB)} \quad = \quad \text{OBO(dB)} + \Delta_{E_b/N_0}(\text{OBO})(\text{dB}) \tag{5.45}$$

where $\Delta_{E_b/N_0}(\text{OBO})(\text{dB})$, so called E_b/N_0 degradation, is the increment of the received $E_b/N_0(\text{dB})$ required to maintain a given BER (say, $P_b = 10^{-4}$) with respect to the case of a perfectly linear amplifier. The optimum OBO of the system gives the minimum value of (5.45).

The output backoff (OBO) is defined as the ratio of a maximum possible output

power to the average in-band signal output power of the amplifier,

$$\begin{aligned} \text{OBO} &= \frac{1/2 \max\{\mathcal{F}^2(A(t))\}}{\sum_{q=1}^{M}\{(H^{(1)})^2 P + (\widetilde{H}_q^{(n)})^2 P\}} && (5.46) \\ &= \frac{\max\{\mathcal{F}^2(A(t))\}}{2MP(H^{(1)})^2(1+\bar{\varrho})}. && (5.47) \end{aligned}$$

The factor of 1/2 in (5.46) comes from the carrier term. It is worthwhile mentioning that, in the defined OBO (5.46), we do not include the out-of-band signal power in the denominator. This definition basically accounts for the in-band power loss from the nonlinear amplifier, which was discussed in Section 5.3.3. Note that for a given amplifier operation region (i.e., the same degree of nonlinearity), the OBO defined in (5.47) is larger than

$$\begin{aligned} \text{OBO}_\text{O} &= \frac{1/2 \max\{\mathcal{F}^2(A(t))\}}{\sum_{q=1}^{M}\{(H^{(1)})^2 P + (\widetilde{H}_q^{(n)})^2 P\} + \{2\sum_{q=l_{min}}^{q=l_{max}}(\widetilde{H}_q^{(n)})^2 P\}} \\ &= \text{OBO}(1-\Upsilon) && (5.48) \end{aligned}$$

which includes the out-of-band signal power. Hence, the power loss $(1-\Upsilon)$, mentioned in the previous section, is thus taken into account for the power optimization (i.e., in TD).

In order to examine the coded system performance in the presence of nonlinearities, we define the coding gain $G(\text{OBO})$ as the difference between the required E_b/N_0 to meet $P_b = 10^{-4}$ for coded system and uncoded system:

$$\begin{aligned} G(\text{OBO})(\text{dB}) &= E_b/N_0|_{uncoded}(\text{OBO})(\text{dB}) - E_b/N_0|_{coded}(\text{OBO})(\text{dB}) \\ &= G(\text{linear})(\text{dB}) + \Delta G(\text{OBO})(\text{dB}) && (5.49) \end{aligned}$$

where the coding gain in a linear channel

$$G(\text{linear})(\text{dB}) = E_b/N_0|_{uncoded}(\text{linear})(\text{dB}) - E_b/N_0|_{coded}(\text{linear})(\text{dB}) \quad (5.50)$$

and the additional coding gain in a nonlinear channel over the coding gain in a linear channel,

$$\begin{aligned} \Delta G(\text{OBO})(\text{dB}) &= \Delta_{E_b/N_0}|_{uncoded}(\text{OBO})(\text{dB}) - \Delta_{E_b/N_0}|_{coded}(\text{OBO})(\text{dB}) \\ &= \text{TD}(\text{OBO})|_{uncoded}(\text{dB}) - \text{TD}(\text{OBO})|_{coded}(\text{dB}). && (5.51) \end{aligned}$$

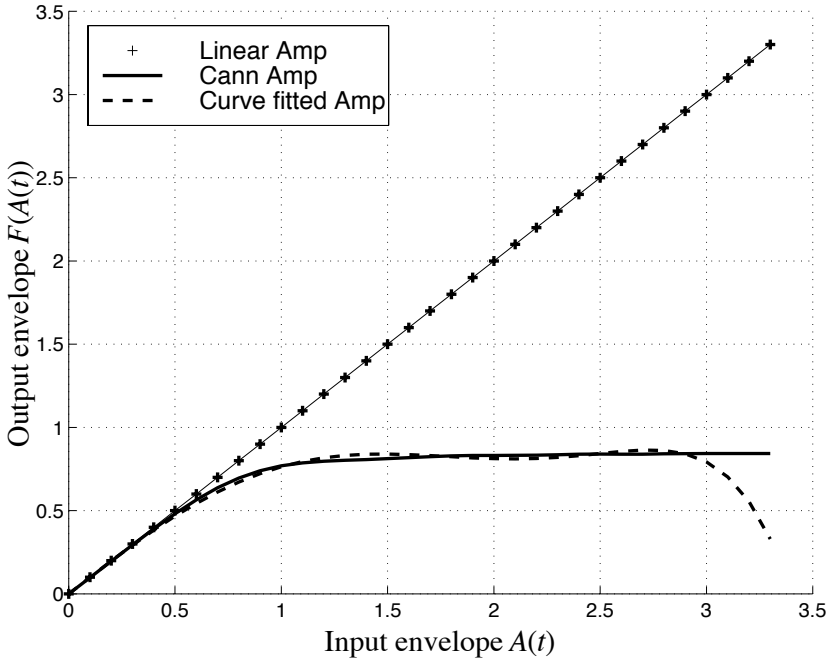

Figure 5.4: AM/AM of the amplifier model.

5.4.2 System Parameters

The average output power of the amplifier depends on the average input power to the amplifier, which is the the average of the square of the input envelope

$$\frac{1}{T}\int_0^T E[A^2(t)]dt \;=\; 2PM. \tag{5.52}$$

By letting $P = \chi/2M$, the average input power becomes

$$\frac{1}{T}\int_0^T E[A^2(t)]dt = \chi.$$

and the maximum value of the square of the envelope, $A^2(t)$,

$$\max_t A^2(t) = 2M^2P = M\chi$$

Hence, the PMEPR

$$\max_t A^2(t)/\{\frac{1}{T}\int_0^T E[A^2(t)]dt\} = M$$

which increases with M. This makes it difficult to use a polynomial model when there is a large number of carriers, M, since the polynomial model curve fitting usually diverges in the saturation region over the long input range.

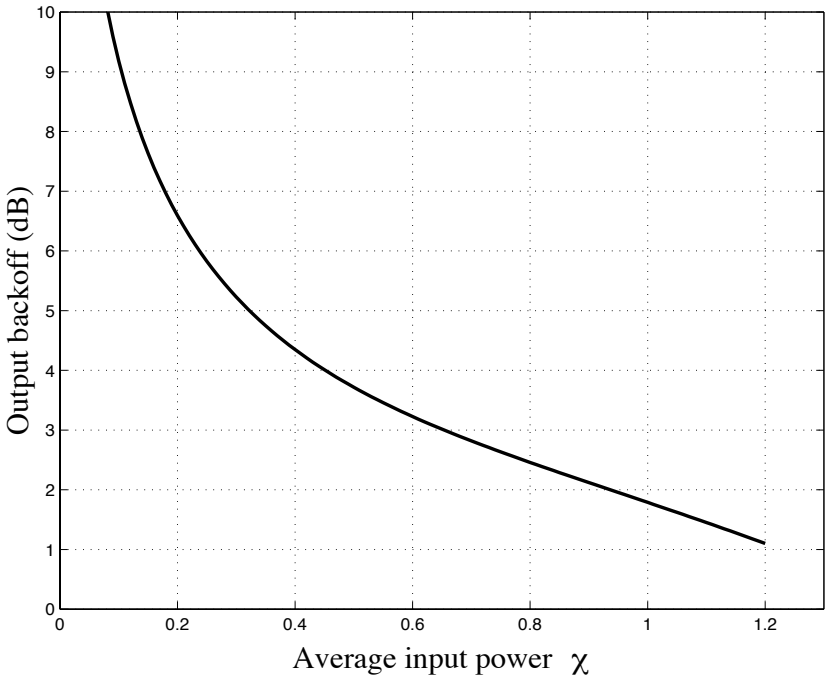

Figure 5.5: OBO vs. average input power χ.

Figure 5.4 shows the AM-AM $\mathcal{F}(A(t))$ where coefficients[1] of the polynomials are α_1=1.000, $\alpha_3 = -0.274$, $\alpha_5 = 0.0394$, $\alpha_7 = -0.002$, and $\alpha_k = 0$ for $k > 7$. Clearly, the polynomial model diverges when $A(t)$ becomes larger than 3. So, we need to confine the peak envelope to be less than 3. Even, a higher n can not extend the saturation region much further.

As a result, this analytical technique can be applied when the number of carriers are between 4 and 10. The lower (4) limit is from the Gaussian approximation assumption and the upper limit (10) is from the polynomial curve fitting. However, the lower limit can be decreased if we consider high N. The upper limit can be increased if our interest is in weak nonlinearities. Moreover, the performance in terms of OBO for high M is similar to that with $M = 10$ carriers, since the envelope statistics becomes asymptotically the same for large M, which is Rayleigh. Figure 5.5 shows the OBO versus the average input power χ. In the rest of this thesis, we restrict our interest to ten carriers ($M = 10$). Also, for the results to follow, we use spreading

[1]The coefficients are first obtained from curve fitting (least square) the Cann's bandpass solid state amplifier model shown in Figure 2.3 (b). Then, the coefficient are normalized so that linear α_1 is one (i.e., α_1=1.000).

gain factor $N_u = MT_b/T_c$, which is related to N as $N = R_c N_u$. For the same N_u, both coded and uncoded systems possess the same bandwidth; however, the effective spreading gain N of the coded system is smaller than that of the uncoded system by a factor of R_c^{-1}.

5.4.3 Performance Evaluation: BER, TDD, and ACPR

Figures 5.6(a) and (b), plot the uncoded system BER performance in AWGN and AWGN with multipath fading, respectively. BER performance of each plot is obtained for the spreading gain ($N_u = N$) 1, 4, 16, and 1000 at OBO = 2.5 dB. As can be seen in both figures, the BER degradation from the nonlinearity decreases as the spreading gain increases. However, even with a very large spreading gain $N_u = 1000$, there is still a residual E_b/N_0 degradation from the nonlinearity. This is due to the $\bar{\varrho}$ term in (5.28), which can not be eliminated even with an infinite N_u.

The TD for the uncoded system in AWGN and AWGN with fading are shown in Figures 5.7(a) and (b), respectively. The target BER is $P_b = 10^{-4}$ and all the remaining TD curves are also plotted for this target BER. As we may have expected, the E_b/N_0 degradation (difference between the curve and straight line) is large at low OBO. However, the difference rapidly decays as the OBO becomes large. Hence, for the large OBO, the main source of the power loss comes from the inefficient operation of the amplifier. Again, this loss at large OBO can be reduced by using the dc bias controlled scheme discussed in Chapter 4. The E_b/N_0 degradation in low OBO can be reduced by the large spreading gain factor N_u as can be seen in Figures 5.7. The optimum OBO, in terms of minimizing the dc power of the considered system, are found to be about 4, 3, and 2.5 dB in AWGN alone, and about 3, 2.5, and 1.5 dB in the multipath fading channel for the spreading gain (N_u) 1, 2, and 4, correspondingly. The result for the unspreaded system ($N_u = 1$) in AWGN shows a comparable result to that of Santella [51].

One interesting observation we have made is that the E_b/N_0 degradation in AWGN with fading is smaller than that of the AWGN alone, especially for small spreading factors. For the OBO 3 – 4 dB with $N_u = 1$, the E_b/N_0 degradation in fading is 1.7 – 0.3 dB where as suppose 2.5 – 0.8 dB in AWGN alone. These differences between the

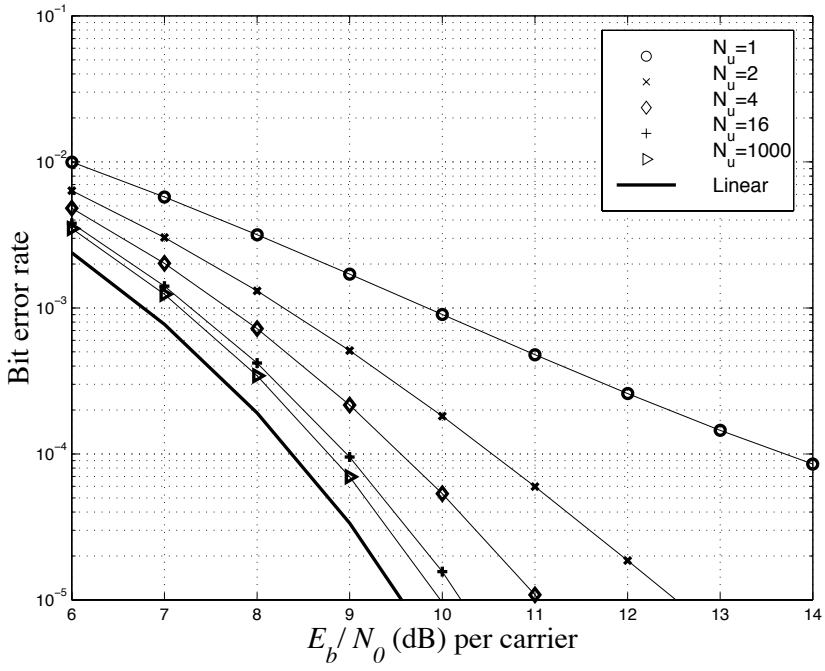

(a)

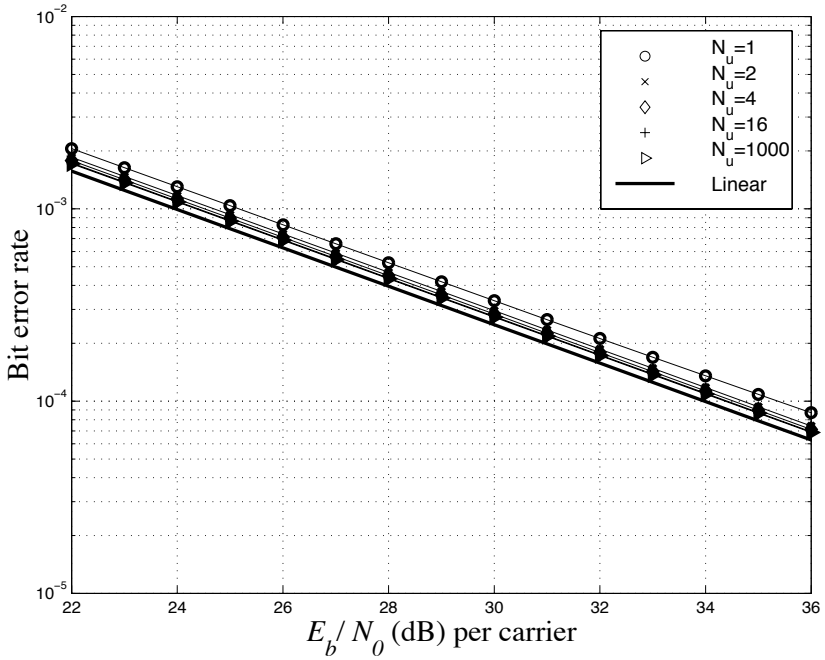

(b)

Figure 5.6: Uncoded system BER with OBO = 2.5 dB for different values of the spreading factor N_u: (a) in AWGN and (b) with fading.

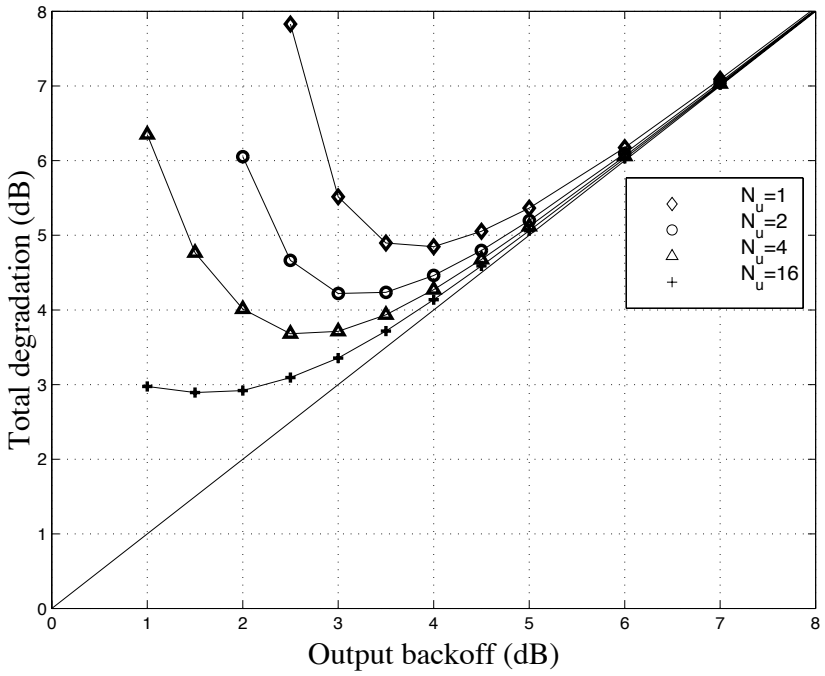

(a)

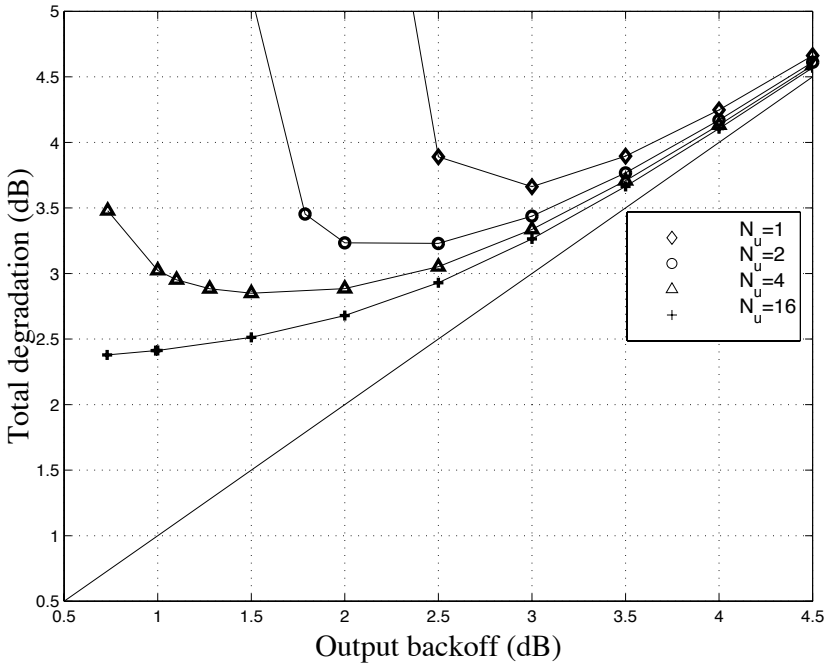

(b)

Figure 5.7: Total degradation (dB) of uncoded systems in: (a) AWGN and (b) with fading.

two channels become smaller as the spreading gain factor increases. The reason for this may be that when the signals are deeply faded (i.e. $\beta_q \approx 0$, which dominates the BER performance in fading), the intermodulation products are also faded, reducing its nonlinear effects, as can be seen from the term β_q in the denominator of (5.28). However, it is important to note that our fading model is slow fading, and the reduced nonlinear effects in fading channel may not be true for the fast fading channel (with high Doppler spread). Also, in the bit error floor region, the BER degradation in the fading can cause significant E_b/N_0 degradation, which will be seen in multi-user environment in Chapter 6.

For the coded systems in both AWGN and AWGN with multipath fading, we obtain upper bounds on the BER. Figure 5.8 shows the upper bound on the BER for OBO = 2.5 dB for N_u = 2, 4, and 16. We see a trend (less E_b/N_0 degradation with a larger spreading gain) similar to that of the uncoded systems, but at smaller BERs for a given E_b/N_0. The TDs for both AWGN and AWGN with fading channels are shown in Figure 5.9. The optimum OBOs for the system are found to be about 2.5 and 2 dB for both channels for the spreading factors (N_u) 2 and 4, respectively.

Figure 5.10 shows the coding gain in AWGN for different values of the spreading gain, N_u. The difference between the horizontal line and the curve is the ΔG(OBO). This additional gain increases as we operate in a more nonlinear region (lower OBO), especially for low values of N_u. The reason for this increased gain in low OBOs is not that the coded systems work better in nonlinear channel but that the performance of uncoded systems with small spreading factor is very sensitive to the nonlinearities, as can be seen in Figure 5.6(a). As the spreading gain increases, the nonlinear effects reduce and the coding gains in low OBOs become similar to the coding gain in the linear channel. Similarly, in the fading channel, since the nonlinear effects are negligible, we have found that ΔG(OBO) ≈ 0 for all OBO and G(linear) =27.6 dB. Note that the additional degradation (less than 2dB at $P_b = 10^{-4}$) from the nonlinearity in the fading channel is negligible, compared to the degradation from the fading itself (more than 25 dB at $P_b = 10^{-4}$) from AWGN. The E_b/N_0 degradation in AWGN is dominated by the nonlinearity, whereas in a fading channel the degradation is dominated by deep fades, not the nonlinearity even in the case of low OBO.

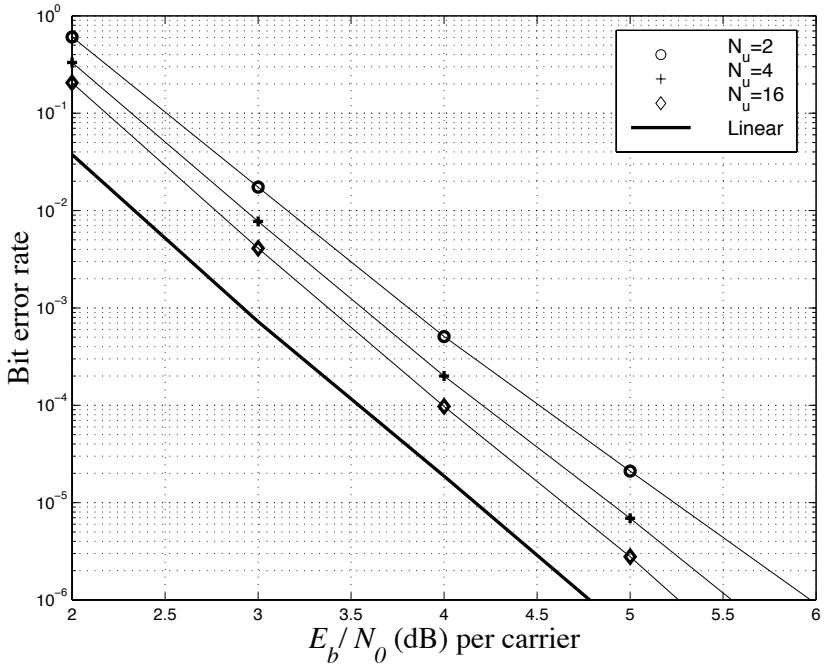

(a)

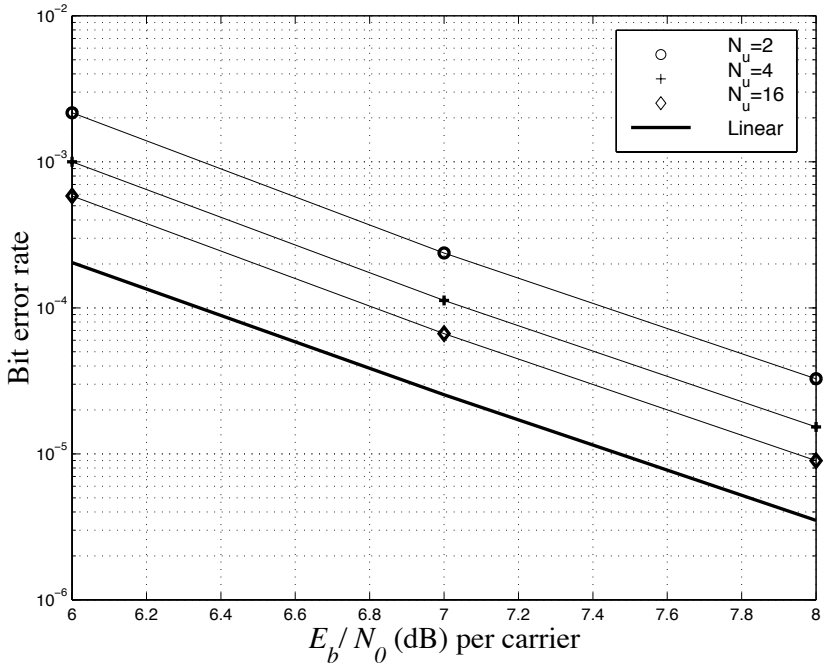

(b)

Figure 5.8: Upper bounds on BER of the coded systems with OBO = 2.5 dB for different values of the spreading factor N_u: (a) in AWGN and (b) with fading.

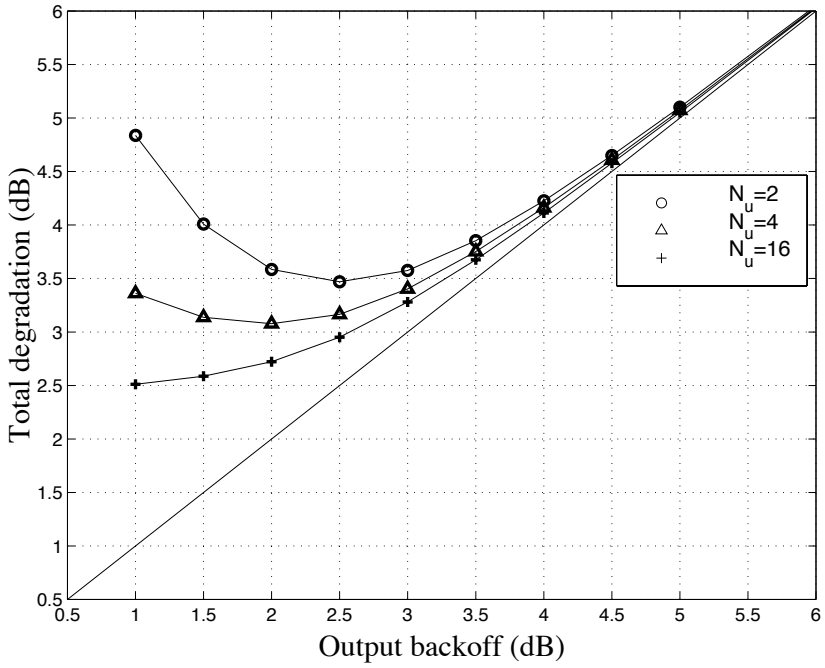

(a)

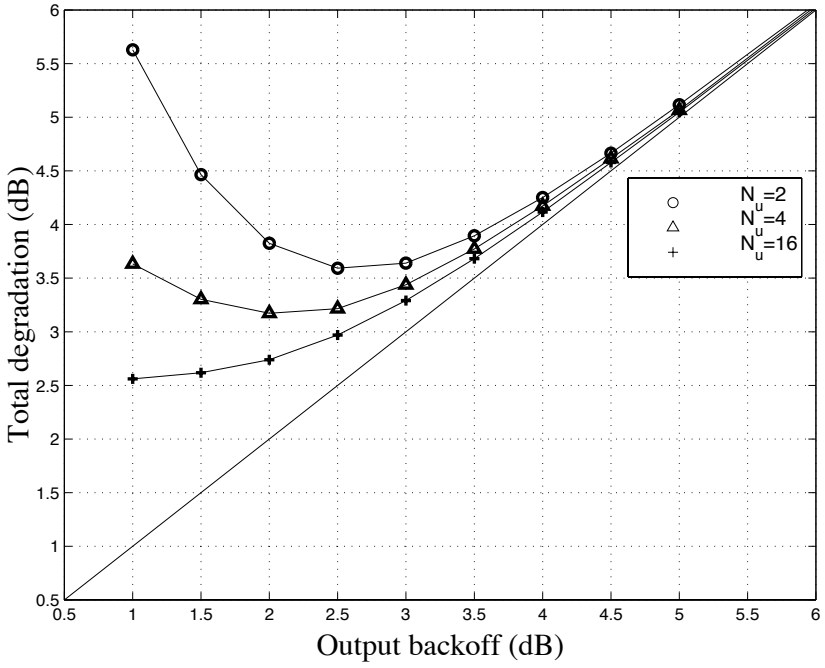

(b)

Figure 5.9: Total degradation (dB) of coded systems in: (a) AWGN and (b) with fading.

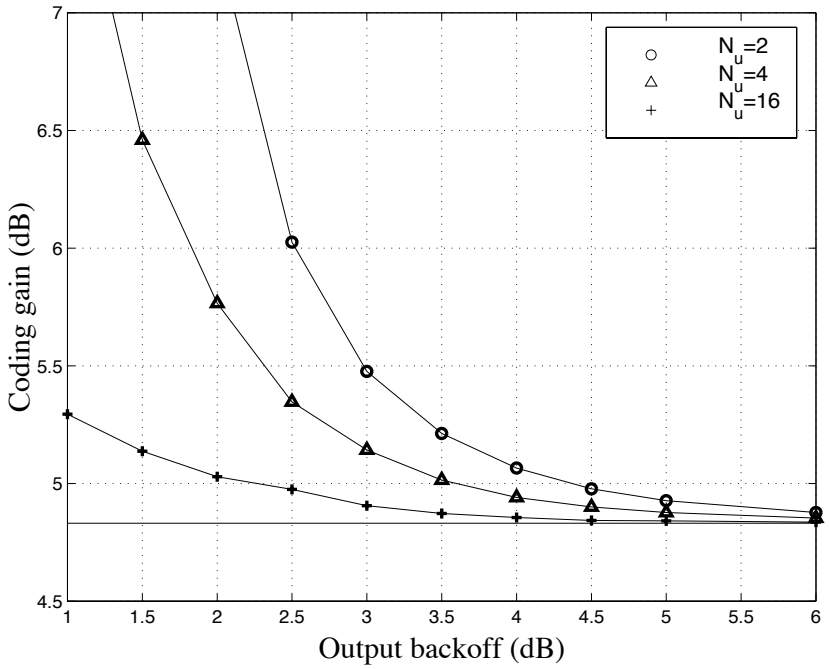

Figure 5.10: Coding gain (dB) in AWGN.

The carrier power of the intermodulation products which fall outside of the main channel are plotted along with the main channel carrier power at OBO = 2.5 dB in Figure 5.11(a). We normalize the center carrier power to be one. From Figure 5.11(a), we see the power regrowth outside of the main channel (the main channel corresponds to the carrier frequency index from 1 to 10). This out-of-band regrowth is more visible, if the figure is plotted in dB scale as shown in Figure 5.11(b). In addition, Figure 5.11(b) illustrates the out-of-band carrier power from the 3rd, 5th, and 7th order polynomial term by term. The closer the out-of-band signals are to the main channel, the higher the interference power is, and these out-of-band carrier powers are dominated by the intermodulation products from the 3rd order polynomial. Figure 5.12 shows the adjacent channel power ratio (ACPR) as a function of OBO. As can be seen, the ACPR (dB) reduces linearly (slowly) with the OBO (dB), whereas the E_b/N_0 degradation (dB) reduces rapidly with the OBO (dB).

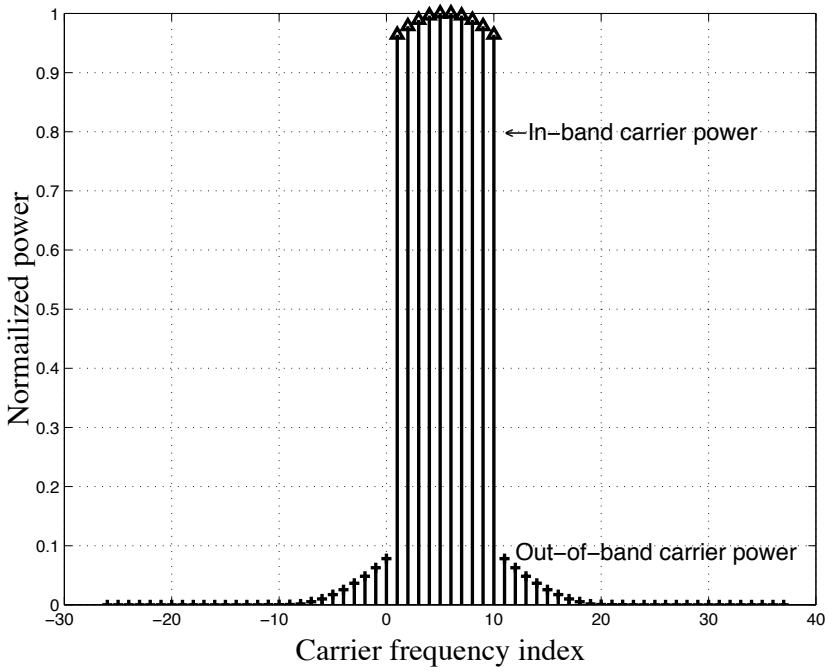

(a)

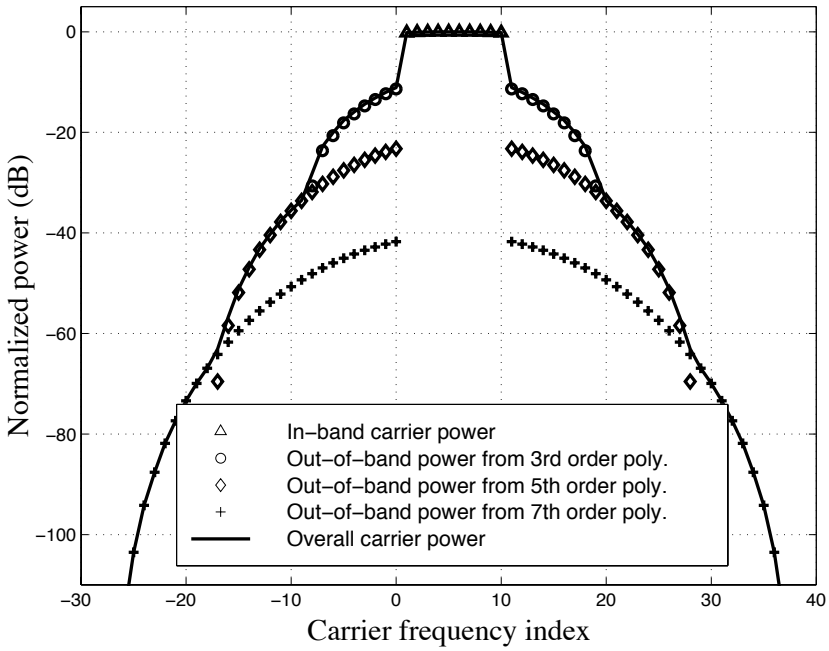

(b)

Figure 5.11: Output power distribution at OBO=2.5 (dB): (a) in a linear scale and (b) in dB.

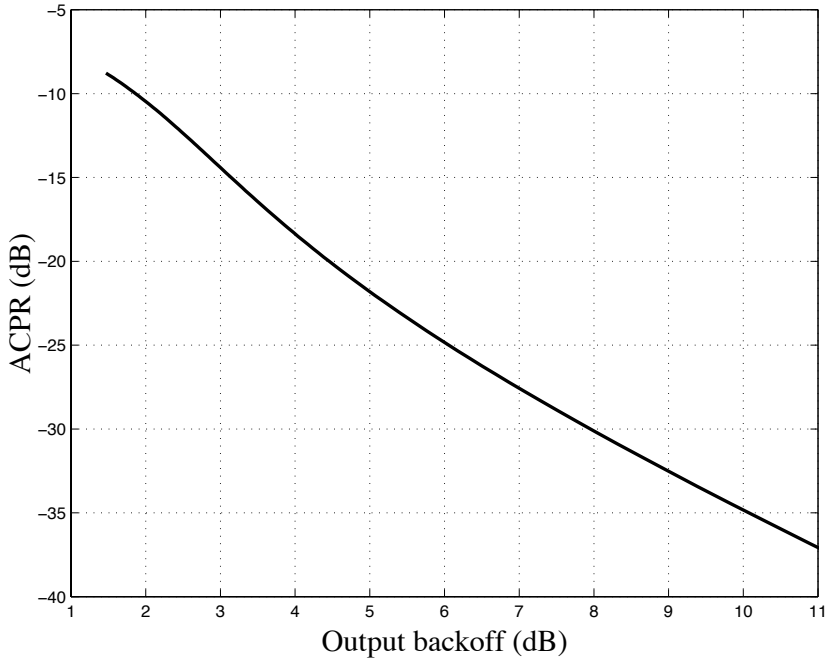

Figure 5.12: Adjacent channel power ratio (dB) vs. different values of OBO (dB).

5.5 Conclusion

In this chapter, the performance of a nonlinearly amplified, coded MCSS system has been analyzed in the presence of additive white Gaussian noise and multipath fading. We quantified the in-band and out-of-band interference from the nonlinearity by the E_b/N_0 degradation and the adjacent channel power ratio (ACPR), respectively. We also optimized power consumption of the systems in terms of TD, with a conventional fixed dc bias amplifier.

The obtained TD with the 7th order polynomial suggests that for an unspreaded system, the optimum OBO is about 2.5 – 4 dB for the coded and uncoded systems depending on the channel (AWGN or multipath fading). On the other hand, with spreading, the TD and the optimum OBO can be further reduced by more than 1 dB (this reduction is considerable in low OBO). This reduction is from the interference rejection capabilities of spread spectrum systems, which in turn reduce the effects from the intermodulation products. Thus, the BER degradation from the nonlinearities can be reduced significantly by the spread spectrum techniques. However, it is important to note that the ACPR (dB) reduces slowly with the OBO (dB) regardless of the

spreading gain factors. Hence, when the adjacent channel interference is a major concern, the OBO should be either increased or the envelope variations be reduced.

Interestingly, it was observed that in AWGN with independent slow flat fading for each carrier, the E_b/N_0 degradation from a nonlinearity is smaller than in AWGN alone for the uncoded MCSS system, especially those with small spreading factors.

Acknowledgments

The authors would like to thank Navin Kashyap and John D. Choi for their helpful comments on this chapter.

CHAPTER 6

Performance Analysis and Power Optimization of Single-Cell Multi-User MC-CDMA Systems

6.1 Introduction

In the last chapter, we analyzed the performance of single user MCSS systems in the presence of nonlinearities. Here, we extend our analysis to multi-user systems, in particular, single cell MC-CDMA systems. Furthermore, we will answer the questions raised in Chapter 1 and 2, as to how user location, which determines the degree of nonlinearity, affects the desired user's BER and how we find the sets of nonlinearities which will ensure minimum power consumption for all users in a given cell. We will explore answers using our optimization methods and analytical means which we will present in this chapter, and which we presented in the preceding chapters.

This chapter is organized as follows. In Section 6.2 the coded MC-CDMA system and the channel model are given. Section 6.3 presents the analysis of BER of the system, which is an extension of Chapter 5. In Section 6.4, we discuss numerical results including the performance trade off between the amplifier output backoff (OBO), user locations, and the BER sensitivity (E_b/N_o degradation). In addition, we optimize power consumption with conventional fixed dc bias amplifiers. In doing so, we identify the inherent power consumption problem for conventional amplifiers, when used in power controlled cellular systems. As a simple but effective solution to this problem, we apply dc bias controlled amplifiers presented in Chapter 4, and also

quantify power consumption. In Section 6.5, we conclude this chapter with a brief summary of our findings.

6.2 System and Channel Model

6.2.1 Transmitter

Before continuing, we briefly review transmitter model discussed in Chapter 2. The convolutionally encoded information sequence is interleaved and converted from a serial stream to M parallel streams. The binary code stream for the q-th carrier of a k-th user is denoted by $\{d_{k,q}^{(j)}\}$ where $d_{k,q}^{(j)} \in \{\pm 1\}$. The signal on the q-th carrier of the user k is then given by $d_{k,q}(t) = \sum_{j=-\infty}^{\infty} d_{k,q}^{(j)} p_{T_s}(t - jT_s)$ where $T_s = MT_bR_c$ is the symbol duration and $p_{T_s}(t)$ is a unit rectangular pulse in $t \in [0, T_s]$. The information bit duration before the parallel to serial process is T_b and the code rate is R_c. The signal on q-th carrier is then multiplied by an pseudo-random spreading code $a_{k,q}(t)$, where $a_{k,q}(t) = \sum_{j=-\infty}^{\infty} \sum_{i=0}^{N-1} a_{k,q}^{(i)} p_{T_c}(t - iT_c - jT_s)$ and the chip sequence $\{a_{k,q}^{(i)}\} \in \{\pm 1\}$ is a sequence of iid random variables with equal probabilities. Each spreading code has a chip duration of $T_c = T_s/N$ where N is the spreading gain of the system. Finally, the signals on each carrier are added together before amplification. The output signal of the modulator of the k-th user

$$x_k(t) = \sqrt{2P_k} \sum_{q=1}^{M} a_{k,q}(t) d_{k,q}(t) \cos\{(w_c + w_q)t + \theta_{k,q}\} \tag{6.1}$$

where P_k is the power per carrier of the k-th user, w_c is the carrier frequency and $\theta_{k,q}$ is an iid random variable uniformly distributed over $[0, 2\pi)$. The separation between q-th carrier frequency and center frequency w_c is denoted by $w_q = 2\pi q/T_c$.

The modulated signal is first nonlinearly amplified, then distorted by multipath fading and finally, corrupted by multiple access interference as well as AWGN.

6.2.2 Channel Model

The channel model adopted for each user is identical to the channel model used in Chapter 5, except additional assumptions needed for multi-user environment. The

additional assumptions made in this chapter are: each user undergoes different (independent) fading, and the propagation loss factor, which is a function of user distance to the base, is included in the fading channel. The amplifier and multipath fading model for each user are the same models used in Chapter 5. Hence, we only explain necessary parameters for the channel, and the common parameters are referred to Chapter 5.

Amplifier Model

The AM/AM of the amplifier for user k is represented by the odd order polynomial

$$\mathcal{F}(A_k(t)) = \alpha_1 A_k(t) + \alpha_3 A_k^3(t) + \alpha_5 A_k^5(t) + \ldots + \alpha_n A_k^n(t) \tag{6.2}$$

as in Chapter 5, where $A_k(t)$ denote the signal envelope of $x_k(t)$. The amplifier output signal of user k

$$\begin{aligned} y_k(t) &= \{\alpha_1 + \alpha_3 A_k^2(t) + \cdots + \alpha_n A_k^{n-1}(t)\}\, x_k(t) \\ &= x_k^{(1)}(t) + x_k^{(3)}(t) + \cdots + x_k^{(n)}(t) \end{aligned} \tag{6.3}$$

where $x_k^{(1)}(t) = \alpha_1 x_k(t)$ denotes the linearly amplified signal term, and $x_k^{(n)}(t)$ (for $n \geq 3$) denotes the amplified signal term from the n-th order nonlinearity, given by

$$x_k^{(n)}(t) = \alpha_n (\sqrt{2P_k})^n \sum_{l_1=1}^{M} \sum_{l_2=1}^{M} \cdots \sum_{l_n=1}^{M} \widetilde{a}_{k,n}(t) \widetilde{d}_{k,n}(t) \cos\{(w_c + w_{\jmath_n})t + \psi_{k,\jmath_n}\} \tag{6.4}$$

where

$$\widetilde{a}_{k,n}(t) = a_{k,l_1}(t)\, a_{k,l_2}(t) \cdots a_{k,l_n}(t) \tag{6.5}$$

$$\widetilde{d}_{k,n}(t) = d_{k,l_1}(t)\, d_{k,l_2}(t) \cdots d_{k,l_n}(t) \tag{6.6}$$

and where the index $\jmath_n = l_1 + l_2 - l_3 + \cdots + l_{n-1} - l_n$, i.e., $w_{\jmath_n} = 2\pi \jmath_n / T_c = w_{l_1} + w_{l_2} - w_{l_3} + \cdots + w_{l_{n-1}} - w_{l_n}$, and the phase $\psi_{k,\jmath_n} = \theta_{k,l_1} + \theta_{k,l_2} - \theta_{k,l_3} + \cdots + \theta_{k,l_{n-1}} - \theta_{k,l_n}$.

As explained in detail in Section 5.2.2, the nonlinearly amplified signal term $x_k^{(n)}(t)$ can be rewritten as the sum of the attenuated version of the original signal and the

interfering signal as

$$x_k^{(n)}(t) = \alpha_n(\sqrt{2P_k})^{n-1}\Lambda_n(M)x_k(t) + \alpha_n(\sqrt{2P_k})^n \underbrace{\sum_{l_1=1}^{M}\sum_{l_2=1}^{M}\cdots\sum_{l_n=1}^{M}}_{\mathcal{A}_n^c} \widetilde{a}_{k,n}(t)\widetilde{d}_{k,n}(t)\cos\{(w_c + w_{\jmath_n})t + \psi_{k,\jmath_n}\} \quad (6.7)$$

where

$$\mathcal{A}_n = \{(l_1, l_2, \ldots, l_n) : \bigvee_{\pi}((l_{\pi_1} = l_3) \wedge (l_{\pi_2} = l_5) \wedge \cdots \wedge (l_{\pi_r} = l_n))\} \quad (6.8)$$

where the OR ($\bigvee$) operation runs over all possible permutations of π of every combination of $r = \frac{n-1}{2}$ distinct integers from the set $\{1, 2, 4, \ldots, n-1\}$. Set $\mathcal{A}_n^c$ is the complement of set $\mathcal{A}_n$ and $\Lambda_n(M)$ is the number of in-phase signal from the $x_k^{(n)}(t)$.

Multipath Fading Model with a Propagation Loss

Each user undergoes independent frequency selective fading in the transmitted bandwidth but flat (frequency non-selective) fading for each carrier. Hence, the low-pass equivalent channel response for the q-th carrier of the k-th user

$$h_{L,k,q}(t) = \widehat{\beta}_{k,q}(t)\exp(j\varphi_{k,q}(t))\delta(t) \quad (6.9)$$

where $\widehat{\beta}_{k,q}(t) = \sqrt{g_k}\beta_{k,q}(t)$. $\beta_{k,q}(t)$ is an iid Rayleigh distributed random variable with $E[\beta_{k,q}^2(t)] = 1$. The channel propagation gain g_k of the k-th user is defined as $g_k = r_k^{-4}$, and r_k is the distance (normalized to the square root value of the product of the height of the base station antenna and the height of the mobile unit) between the user k and the base station. The phase $\varphi_{k,q}(t)$ is an iid random variable uniformly distributed over $[0, 2\pi)$. In this model, we assume a slowly changing Rayleigh fading for each carrier so that the fades ($\beta_{k,q}(t)$ and $\varphi_{k,q}(t)$) are constant over the symbol duration. In the rest of this chapter, we omit t in $\beta_{k,q}(t)$ and $\varphi_{k,q}(t)$. The independence of $\beta_{k,q}$ and $\varphi_{k,q}$ on the transmitted symbols can be justified by the use of sufficient interleaving. The random variables $\beta_{k,q}$ and $\varphi_{k,q}$ are constant over the symbol duration but independent from the symbol to symbol.

Figure 6.1 summarizes the channel model. Due to the nonlinear distortion, the amplifier output signal of each user consists of the desired signal and the intermodulation products. In order to account for the asynchronous transmission in the reverse

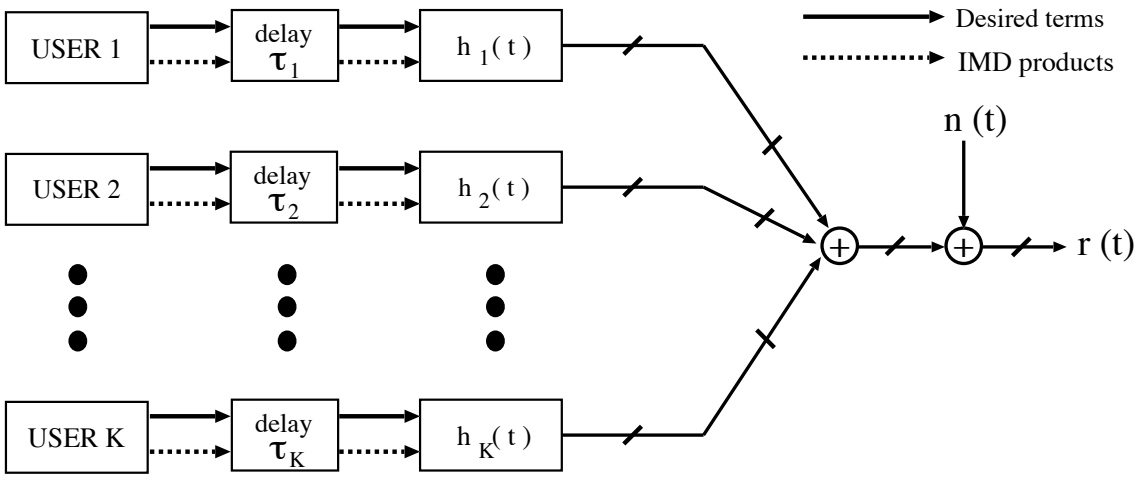

Figure 6.1: Channel model.

link, the random delay, uniformly distributed over $[0, T_s]$, is added to the starting bit time of each user.

The received signal after the fading and AWGN channel

$$r(t) \;=\; n(t) + \sum_{k=1}^{K} S_k(t-\tau_k) + \sum_{k=1}^{K} I_k(t-\tau_k) \tag{6.10}$$

where a desired signal of the k-th user, $S_k(t)$, is

$$H_k^{(1)}\sqrt{2P_k}\sum_{q=1}^{M}\widehat{\beta}_{k,q}a_{k,q}(t)d_{k,q}(t)\cos\{(w_c+w_q)t+\widehat{\theta}_{k,q}\} \tag{6.11}$$

and the interference signal of the k-th user nonlinearities

$$I_k(t) \;=\; I_k^{(3)}(t) + I_k^{(5)}(t) + \cdots + I_k^{(n)}(t) \tag{6.12}$$

where the interference from the n-th order nonlinearity $I_k^{(n)}(t)$ is

$$\alpha_n(\sqrt{2P_k})^n \sum_{l_1=1}^{M}\sum_{l_2=1}^{M}\cdots\sum_{l_n=1}^{M} \mathrm{I}_{\{\mathcal{A}_n^c\}}\widehat{\beta}_{\jmath_n}\widetilde{a}_{k,n}(t)\widetilde{d}_{k,n}(t)\cos\{(w_c+w_{\jmath_n})t+\widehat{\psi}_{k,\jmath_n}\} \tag{6.13}$$

where $H_k^{(1)} = \{\alpha_1 + \alpha_3(\sqrt{2P_k})^2\Lambda_3(M) + \cdots + \alpha_n(\sqrt{2P_k})^{n-1}\Lambda_n(M)\}$, $\widehat{\theta}_{k,q} = \theta_{k,q} + \varphi_{k,q}$, and $\widehat{\psi}_{k,\jmath_n} = \psi_{k,\jmath_n} + \varphi_{k,\jmath_n}$. The indicator function, $\mathrm{I}_{\{\zeta\}}$, equals one if the indices in the summation belong to set ζ, and, zero if not.

6.3 Performance Analysis

In this section, we first analyze the demodulator output statistics and then derive the average BER of each user for the uncoded systems. For the coded systems, we obtain an upper bound on the average BER. For the receiver, we consider a conventional single user matched filter receiver (a filter matched to the signal before the nonlinearities), which is not an optimum receiver even without nonlinearities. However, we consider this type of receiver because of its wide popularity in practice.

6.3.1 Demodulator and Its Output Statistics

The coherently demodulated symbol $Z_{l,q}$, after the integrate-and-dump filter of the q-th subcarrier of the l-th user for time, $t \in [\tau_l, \tau_l + T_s]$ is as follows:

$$\begin{aligned} Z_{l,q} &= \int_{\tau_l}^{T_s+\tau_l} r(t)\, a_{l,q}(t-\tau_l) \cos\{(w_c + w_q)(t-\tau_l) + \widehat{\theta}_{l,q}\}\, dt \\ &= \eta + D_{l,q} + S_{l,q} + \widehat{S}_{l,q} + J_{non,l,q} + I_{non,l,q} + \widehat{I}_{non,l,q} \end{aligned} \tag{6.14}$$

where

- η is a Gaussian distributed random variable with mean 0 and variance $\frac{N_0 T_s}{4}$.
- $D_{l,q}$ is the desired term for the q-th carrier of the l-th user.
- $J_{non,l,q}$ is the nonlinear interference term to the q-th carrier from the l-th user itself.
- $S_{l,q}$ is the linear interference from the q-th carrier of the other users.
- $\widehat{S}_{l,q}$ is the linear interference from the other (not q) carriers of the other users.
- $I_{non,l,q}$ is the nonlinear interference from the q-th carrier of the other users.
- $\widehat{I}_{non,l,q}$ is the nonlinear interference from the other (not q) carriers of the other users.

Without loss of generality, if we let $\tau_l = 0$, the desired term of the l-th user

$$D_{l,q} = H_l^{(1)} \sqrt{\frac{P_l}{2}} \widehat{\beta}_{l,q} d_{l,q}^{(0)} T_s \tag{6.15}$$

and the linear interference from the other users

$$S_{l,q} = \sum_{k=1,k\neq l}^{K} H_k^{(1)} \sqrt{\frac{P_k}{2}} \widehat{\beta}_{k,q} \cos\{\widehat{\theta}_{k,q} - \widehat{\theta}_{l,q} - w_q \tau_k\} \int_0^{T_s} a_{l,q}(t) a_{k,q}(t-\tau_k) d_{k,q}(t-\tau_k) dt \quad (6.16)$$

and

$$\widehat{S}_{l,q} = \sum_{k=1,k\neq l}^{K} H_k^{(1)} \sqrt{\frac{P_k}{2}} \sum_{m=1,m\neq q}^{M} \widehat{\beta}_{k,m} \int_0^{T_s} a_{l,q}(t) a_{k,m}(t-\tau_k) d_{k,m}(t-\tau_k) \cos\{(w_q - w_m)t + (w_c + w_m)\tau_k + \widehat{\theta}_{l,q} - \widehat{\theta}_{k,m}\} dt. \quad (6.17)$$

These equations (6.16) and (6.17) can be further simplified as

$$S_{l,q} = \sum_{k=1,k\neq l}^{K} H_k^{(1)} \sqrt{\frac{P_k}{2}} \widehat{\beta}_{k,q} \cos\{\widehat{\theta}_{k,q} - \widehat{\theta}_{l,q} - w_q \tau_k\} [d_{k,q}^{(-1)} R_{k_q,l_q}(\tau_k) + d_{k,q}^{(0)} \widehat{R}_{k_q,l_q}(\tau_k)] \quad (6.18)$$

and

$$\widehat{S}_{l,q} = \sum_{k=1,k\neq l}^{K} H_k^{(1)} \sqrt{\frac{P_k}{2}} \sum_{m=1,m\neq q}^{M} \widehat{\beta}_{k,m} \mathrm{sinc}(\frac{\Delta(w_q - w_m)}{2}) \Delta \cos\left\{\frac{\Delta(w_q - w_m)}{2} + (w_c + w_m)\tau_k + \widehat{\theta}_{l,q} - \widehat{\theta}_{k,m}\right\} \left\{d_{k,m}^{(-1)}[C_{k_m,l_q}(i+1-N) - C_{k_m,l_q}(i-N)] + d_{k,m}^{(0)}[C_{k_m,l_q}(i+1) - C_{k_m,l_q}(i)]\right\} \quad (6.19)$$

where $i = \lfloor \tau_k / T_c \rfloor$, $\Delta = \tau_k - iT_c$, the continuous partial cross correlation functions

$$R_{k_m,l_q}(\tau) = \int_0^{\tau} a_{k,m}(t-\tau) a_{l,q}(t) dt \quad (6.20)$$

$$\widehat{R}_{k_m,l_q}(\tau) = \int_{\tau}^{T_s} a_{k,m}(t-\tau) a_{l,q}(t) dt \quad (6.21)$$

and the discrete aperiodic cross correlation function

$$C_{k_m,l_q}(i) = \begin{cases} \sum_{j=0}^{N-1-i} a_{k,m}^{(j)} a_{l,q}^{(j+i)}, & 0 \leq i \leq N-1 \\ \sum_{j=0}^{N-1+i} a_{k,m}^{(j-i)} a_{l,q}^{(j)}, & 1-N \leq i < 0 \\ 0, & \text{otherwise.} \end{cases} \quad (6.22)$$

It can be easily shown that the continuous partial and the discrete aperiodic cross correlation function are related as

$$R_{k_m,l_q}(\tau) = T_c C_{k_m,l_q}(i-N) + (\tau - iT_c)[C_{k_m,l_q}(i+1-N) - C_{k_m,l_q}(i-N)] \quad (6.23)$$

$$\widehat{R}_{k_m,l_q}(\tau) = T_c C_{k_m,l_q}(i) + (\tau - iT_c)[C_{k_m,l_q}(i+1) - C_{k_m,l_q}(i)]. \quad (6.24)$$

The (6.19) are obtained using the following equality in [27],

$$\int_0^{T_s} d(t-\tau)a_{k,m}(t-\tau)a_{l,q}(t)\cos(wt+\varphi)dt = \Delta \mathrm{sinc}(\frac{\Delta}{2})\cos(\frac{\Delta w}{2}+\varphi)$$
$$\left\{d^{(-1)}[C_{k,l}(i+1-N) - C_{k,l}(i-N)] + d^{(0)}[C_{k,l}(i+1) - C_{k,l}(i)]\right\}. \quad (6.25)$$

Finally, the nonlinear interference terms

$$J_{non,l,q} = J^{(3)}_{non,l,q} + J^{(5)}_{non,l,q} + \cdots + J^{(n)}_{non,l,q} \quad (6.26)$$

$$I_{non,l,q} = I^{(3)}_{non,l,q} + I^{(5)}_{non,l,q} + \cdots + I^{(n)}_{non,l,q} \quad (6.27)$$

$$\widehat{I}_{non,l,q} = \widehat{I}^{(3)}_{non,l,q} + \widehat{I}^{(5)}_{non,l,q} + \cdots + \widehat{I}^{(n)}_{non,l,q} \quad (6.28)$$

where

$$J^{(n)}_{non,l,q} = \alpha_n \frac{(\sqrt{2P_l})^n}{2}\widehat{\beta}_{l,q}\sum_{l_1=1}^{M}\sum_{l_2=1}^{M}\cdots\sum_{l_n=1}^{M} \mathrm{I}_{\{A'_{n,q}\}}\, d^{(0)}_{l,l_1}d^{(0)}_{l,l_2}\cdots d^{(0)}_{l,l_n}$$
$$\cos(\psi_{l,\jmath_n} - \theta_{l,q})\int_0^{T_s}\widetilde{a}_{l,n}(t)a_{l,q}(t)\,dt \quad (6.29)$$

$$I^{(n)}_{non,l,q} = \sum_{k=1,k\neq l}^{K}\alpha_n\frac{(\sqrt{2P_k})^n}{2}\widehat{\beta}_{k,q}\sum_{l_1=1}^{M}\sum_{l_2=1}^{M}\cdots\sum_{l_n=1}^{M}\mathrm{I}_{\{\mathcal{A}'_{n,q}\}}\cos\{\widehat{\psi}_{k,\jmath_n} - \widehat{\theta}_{l,q} - w_q\tau_k\}$$
$$\int_0^{T_s} a_{l,q}(t)\widetilde{a}_{k,n}(t-\tau_k)\widetilde{d}_{k,n}(t-\tau_k)\,dt \quad (6.30)$$

$$\widehat{I}^{(n)}_{non,l,q} = \sum_{k=1,k\neq l}^{K}\alpha_n\frac{(\sqrt{2P_k})^n}{2}\sum_{m=1,m\neq q}^{M}\widehat{\beta}_{k,m}\sum_{l_1=1}^{M}\sum_{l_2=1}^{M}\cdots\sum_{l_n=1}^{M}\mathrm{I}_{\{\mathcal{A}'_{n,m}\}}$$
$$\int_0^{T_s}\cos\{(w_q - w_m)t + (w_c + w_m)\tau_k + \widehat{\theta}_{l,q} - \widehat{\psi}_{k,\jmath_n}\}$$
$$a_{l,q}(t)\,\widetilde{a}_{k,n}(t-\tau_k)\,\widetilde{d}_{k,n}(t-\tau_k)\,dt \quad (6.31)$$

where set $\mathcal{A}'_{n,q}$ is defined as $\{(l_1, l_2, \ldots, l_n) : (\jmath_n = q)\} \cap \mathcal{A}^c_n\}$, and $\jmath_n = l_1 + l_2 - l_3 + \cdots + l_{n-1} - l_n$. In $\widehat{I}_{non,l,q}$, the interference from the out-of-band carrier components are not included, since its effects are negligible.

Conditional Variance

The conditional variances of the linear interference are obtained as

$$\mathrm{Var}[S_{l,q}|\beta_{l,q}] = \sum_{k=1,k\neq l}^{K} (H_k^{(1)})^2 \frac{g_k P_k T_s^2}{4} \frac{2}{3N} \tag{6.32}$$

$$\mathrm{Var}[\widehat{S}_{l,q}|\beta_{l,q}] = \sum_{k=1,k\neq l}^{K} (H_k^{(1)})^2 \frac{g_k P_k T_s^2}{4N\pi^2} \sum_{m=1,m\neq q}^{M} \frac{1}{(m-q)^2} \tag{6.33}$$

using the following facts that

$$E[R_{k_m,l_q}^2(\tau_k) + \widehat{R}_{k_m,l_q}^2(\tau_k)] = \frac{2}{3N} \tag{6.34}$$

and

$$E[C_{k_m,l_q}(i)C_{k_m,l_q}(j)] = \begin{cases} N-|i|, & i=j \\ 0, & i\neq j \end{cases} \tag{6.35}$$

and, from [27],

$$E[\Delta^2 \mathrm{sinc}^2(\frac{\Delta}{2})\cos^2(\frac{\Delta w}{2}+\varphi)] = [\frac{T_c}{2\pi(m-q)}]^2. \tag{6.36}$$

Similar to the derivation of (5.22) in Chapter 5, the conditional variance of $J_{non,l,q}^{(n)}$ is obtained as

$$\mathrm{Var}[J_{non,l,q}^{(n)}|\beta_{l,q}] = \frac{P_l \beta_{l,q}^2 T_s^2}{4N} \{(H_{l,q}^{(n)})^2\} \tag{6.37}$$

$$(H_{l,q}^{(n)})^2 = \alpha_n^2 (2P_l)^{n-1} \sum_i |G_{i,q}(n)|^2. \tag{6.38}$$

The summation in (6.38) runs over the set of groups, and $|G_{i,q}(n)|$ denotes the size of each group, equivalently, the number of index vector $(l_1, l_2, l_3, \ldots, l_n)$ which belong to the group $G_{i,q}(n)$. The notion of group is explained in detail in Section 5.3. Also, similar to the derivations of (6.33) and (6.33), the conditional variances of $I_{non,l,q}^{(n)}$ and $\widehat{I}_{non,l,q}^{(n)}$ are derived as

$$\mathrm{Var}[I_{non,l,q}^{(n)}|\beta_{l,q}] = \sum_{k=1,k\neq l}^{K} \frac{g_k P_k T_s^2}{6N} (H_{k,q}^{(n)})^2 \tag{6.39}$$

$$\mathrm{Var}[\widehat{I}_{non,l,q}^{(n)}|\beta_{l,q}] = \sum_{k=1,k\neq l}^{K} \frac{g_k P_k T_s^2}{4N\pi^2} \sum_{m=1,m\neq q}^{M} \frac{(H_{k,m}^{(n)})^2}{(m-q)^2}. \tag{6.40}$$

Hence, the variance of $Z_{l,q}$,

$$\begin{aligned}\mathrm{Var}[Z_{l,q}|\beta_{l,q}] &= \frac{N_0 T_s}{4} + \frac{\widehat{\beta}_{l,q}^2 P_l T_s^2}{4N}(\widetilde{H}_{l,q}^{(n)})^2 + \sum_{k=1,k\neq l}^{K} \frac{g_k P_k T_s^2}{6N}\{(H_k^{(1)})^2 + \widetilde{H}_{l,q}^{(n)})^2\} \\ &\quad + \sum_{k=1,k\neq l}^{K} \frac{g_k P_k T_s^2}{4N\pi^2} \sum_{m=1,m\neq q}^{M} \frac{1}{(m-q)^2}\{(H_k^{(1)})^2 + (\widetilde{H}_{k,m}^{(n)})^2\}\} \quad (6.41)\end{aligned}$$

where

$$(\widetilde{H}_{k,q}^{(n)})^2 = (H_{k,q}^{(3)})^2 + (H_{k,q}^{(5)})^2 + \cdots + (H_{k,q}^{(n)})^2 \quad (6.42)$$

and the conditional mean

$$E[Z_{l,q}|\beta_{l,q}] = \sqrt{2P_l}\widehat{\beta}_{l,q} d_{l,q}^{(0)} T_s H_l^{(1)}/2. \quad (6.43)$$

6.3.2 Bit Error Rate Performance

Uncoded System Performance

If we approximate the multiple access interference and the nonlinear interference by a Gaussian random variable, the conditional BER of the q-th subcarrier of the l-th user is

$$P_{b,l,q|\beta_{l,q}} = Q\left(\sqrt{\mathrm{SNR}(\beta_{l,q})}\right) \quad (6.44)$$

where $Q(x) = (1/\sqrt{2\pi})\int_x^\infty \exp(-u^2/2)du$. The conditional $\mathrm{SNR}(\beta_q)$ given $\beta_{l,q}$,

$$SNR(\beta_q) = \frac{E^2[Z_{l,q}|\beta_{l,q}]}{\mathrm{Var}[Z_{l,q}|\beta_{l,q}]} = \frac{2\beta_{l,q}^2\bar{\gamma}}{(1+\bar{\varrho}_l)(1+v_{l,q}^K\bar{\gamma}) + \beta_{l,q}^2\bar{\gamma}\frac{\varrho_{l,q}}{N}} \quad (6.45)$$

where

- $\bar{\gamma}_{l,q} = [(H_l^{(1)})^2 + (\widetilde{H}_{l,q}^{(n)})^2]g_l P_l T_s/N_0$: average received symbol-energy-to-noise power density ratio (E_s/N_0) on the q-th carrier of the l-th user.
- $\bar{\gamma}_l = \frac{1}{M}\sum_{q=1}^{M}\bar{r}_{l,q}$: E_s/N_0 per carrier of the l-th user.
- $\varrho_{l,q} = [(\widetilde{H}_{l,q}^{(n)})^2]/(H_l^{(1)})^2$: normalized nonlinear interference variance on a q-th carrier of the l-th user.
- $\bar{\varrho}_l = \frac{1}{M}\sum_{q=1}^{M}\varrho_{l,q}$: normalized nonlinear interference variance of the l-th user per carrier.

- $v_{l,q}^K = \frac{1}{N}\sum_{k=1,k\neq l}^{K}\{(\frac{1}{1+\bar{\varrho}_k})(\frac{2}{3}(1+\varrho_{k,q}) + \frac{1}{\pi^2}\sum_{m=1,m\neq q}^{M}\frac{1+\varrho_{k,m}}{(m-q)^2})\}$.

In (6.45), from the perfect power control assumption, $\bar{\gamma}_l = \bar{\gamma}_k = \bar{\gamma}$ for all k. The average received bit-energy-to-noise power density ratio (E_b/N_0) per carrier is $R_c^{-1}\bar{\gamma}$.

Hence, the unconditional bit error rate of q-th subcarrier of l-th user

$$P_{b,l,q} = \frac{1}{2} - \frac{1}{\sqrt{2\pi}}\int_{u=0}^{\sqrt{\frac{2N}{\varrho_{l,q}}}}\exp\{-\frac{u^2}{2}[1+\frac{(1+\bar{\varrho}_l)(1+\bar{\gamma}v_{l,q}^K)}{\bar{\gamma}(1-\frac{\varrho_{l,q}u^2}{2N})}]\}du \tag{6.46}$$

and the average BER of l-th user,

$$P_{b,l} = \frac{1}{M}\sum_{q=1}^{M}P_{b,l,q}. \tag{6.47}$$

Upper Bounds on the Bit Error Rate for Coded Systems

For the coded system, we consider a convolutional code of rate $R_c = 1/2$ with constraint length 7 with maximum likelihood decoding as in Chapter 5. We assume that a perfect channel estimate is available so that we can weight the output of the integrate-and-dump filter by the factor

$$g_{l,i} = E[Z_{l,i}|\beta_{l,i}, d_l^{(i)} = 1]/\mathrm{Var}[Z_{l,i}|\beta_{l,i}]. \tag{6.48}$$

We also assume that we have a sufficiently large sized interleaver so that code symbols are independent of each other after the deinterlever. Bounds on the BER of user l can be expressed as follows [85, page 327]

$$P_{b,l} \leq \sum_{d=d_{free}}^{\infty} w_d P_{l,2}(d) \tag{6.49}$$

where w_d is the total number of nonzero information bits on a path with hamming distance d, d_{free} is the free distance of the code, and $P_{l,2}(d)$ is the error probability between two codewords which differ in d symbols. We use truncated w_d up to approximately $d = 30$ which are tabulated in [86].

Similar to the derivation of (5.39), the pairwise error probability can be upper bounded by

$$P_{l,2}(d) \leq \frac{1}{\pi}\int_0^{\pi/2} I_{in}^d(\theta)\, d\theta \tag{6.50}$$

where

$$I_{in}(\theta) = \int_0^{\infty} \exp\{-\frac{1}{2\sin^2\theta}\mathrm{SNR}_{min}(\beta_{l,i})\} f_{\beta_{l,i}}(\beta_{l,i}) d\beta_i \tag{6.51}$$

and $f_{\beta_{l,i}}(\beta_{l,i})$ is a pdf of the Rayleigh random variable, and

$$\mathrm{SNR}_{min}(\beta_{l,i}) = \frac{2\beta_{l,q}^2 \bar{\gamma}}{(1+\bar{\varrho}_l)(1+v_l^K\bar{\gamma}) + \beta_{l,q}^2 \bar{\gamma}\frac{\varrho_l}{N}}. \tag{6.52}$$

The ϱ_l and v_l^K in the above equation, are taken from the maximum value of $\varrho_{l,q}$ and $v_{l,q}^K$ among the M carriers, respectively. In other words, $\varrho_l = \varrho_{l,\hat{q}}$, and $v_l^K = v_{l,\hat{q}}^K$, for $\hat{q} = \lfloor (M+1)/2 \rfloor$.

By a change of variable (letting $\mathrm{SNR}_{min}(\beta_{l,i}) = y$), (6.51) becomes

$$I_{in}(\theta) = \int_0^{\frac{1}{\nu}} \exp\{-\frac{y}{2\sin^2\theta}\}\left(\frac{u}{(1-\nu y)^2}\exp\{-\frac{uy}{1-\nu y}\}\right) dy \tag{6.53}$$

where $u = (1+\bar{\varrho}_l)(1+v_l^K\bar{\gamma})/(2\bar{\gamma})$ and $v = \varrho_l/(2N)$.

6.3.3 Approximation of $P_{l,2}(d)$

In the multiple access systems, the spreading gain N is usually much larger than the number of users. For large N, (6.52) can be approximated by

$$\mathrm{SNR}_{min}(\beta_{l,i}) \approx \frac{2\beta_{l,q}^2 \bar{\gamma}}{(1+\bar{\varrho}_l)(1+v_l^K\bar{\gamma})} \tag{6.54}$$

and, it can be easily shown that

$$P_{l,2}(d) \leq \frac{1}{2} - \frac{1}{2}\sum_{i=0}^{d-1} \binom{2i}{i} \frac{\lambda(1-\lambda^2)^i}{2^{2i}} \tag{6.55}$$

where

$$\lambda = \sqrt{\frac{\bar{\gamma}}{(1+\bar{\varrho}_l)(1+v_l^K\bar{\gamma})+\bar{\gamma}}}. \tag{6.56}$$

6.4 Numerical Results and Discussion

In this section, we first describe basic system parameters considered in the performance evaluation. In particular, we discuss user location configuration, and we

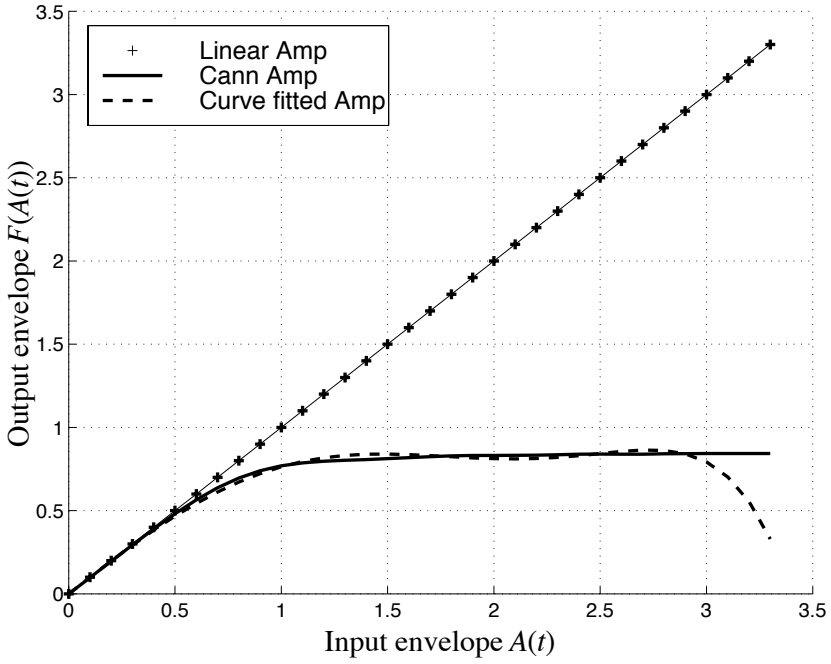

Figure 6.2: AM/AM of the amplifier model.

explain how we set the amplifier operation point (i.e., OBO) of each user, depending on the user locations. Then, we numerically evaluate BER and E_b/N_0 degradation. Finally, we discuss user power consumption problems and our approach to resolving them.

6.4.1 System Parameters

The considered amplifier AM-AM model, which was also used in Chapter 5, is shown in Figure 6.2, where the polynomial coefficients are: α_1=1.000, $\alpha_3 = -0.274$, $\alpha_5 = 0.0394$, $\alpha_7 = -0.002$, and $\alpha_k = 0$ for $k > 7$. In addition, for the results to follow, we consider $M = 10$ subcarriers and denote the spreading gain factor as $N_u = MT_b/T_c$ instead of N, where $N = R_c N_u$.

We assume that every user has an identical amplifier. The amplifier output backoff (OBO) of user k is defined as the ratio of maximum output power to the average in-

band output power, which is given by

$$\begin{aligned} \mathrm{OBO}_k &= \frac{1/2 \max\{\mathcal{F}^2(A_k(t))\}}{\sum_{q=1}^{M}\{(H_k^{(1)})^2 P_k + (\widetilde{H}_{k,q}^{(n)})^2 P_k\}} \\ &= \frac{\max\{\mathcal{F}^2(A_k(t))\}}{2MP_k(H_k^{(1)})^2(1+\bar{\varrho}_k)}. \end{aligned} \tag{6.57}$$

It should be noted that $\mathcal{F}(A_k(t))$ is the same for all users, since every user uses an identical amplifier. However, because of the power control requirement, the user amplifier operation points are different according to their locations. For example, the OBO of user l at r_l is related to the OBO of user k at r_k by

$$\mathrm{OBO}_l/\mathrm{OBO}_k = (r_k/r_l)^{\psi}. \tag{6.58}$$

Since the channel propagation loss factor (ψ) in cellular radio environments is usually 4, we use the same factor in our study.

In order to represent general cases, we consider two deterministic locations, r_1 and r_2, from the base station with $r_2/r_1 = 20$. The user at r_2 can operate his amplifier in very nonlinear regions (for example, OBO in the range 0 - 2 dB). However, the user at r_1 operates virtually in the linear region from the power control requirement: the OBO of the user at r_1 should be less than that of the user at r_2 by 52 dB ($40 \log 20$). Hence, in the following, we evaluate the performance of the user of interest (User A) as a function of the OBO of the users located at r_2, regardless of the position of User A (r_1 or r_2).

6.4.2 Performance Evaluation

Figures 6.3(a) and (b), plot the uncoded system BER of User A in AWGN and AWGN with multipath fading, respectively. The BER performance of each plot is obtained for the spreading factors ($N_u = N$) 80, 160, and, 300 when all $K = 30$ users (including User A) are located at r_2. BER is obtained for OBO = 2.5 dB and linear amplification. As shown in both figures, the BER degradation, from the nonlinearity and multiple access interference, decreases as the spreading factor increases. However, the additional degradations, due to nonlinearities, remain even with higher N_u.

Figure 6.4 shows uncoded system BER of User A for different numbers of users when all users (including User A) are at r_2 with $N_u = 300$. Once again, OBO = 2.5 dB

and linear amplification is considered. As the number of users increases, the BER degrades. The nonlinear effects cause additional degradations to the already increased BER due to the multiple access interference and multipath fading. Figure 6.5 shows the uncoded system BER of User A for different OBOs when all $K = 30$ users (including User A) are at r_2 with spreading factor $N_u = 300$. The BER increases as the OBO decreases due to the increased nonlinear signal distortion. In the fading channel, the BER decay rate is not as steep as in the AWGN channel. This results in a higher BER than that in the AWGN channel. In addition, a BER floor occurs for a large E_b/N_0 due to the multi-user interference. The results obtained in the uncoded systems suggest that the degradation from the nonlinearities is not as considerable as from the multiple access interference and fading alone.

In order to examine the nonlinear effects as a function of user locations, we consider two more possible configurations: when User A is at r_2 and $K-1$ other users are at r_1, and when User A is at r_1 and $K-1$ other users are at r_2. In these scenarios, the number of users is $K = 30$, and the spreading factor is $N_u = 300$. Figure 6.6 shows the BER of User A when User A is at r_2 and 29 other users are at r_1. The BER performance in this case is very similar to Figure 6.5 when all the users are at r_2. This similarity in BER suggests that the BER of User A does not depend on the other users' locations. This interpretation becomes more valid in Figure 6.7 when User A is at r_1 and 29 other users are at r_2. There is almost no BER degradation of User A when User A is operating in the linear region (note that User A is at r_1), regardless of the other users' OBOs. This issue will be discussed in detail when we examine coded system performance.

As can be seen in the preceding figures, the uncoded system performances can be poor (BER floor above $P_b = 10^{-2}$), especially in the fading channel or when the number of users in a cell becomes large. Hence, channel coding is usually required to make communication acceptable. For coded system evaluation, we consider a convolutional code of rate $R_c = 1/2$ with constraint length 7. Figures 6.8 and 6.9 show the upper bounds on BER of User A for different values of the spreading factor and the number of users, respectively. In these figures, we examine BER with both OBO =2.5 dB and linear amplification, when all the users (including User A) are at

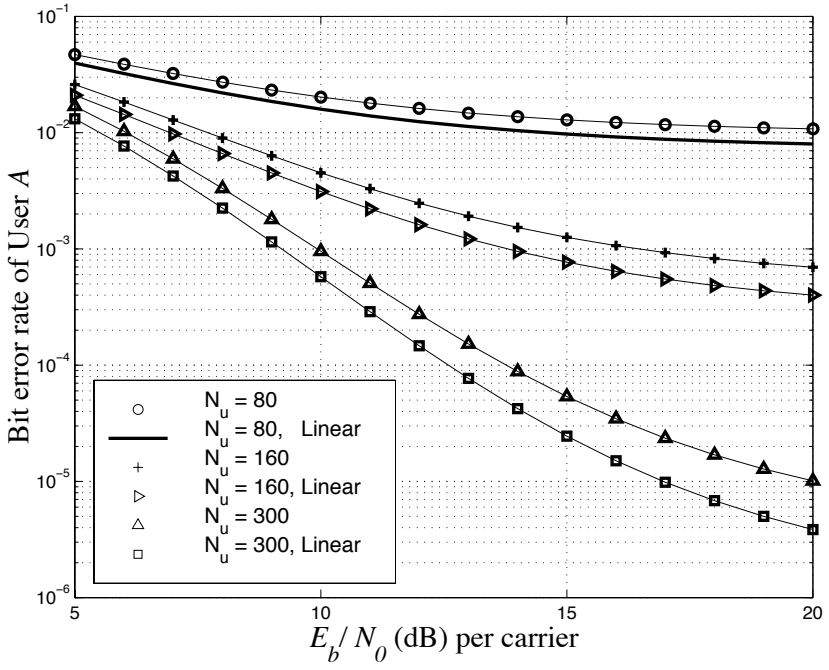

(a)

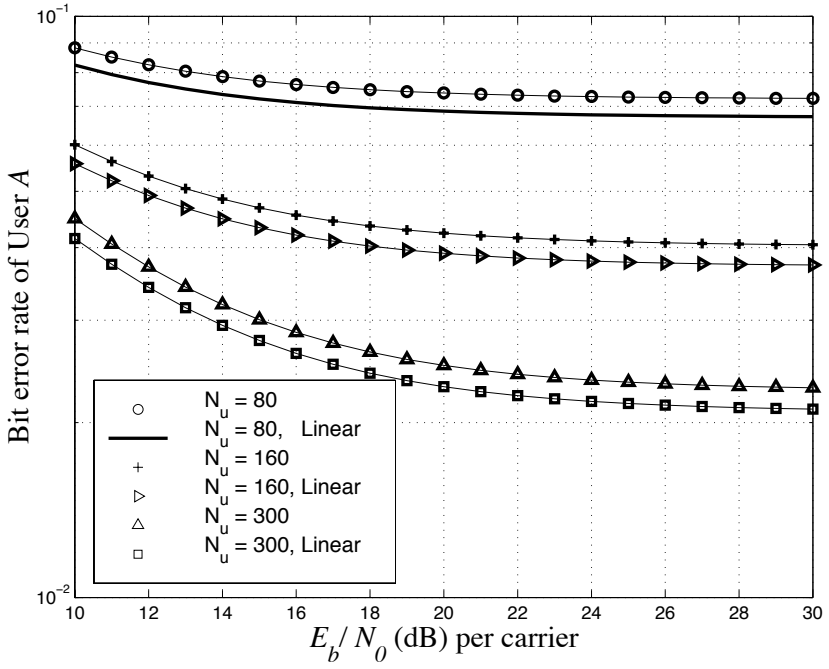

(b)

Figure 6.3: Uncoded system BER when all 30 users are at r_2 with OBO = 2.5 dB for different values of the spreading factor N_u: (a) in AWGN and (b) with fading.

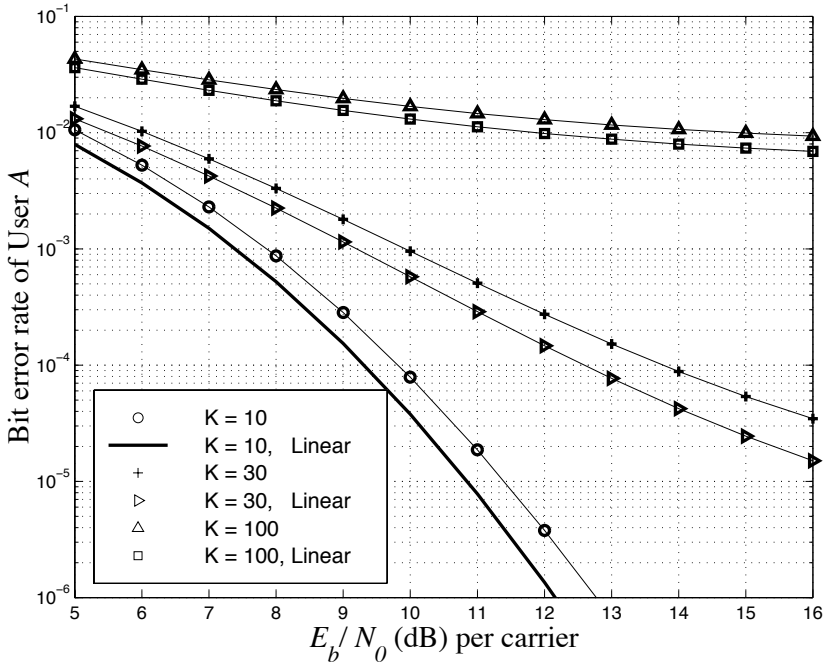

(a)

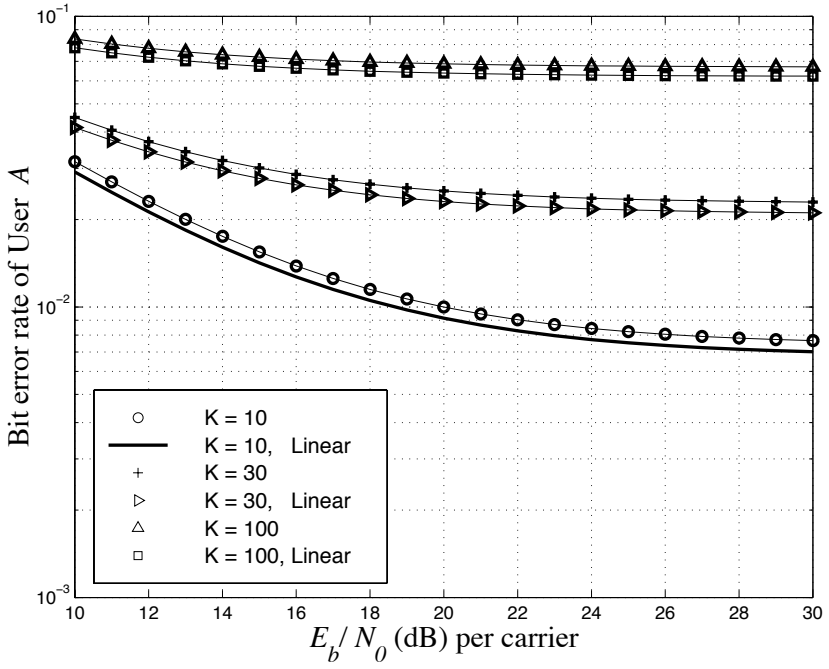

(b)

Figure 6.4: Uncoded system BER when all K users are at r_2 with OBO = 2.5 dB and $N_u = 300$ for different numbers of user, K: (a) in AWGN and (b) with fading.

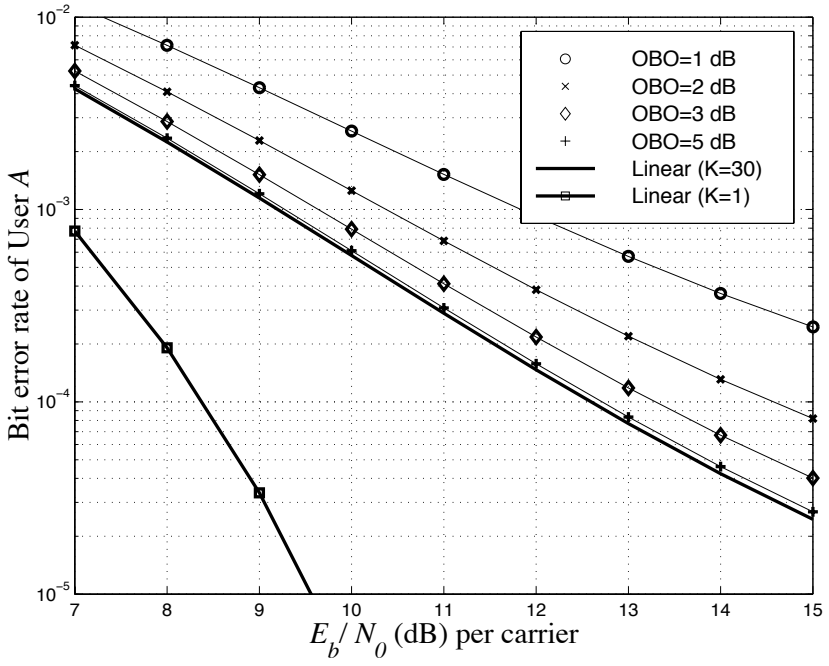

(a)

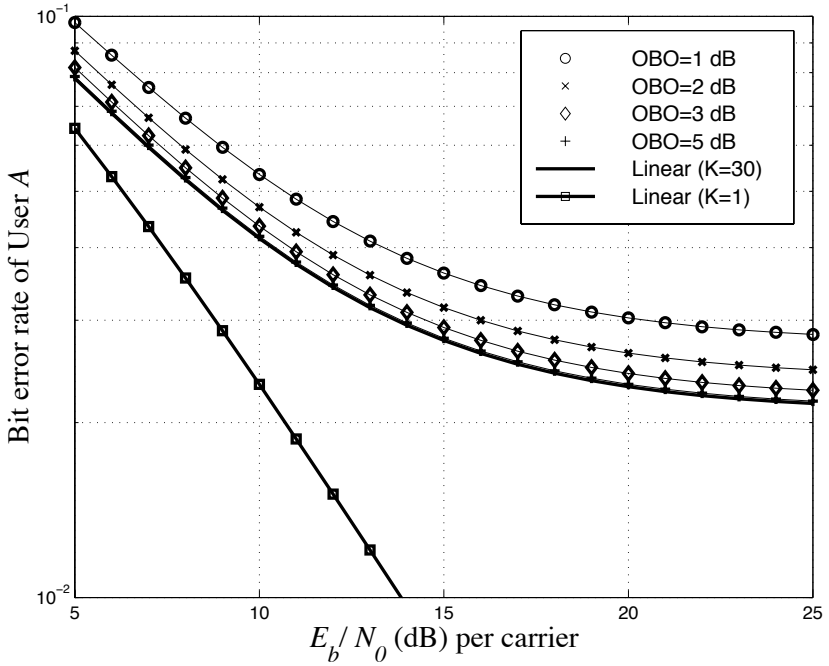

(b)

Figure 6.5: Uncoded system BER when all 30 users are at r_2 for different values of OBO: (a) in AWGN and (b) with fading.

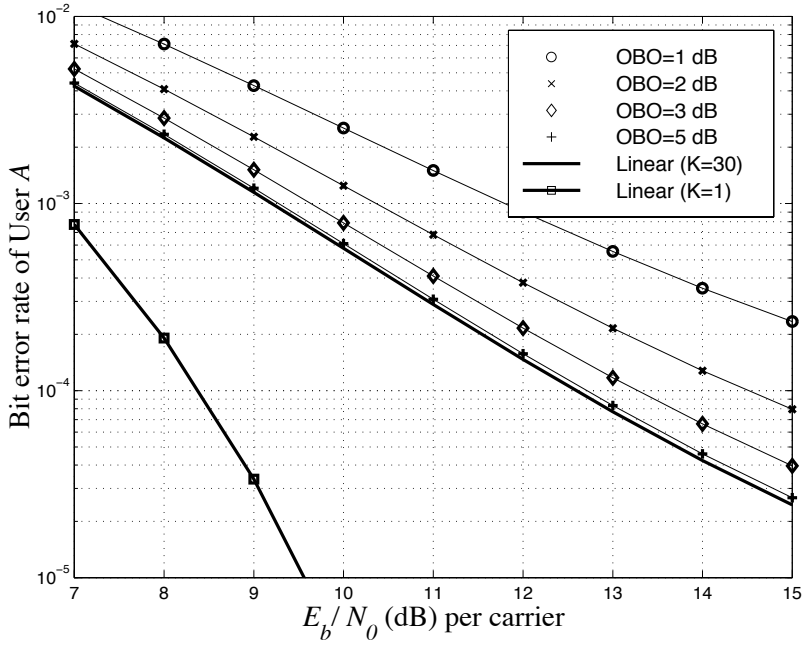

(a)

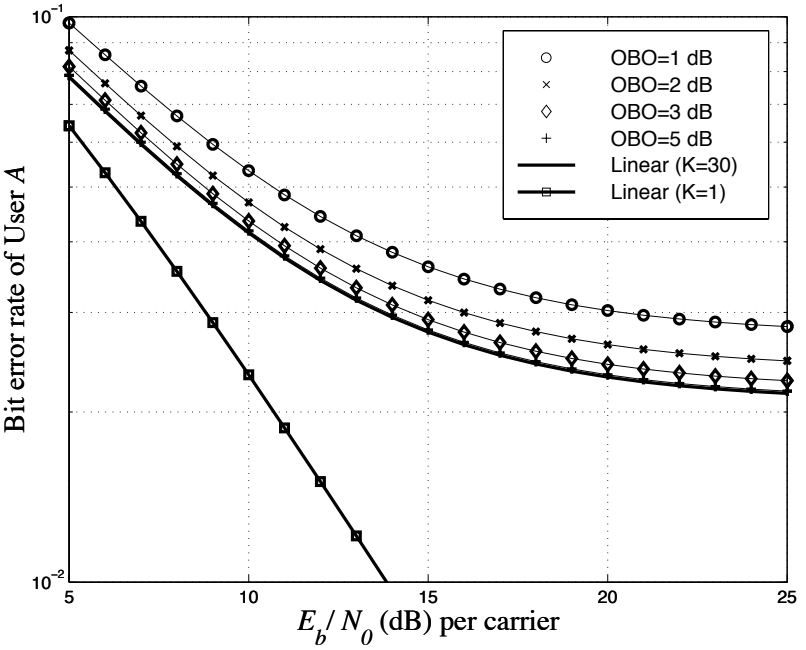

(b)

Figure 6.6: Uncoded system BER when User A is at r_2 and 29 other users are at r_1 for different values of OBO of users at r_2 (User A): (a) in AWGN and (b) with fading.

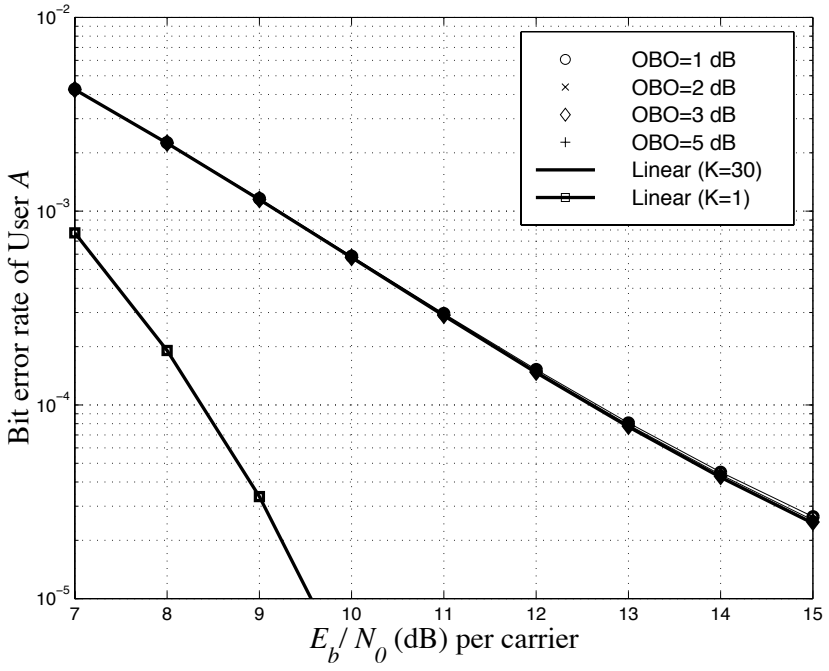

(a)

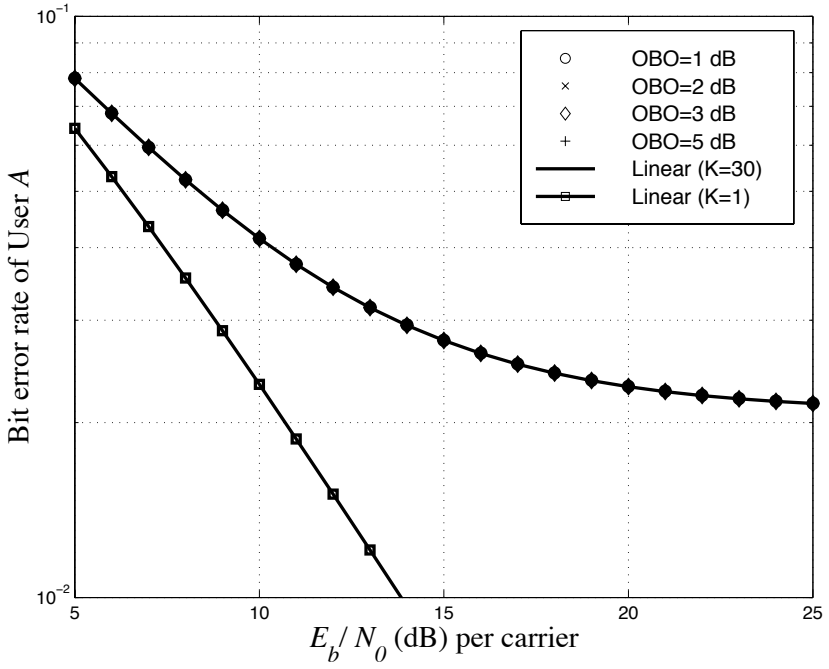

(b)

Figure 6.7: Uncoded system BER when User A is at r_1 and 29 other users are at r_2 for different values of OBO of users at r_2: (a) in AWGN and (b) with fading.

r_2. The results for the coded systems are similar to the uncoded cases, except that BER is much smaller in the coded systems for a given E_b/N_0. At $E_b/N_0 = 5$ dB with $K = 30$ and $N_u = 300$ in AWGN, the uncoded system BER is about 10^{-2} while it is about 10^{-5} in coded systems.

In order to examine the nonlinear effects on the coded system as a function of user locations, we consider three possible configurations as we did for the uncoded systems. The results are shown in Figures 6.10 – 6.12. The trend in the figures is very similar to that in the uncoded case, that is, the BER of User A does not depend on the locations of other users. This trend is quantified in Figure 6.13, by the E_b/N_0 degradation at the BER of 10^{-4}. Again, the E_b/N_0 degradation is the increased in required E_b/N_0 from the linear case at target BER, $P_b = 10^{-4}$. The E_b/N_0 degradation of User A is plotted versus the OBO of the users at r_2. When the amplifier OBO is close to 1 dB, the degradation is as large as 2.2 dB and 6.2 dB in the AWGN and fading channels, respectively. The performances, in both AWGN and AWGN with fading, are noticeable only when User A has low OBOs (i.e., when User A is at r_2 and the OBO of User A is low). The degradation in the fading channel at low OBOs is a little more sensitive to the low OBOs of other users than in the AWGN case. This is because our considered BER (10^{-4}) is near the BER floor region of the fading channel so that a slight increase in BER from additional nonlinear effects causes relatively large E_b/N_0 degradation, unlike in the AWGN case.

The results obtained in both coded and uncoded systems suggest that the main source of the nonlinear degradation of User A is the self-nonlinear interference of User A (low OBO of User A) and not the nonlinear interference of other users. This result can be explained intuitively if we bear in mind that the other users, regardless of their OBOs, all contribute interference (either linear or nonlinear) to User A. As long as the interference power from each of the other users is the same, the interference from the distorted waveforms (from the nonlinearities) of other users is only slightly more than the interference from their undistorted waveforms.

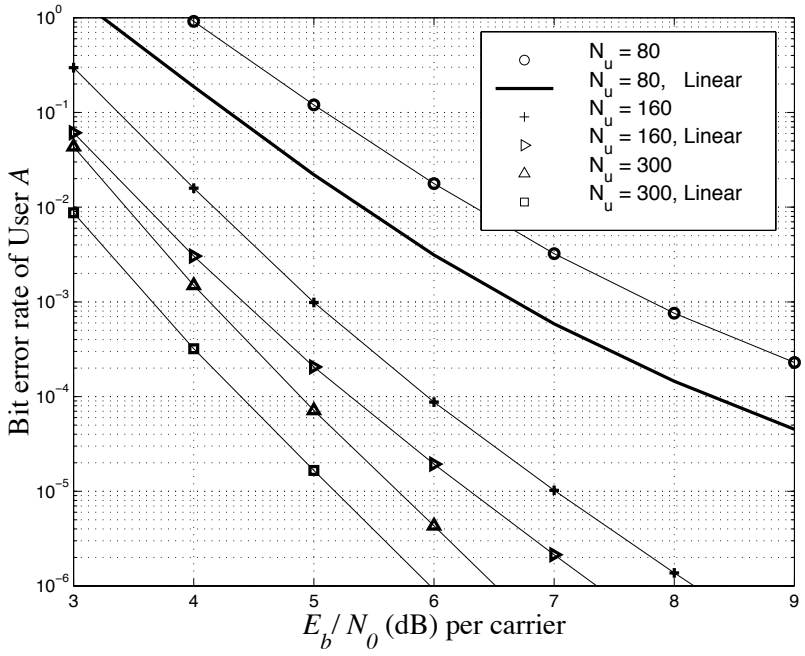

(a)

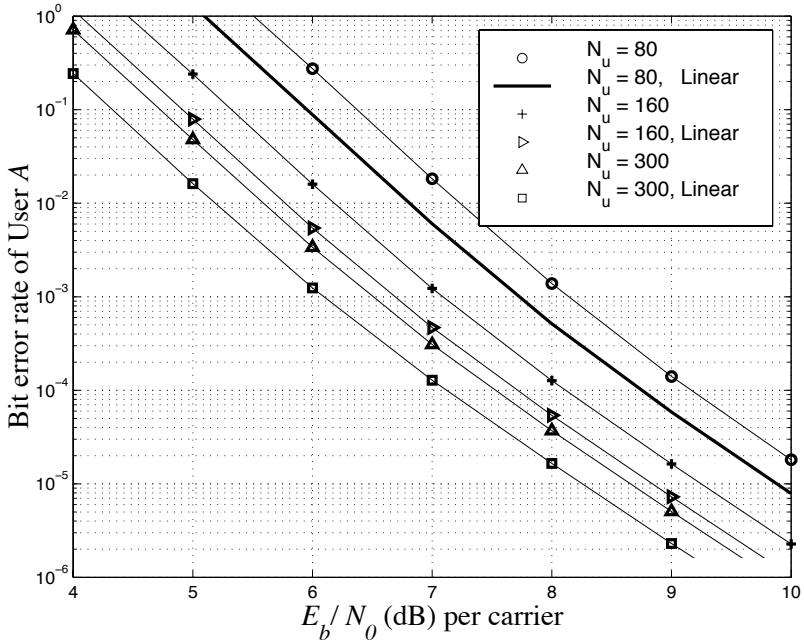

(b)

Figure 6.8: Upper bounds on BER of the coded systems when all 30 users are at r_2 with OBO = 2.5 dB for different values of the spreading factor N_u: (a) in AWGN and (b) with fading.

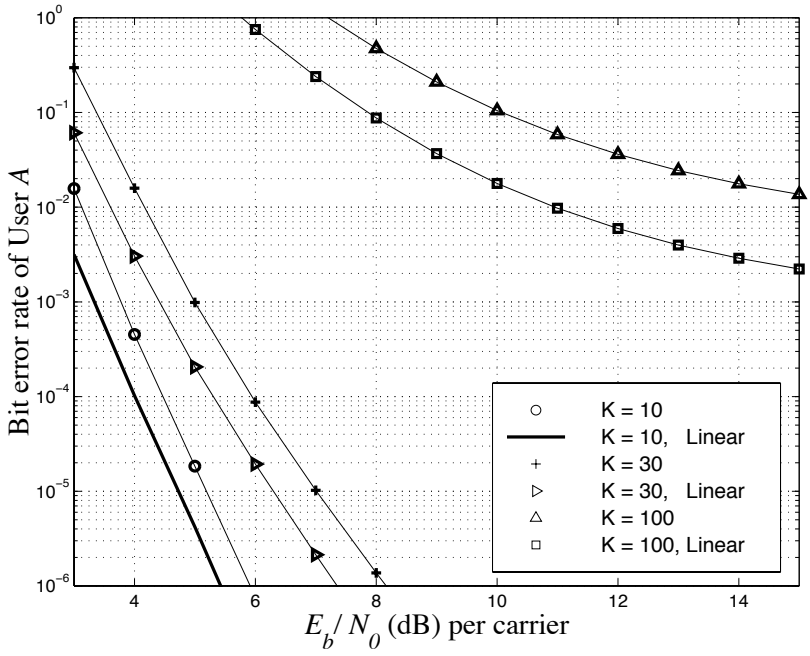

(a)

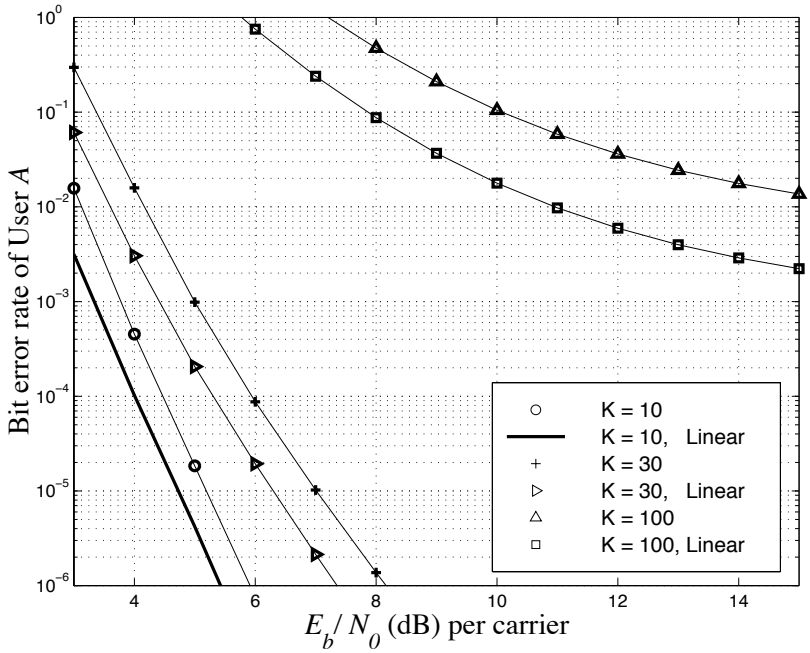

(b)

Figure 6.9: Upper bounds on BER of the coded systems when all K users are at r_2 with OBO = 2.5 dB and $N_u = 160$ for different number of users, K: (a) in AWGN and (b) with fading.

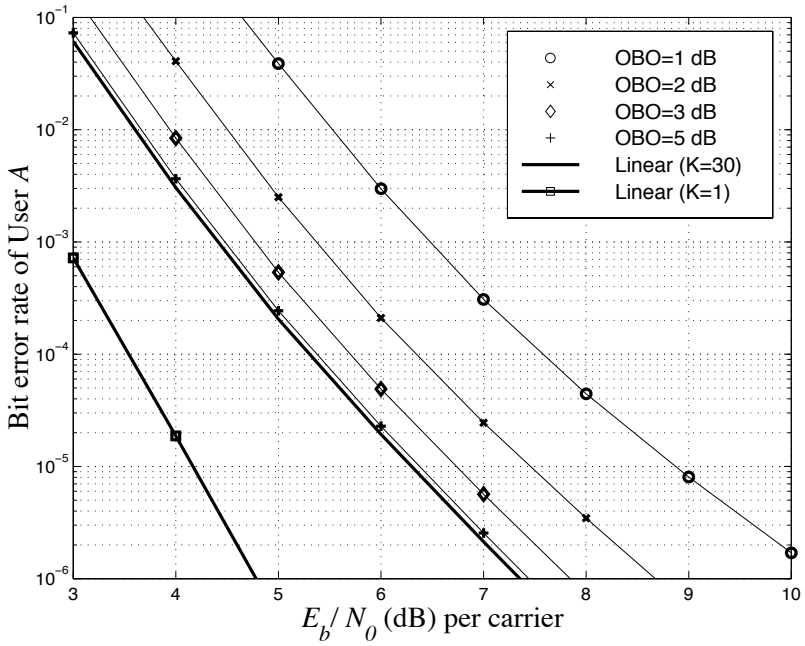

(a)

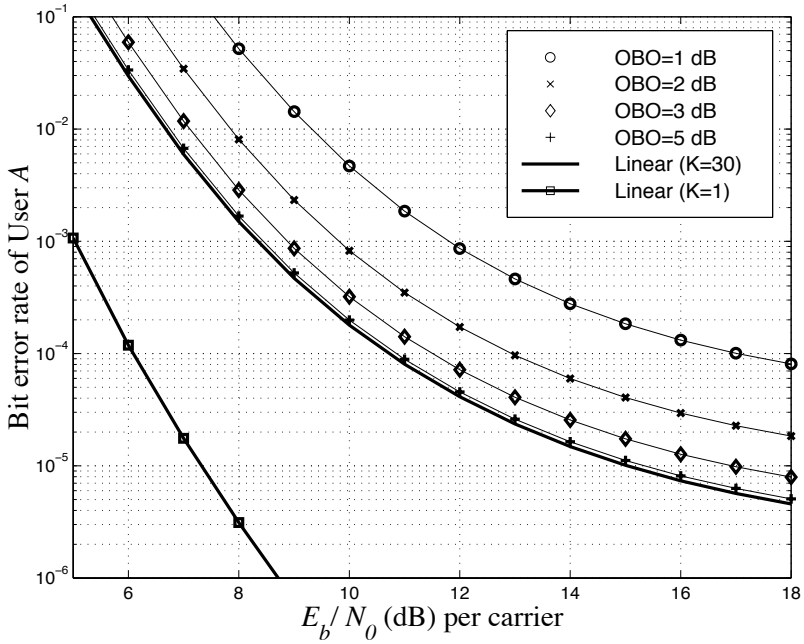

(b)

Figure 6.10: Upper bounds on BER of the coded systems when all 30 users are at r_2 for different values of OBO: (a) in AWGN and (b) with fading.

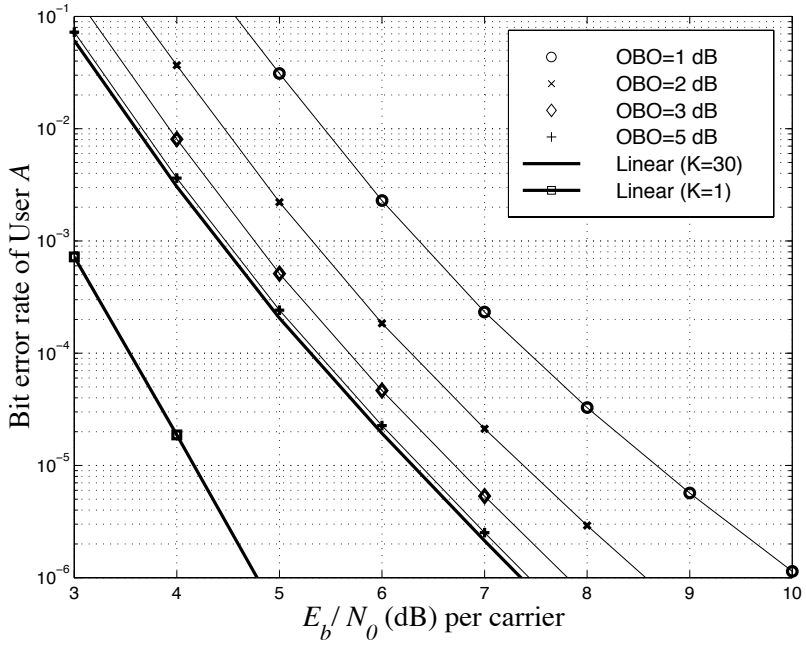

(a)

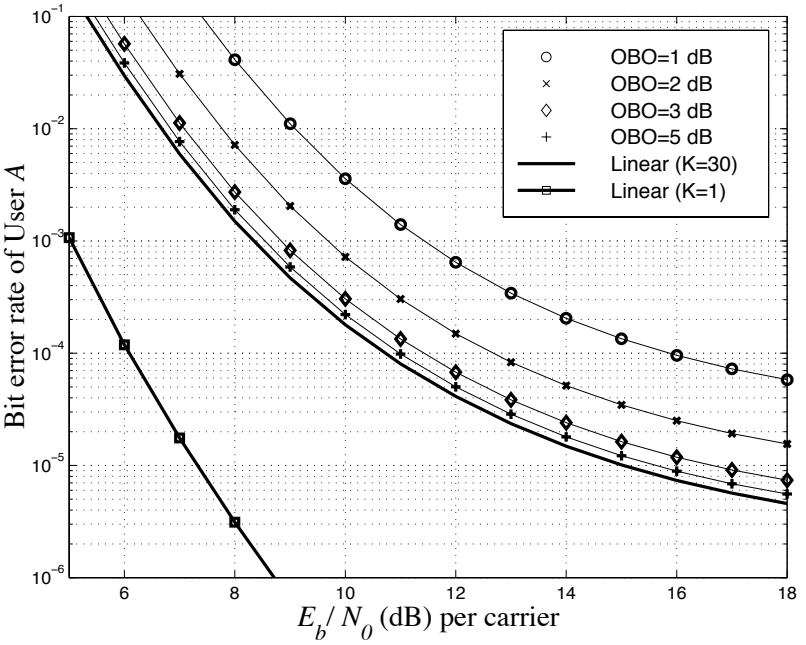

(b)

Figure 6.11: Upper bounds on BER of the coded systems when User A is at r_2 and 29 other users are at r_1 for different values of OBO of users at r_2: (a) in AWGN and (b) with fading.

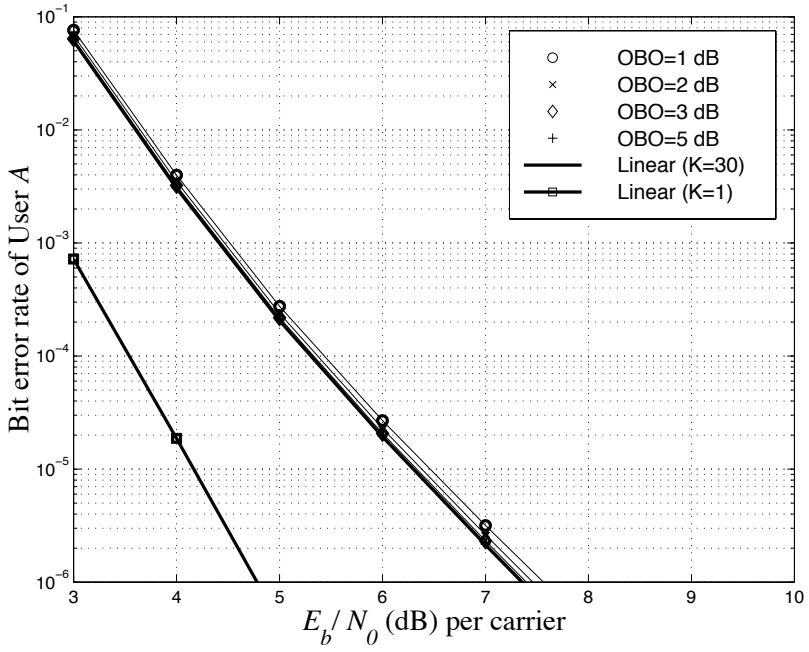

(a)

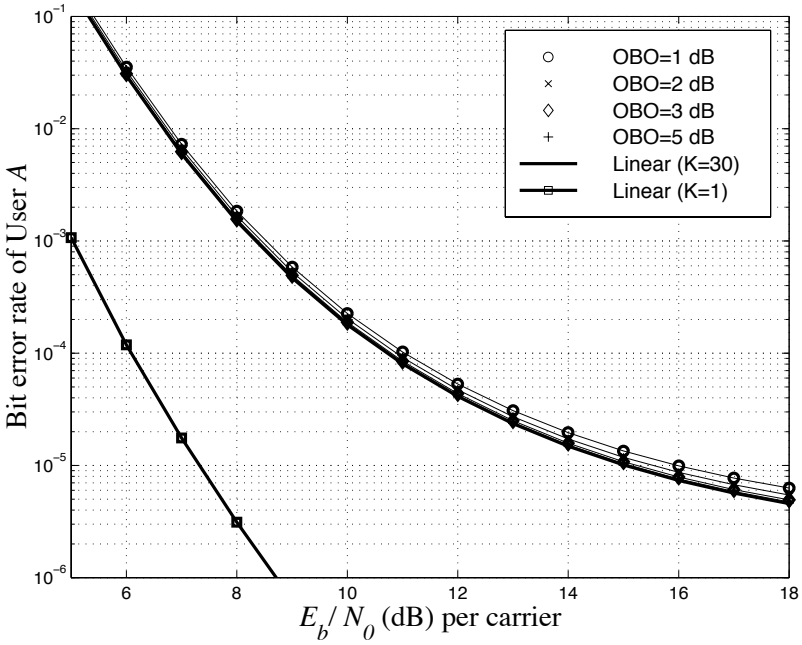

(b)

Figure 6.12: Upper bounds on BER of the coded systems when User A is at r_1 and 29 other users are at r_2 for different values of OBO of users at r_2: (a) in AWGN and (b) with fading.

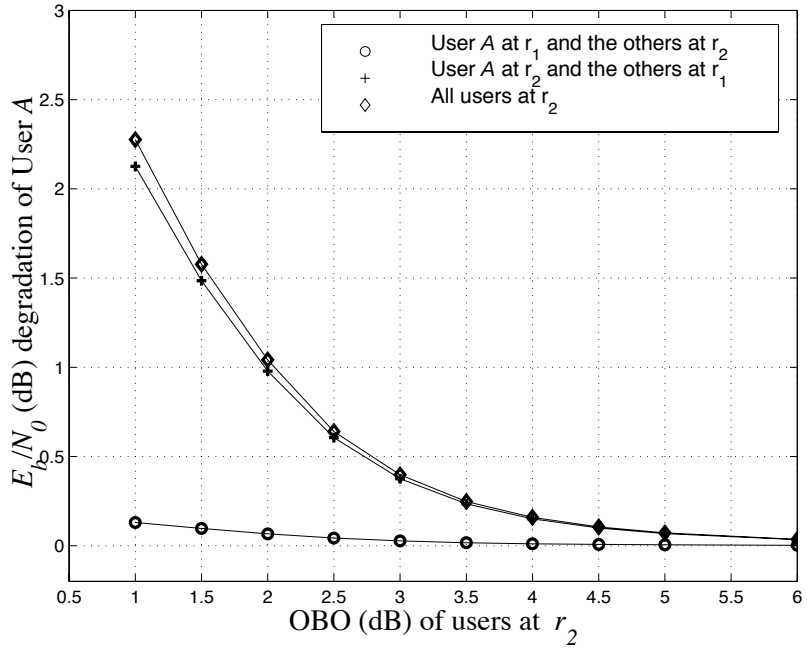

(a)

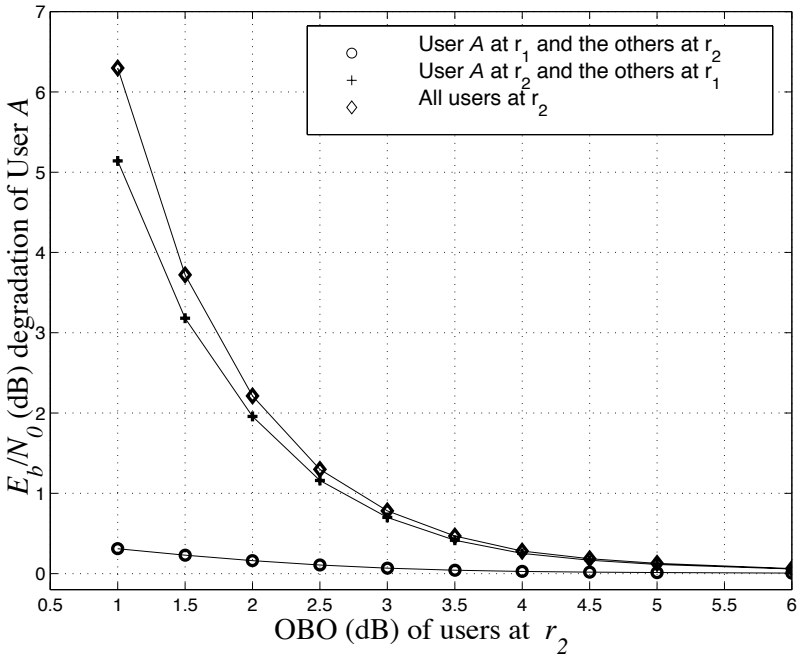

(b)

Figure 6.13: E_b/N_0 (dB) degradation of User A in the coded systems for different configuration of user location: (a) in AWGN and (b) with fading.

6.4.3 Discussion regarding User Power Optimization

In this subsection, we discuss user power optimization in a power controlled single-cell system. The purpose of this subsection is to present a methodology for finding the optimum operation points of the user's amplifiers, which will reduce the overall power consumption in a cell. Hence, the optimization process is mainly conducted to find the optimum OBOs for the users, which ensure the minimum power consumption (i.e. dc power consumption) for a given system. In this thesis, we do not attempt to reduce power consumption by improving the performance of our communication systems. We do, however, attempt to do so by intelligent utilization of the amplifier characteristics. This is accomplished once the optimization with conventional fixed dc bias amplifiers is completed.

In the considered power controlled single-cell systems, the solution to the optimization problem is simple. In essence, once the average output power of a user at the maximum cell radius (R_m) is determined, a user's location will be sufficient to determine his average output power. In addition, when the user at R_m meets a target BER, all the other users in a cell will meet the target BER. This occurs because any user closer to the base station has less nonlinear distortion. Therefore, it is necessary to find the optimum OBO of the user at R_m. However, this is the optimum method only in a power control system. One may argue that users operating in linear regions transmit more power, because of the power control, than necessary to meet the target BER. Nonetheless, in most cases, the excess power sent is insignificant, since the E_b/N_0 degradation rapidly decreases with increasing OBO.

To make our discussion more concrete, we optimize power consumption in the coded systems, considered in the previous subsection, when all 30 users are at r_2. We take r_2 to be R_m. Since we consider a fixed dc bias amplifier, we adopt TD as our objective function, which is the sum of the OBO (dB) and its corresponding E_b/N_0 (dB) degradation at the BER of 10^{-4}. For this case, TD is shown in Figure 6.14. The optimum OBO for the user at R_m is about 2 dB in AWGN and 3 dB in the fading channel. Even when the other 29 users are not at R_m, the obtained OBO is still the optimum OBO for the user at R_m since the other users' nonlinearities do not affect the BER of the user at R_m, as long as the number of users in a cell is 30.

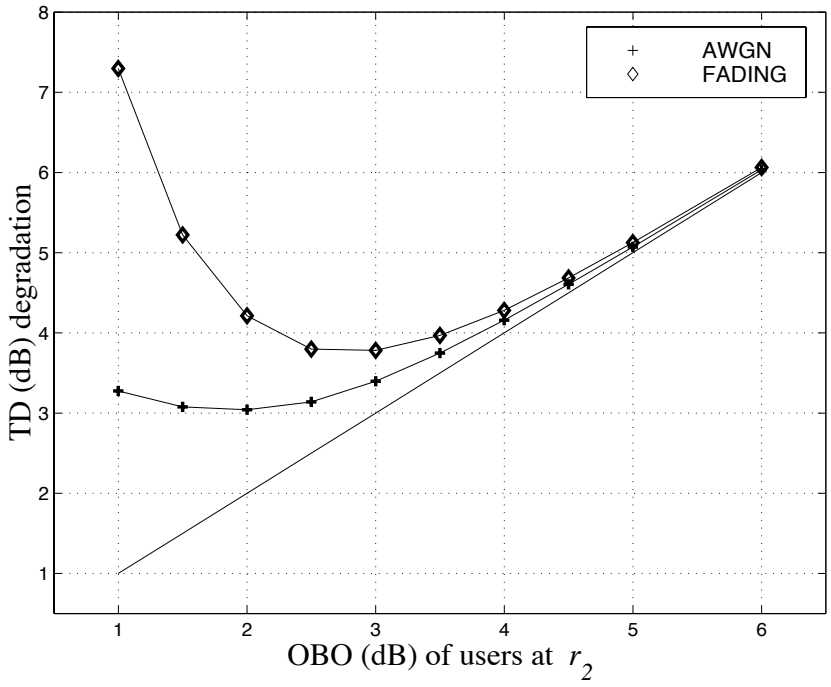

Figure 6.14: TD of the users at r_2 in AWGN and with fading.

We, now, summarize what we have done so far regarding power optimization of power controlled cellular systems, and identify power consumption problems of conventional fixed dc bias amplifiers used in such systems. From the obtained TD, we found the optimum OBO of the user at R_m. Correspondingly, we determined the minimum required dc power level $P_{dc,m}$ (from (3.7) in Chapter 3) of the amplifier to be used in the system, given the required average output power $\overline{P}_{R_m}$. Once the desired dc power level of the amplifier is set, any user at distance r transmits output power $P_{R_m}/\{R_m/r\}^{\psi}$ as shown in Figure 6.15. However, since all the users use $P_{dc,m}$, regardless of their output powers, the average dc power consumption per user is $P_{dc,m}$.

As a result, with a conventional amplifier, the users in a cell expend equal amounts of dc power, which is inefficient for users closer to the base station. As we have discussed in Chapter 4, for the dc bias controlled amplifiers, the dc power can be adjusted proportionally to the transmitted output power (see the dashed line in Figure 6.15): an effective method for reducing power consumption in a power controlled cellular system. We conduct a simplified analysis to gain more insight on further power minimization from the dc bias schemes in the following.

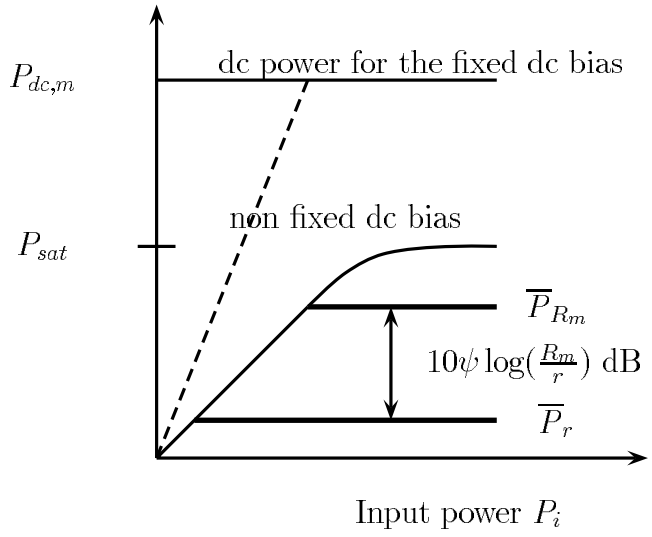

Figure 6.15: Amplifier output and dc power of users when the conventional fixed dc bias amplifiers are used after power optimization.

A dc Bias Controlled Amplifier for Cellular Systems

A circular cell with a radius R_m, as shown in Figure 6.16, is considered for the cell model. In addition, we assume that the user location (X, Y) is uniform over the circular cell with joint probability density function (pdf)

$$f_{X,Y}(x,y) = \frac{1}{\pi R_m^2}.$$

In terms of the distance $R = \sqrt{X^2 + Y^2}$, the pdf of R can be represented as

$$f_R(r) = \frac{2r}{R_m^2} \quad \text{for} \quad 0 \le r \le R_m.$$

For the amplifier models, we consider the ideal dc bias schemes presented in Chapter 4. For the readers' convenience, we reiterate the amplifier dc power characteristics as a function of output power, given as follows:

$$\text{Ideal fixed dc bias} \quad P_{dc,m} \quad \text{for} \quad 0 \le P_o(t) \le P_{sat} \tag{6.59}$$

$$\text{Ideal single dc bias} \quad \begin{cases} P_{dc,m}\sqrt{\frac{P_o(t)}{P_{L,o}}} & \text{for} \quad 0 \le P_o(t) \le P_{L,o} \\ P_{dc,m} & \text{for} \quad P_{L,o} \le P_o(t) \end{cases} \tag{6.60}$$

$$\text{Ideal dual dc bias} \quad \begin{cases} P_{dc,m}\frac{P_o(t)}{P_{L,o}} & \text{for} \quad 0 \le P_o(t) \le P_{L,o} \\ P_{dc,m} & \text{for} \quad P_{L,o}(t) \le P_o(t) \end{cases} \tag{6.61}$$

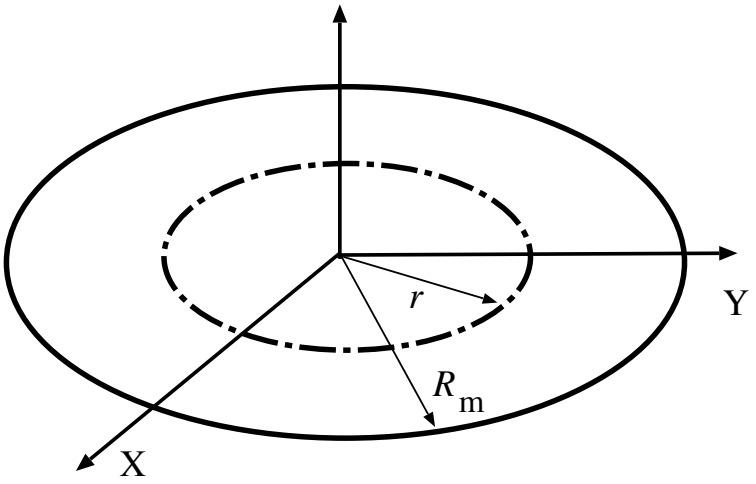

Figure 6.16: Circular cell shape and the maximum radius of the cell.

where $P_{L,o}$ is the maximum amplifier linear output power and is related to the maximum dc power $P_{dc,m}$ and to the saturation output power P_{sat} by

$$P_{L,o} = \frac{P_{dc,m}}{2} = \frac{P_{sat}}{(\frac{4}{\pi})^2}. \tag{6.62}$$

We denote th user's OBO at R_m as

$$\text{OBO}^* = \frac{P_{sat}}{\overline{P}_{R_m}}. \tag{6.63}$$

As we have mentioned in the previous subsection, when a conventional fixed dc bias amplifier is used, the average dc power consumed per user is $P_{dc,m}$, once the dc power level $P_{dc,m}$ is determined from the TD. In order to examine user power savings from the dc bias schemes, we perform a simplified analysis, that is, we consider two extreme cases: constant envelope signals with small OBO* and nonconstant multicarrier signals with large OBO*.

In the case of constant envelope signals, when the propagation loss factor $\psi > 0$, and the OBO$^* \leq (\frac{4}{\pi})^2$, the average dc power consumption per user is

$$\overline{P_{dc}} = \int_{R_l^*}^{R_m} P_{dc,m} f_R(r) dr + \int_0^{R_l^*} P_{dc}(r) f_R(r) dr \tag{6.64}$$

where the conditional average dc power is $P_{dc}(r) = E[P_{dc}|r]$ and

$$R_l^* = \left\{ \frac{\text{OBO}^*}{(\frac{4}{\pi})^2} \right\}^{1/\psi} R_m. \tag{6.65}$$

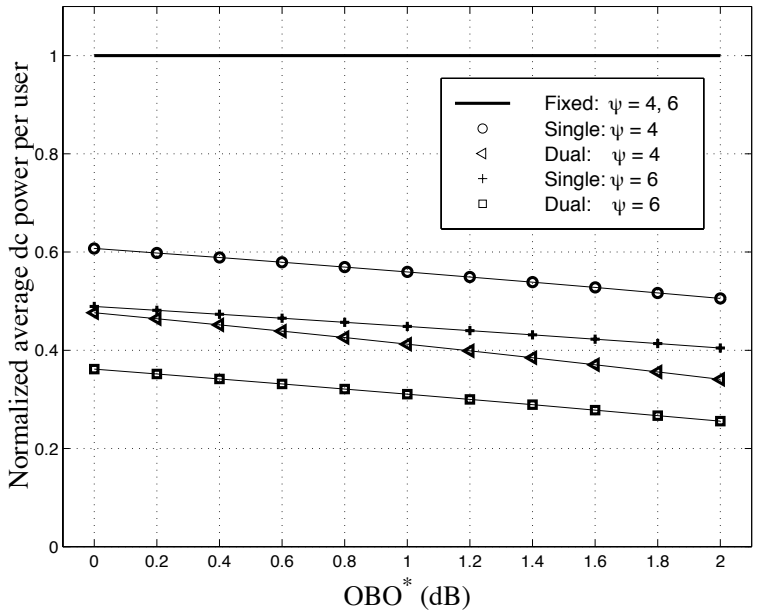

Figure 6.17: Normalized average dc power per user with different dc bias controlled schemes and different values of ψ.

Using the following relationships:

$$P_{dc}(r) = \begin{cases} P_{dc,m} & \text{for fixed bias} \\ \sqrt{2P_{dc,m}\overline{P}_{R_m}/\{R_m/r\}^{\psi}} & \text{for single bias} \\ 2\overline{P}_{R_m}/\{R_m/r\}^{\psi} & \text{for dual bias} \end{cases} \tag{6.66}$$

and

$$\overline{P}_{R_m} = (\frac{4}{\pi})^2 \frac{P_{dc,m}}{2\,\mathrm{OBO}^*} \tag{6.67}$$

we obtain average dc power consumption for the different dc bias schemes as:

$$\overline{P}_{dc} = \begin{cases} P_{dc,m} & \text{for fixed bias} \\ P_{dc,m}\{1 - \frac{\psi/2}{\psi/2+2}[(\frac{\pi}{4})^2\mathrm{OBO}^*]^{\frac{2}{\psi}}\} & \text{for single bias} \\ P_{dc,m}\{1 - \frac{\psi}{\psi+2}[(\frac{\pi}{4})^2\mathrm{OBO}^*]^{\frac{2}{\psi}}\} & \text{for dual bias.} \end{cases} \tag{6.68}$$

In the case of nonconstant envelope signals with large $\mathrm{OBO}^* \gg (\frac{4}{\pi})^2$, the average dc power consumption per user is

$$\overline{P}_{dc} \approx \int_0^{R_m} P_{dc}(r) f_R(r) dr. \tag{6.69}$$

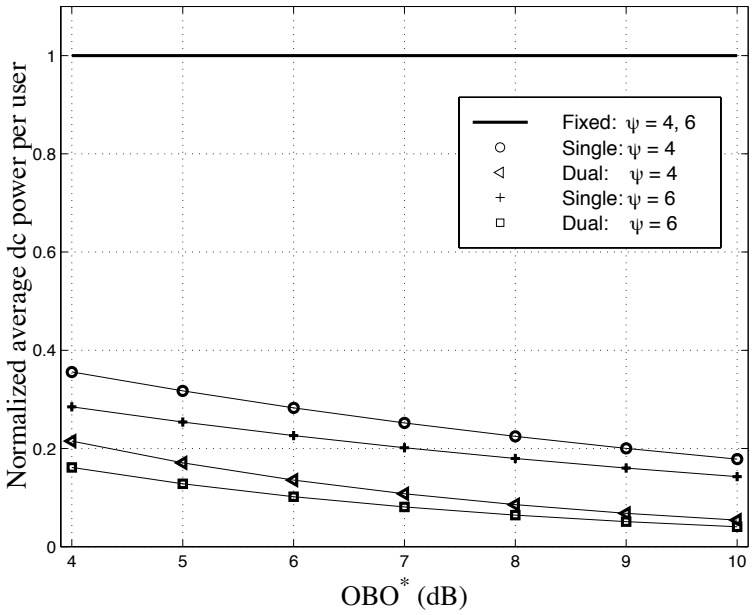

Figure 6.18: Normalized average dc power per user with different dc bias controlled schemes and different values of ψ.

Using (4.16) and (4.17), the average dc power for different bias schemes are obtained from derivations similar to (6.68), and are given by

$$\overline{P_{dc}} \approx \begin{cases} P_{dc,m} & \text{for fixed bias} \\ P_{dc,m}\{\frac{2}{\psi/2+2}\sqrt{(\frac{4}{\pi})\frac{1}{\text{OBO}^*}}\} & \text{for single bias} \\ P_{dc,m}\{\frac{2}{\psi+2}(\frac{4}{\pi})^2\frac{1}{\text{OBO}^*}\} & \text{for dual bias} \end{cases} \tag{6.70}$$

where we assume that the input envelope of the signals is Rayleigh distributed, which is the case when the number of subcarriers is larger than 6.

Figure 6.17 shows the normalized average dc power consumption per user (normalized to the average dc power of the fixed dc bias scheme) for $\psi = 4$ and 6 when the OBO*s are small. When $\psi = 4$, even for $\text{OBO}^* = 0$ dB, the dual bias scheme can reduce dc power consumption by a factor of 2, which in turn doubles the battery life. When a large OBO* is required (which is common in multicarrier systems to meet the ACPR requirement), the power savings from the dc bias scheme can be substantial as shown in Figure 6.18. When $\psi = 4$ and $\text{OBO}^* = 8$ dB, the dual bias scheme can reduce dc power consumption by a factor of 10.

6.5 Conclusion

In this chapter, we have evaluated the performance of single-cell convolutionally coded MC-CDMA systems in the presence of multipath fading and nonlinearities. In particular, we have formulated and examined the problem of the nonlinear effects from the power control used in a cellular system.

The effect of other users' nonlinearities on the BER performance of a desired user has been analytically derived and system power consumption of the users optimized in a power control system. It was found that the nonlinear degradation effects in multi-path and multi-user environments are not as significant as the degradation from multiple access and fading alone. In addition, it was found that the BER for the desired user is mainly affected by the nonlinearities of the user's amplifier, not by the nonlinearities of other users.

We discussed the inherent power consumption problem for conventional amplifiers, used in conventional cellular systems. We presented dc bias controlled amplifiers as effective solutions to this problem and quantified realizable power savings. The power consumption can be about half that of the conventional fixed dc bias scheme, even with constant envelope signals. More importantly this savings can be increased up to 10-fold for nonconstant signals when high OBO is needed.

CHAPTER 7

Conclusions

This thesis has dealt with the performance and power optimization of communication systems in the presence of amplifier nonlinearities. Although the communication system models considered in this thesis are mostly multicarrier systems, the optimization functions and methodology employed in this thesis can be readily used with other types of communication systems, including single-carrier systems. In addition, the insight gained from our numerical results can be very useful for designing low power communication systems. In this chapter, we summarize the results of this thesis and discuss some of the interesting future work suggested from our research.

Despite the existence of a trade-off between the degree of nonlinearities and total system power consumption, to date no justified methods have been offered to optimize power consumption. Only an intuitively justified objective function for power optimization has been used. However, we have demonstrated that the use of the conventional objective function is only valid when the amplifier dc power is constant throughout the entire input power range. We have proposed a general objective function for optimizing power consumption of communication systems with nonlinear power amplifiers. Our objective function is an integral part of this thesis because it allows us to achieve power optimization.

In order to show the usage of our objective function and methodology for power optimization, we have demonstrated optimization procedures for OFDM systems with three different dc bias controlled amplifiers: fixed, single, and dual dc bias controlled amplifiers. The dc power changes according to the envelope in both single and dual

dc bias schemes; whereas it is constant in the fixed dc bias scheme, typical of the conventional amplifier. We first quantified the performance (BER in AWGN and spectral regrowth) and power consumption of OFDM systems with different amplifiers and amplifier operation points. We then optimized power consumption based on the quantified performance and objective function.

The presented optimization procedure can serve as a guideline for optimizing power consumption of amplifiers in communication systems. Furthermore, this optimization has enabled us to quantify power consumption with dc bias controlled amplifiers. As critical by-products, we have demonstrated a significant power reduction using dc bias control schemes for highly nonconstant envelope signals, such as OFDM signals. The dc bias control scheme is found to be an effective method for reducing power consumption when linear amplification is highly desired, such as with ACPR requirements.

Because of the difficulties in analytical performance evaluation of nonlinear systems, time-consuming Monte Carlo computer simulation has been extensively conducted to study the effects of amplifier nonlinearities on multicarrier systems. However, the simulation approach does not provide much insight into the underlying mechanism, and becomes impractical in performance evaluation of multi-user systems. In this thesis, we have analyzed the effect of amplifier nonlinearities on the performance of multicarrier spread spectrum systems in both single-user and multi-user environments. Two performance measures, BER and ACPR, were considered to assess the effects of in-band and out-of-band interference from nonlinear amplification, respectively. A memoryless polynomial model was used to represent the bandpass amplifier amplitude nonlinearities (AM/AM) and a slow frequency nonselective independent Rayleigh fading channel was assumed for each modulated carrier.

In the case of single-user environments, we have obtained analytical results for the BER of uncoded systems and bounds on the BER of convolutionally coded systems. It was found that BER degradation from the nonlinearities can be reduced significantly by spread spectrum techniques in single-user systems. This reduction comes from the interference rejection capabilities of spread spectrum systems, which in turn reduce the effects of the intermodulation products. In addition, it was ob-

served that for uncoded MCSS systems in AWGN, with independent, slow, flat fading for each carrier, the E_b/N_0 degradation from a nonlinearity is smaller than in AWGN alone. This is especially for those MCSS systems with small spreading factors. The reason for this may be that when the signals undergo deep fading, which dominates the BER performance, the intermodulation products from nonlinear amplification are also faded, reducing their nonlinear effects. The obtained ACPR shows its slow (inverse linear) fall-off with the amplifier output backoff. Finally, the optimum amplifier output power backoffs were determined for both coded and uncoded systems when the conventional fixed dc bias amplifier is used.

In the case of multi-user environments, we have analyzed the performance of single-cell MC-CDMA systems, where perfect power control is assumed. More importantly, we were able to answer the questions of how user location, which determines the degree of nonlinearity, affects the desired user's BER as well as to the question of how to find the set of nonlinearities which minimize user power consumption in a cell. It was found that in a power control system, the BER for the desired user is mainly affected by the nonlinearities of the user's amplifier, not by the nonlinearities of other users. In addition, it was found that nonlinear degradation effects on MC-CDMA systems in multi-path and multi-user environments are not as significant as the degradation due to multiple access interference and fading alone.

When we optimized user power consumption with conventional fixed dc bias amplifiers in a power control cellular system, we identified an inherent inefficient usage of power in conventional amplifiers. That is, all the users use equal amounts of dc power, which is unnecessary in a power control system. We presented dc bias control schemes as effective methods for solving this problem and quantified realizable power savings.

There are a number of issues that were not tackled in the course of this research, which would provide interesting topics for further research. The channel Doppler and amplifier phase distortion (AM/PM) effects can be significant in high frequency bands. In the presence of Doppler, the intermodulation products can interfere with the desired carriers, which does not occur in the absence of Doppler. Hence, the Doppler effects in a nonlinear channel are expected to degrade system performance

more severely than in a linear channel. An inclusion of AM/PM effects should be considered together with predistortion techniques since the AM/PM predistortion [41] is not as performance-limited as AM/AM predistortion. Note that the best amplifier characteristics achievable with AM/AM predistortion are those of the soft limiter.

It would be interesting to include multi-user interference cancellation techniques in the framework of our MC-CDMA system. In particular, the subtractive interference cancellation techniques [89] can be applied to remove intermodulation products as well as multiple access interference. Since the interference cancellation techniques do not require as precise power control as the single user correlation receivers do, it would be interesting to examine the trade-offs between total user power consumption and different degree of power control precision.

Finally, it is important to note that the role of the dc bias control scheme, presented in this thesis, is to reduce the average dc power, not the peak dc power. Since the peak dc power is proportional to the peak amplifier output power, the bias control scheme in conjunction with the block coding schemes for reducing PMEPR proposed by Ochiai [35, 36] and Davis [39], could provide an effective approach to integrate the issues of peak dc power.

APPENDICES

APPENDIX A

Power Analysis of Class A dc Bias Controlled Amplifiers

This appendix is a supplement to Chapter 4, and includes a derivation of amplifier characteristics (output and dc power) of the dual dc bias controlled amplifier. This is an extension of work done in the fixed and single dc bias scheme of Saleh's [48] to the dual dc bias scheme. This is needed because only a summary of the bias controlled amplifier characteristics is presented in Yang's work [44], and the actual derivations are not given in his paper. We first review basic parameters of a power amplifier circuit, and derive the amplifier characteristics of ideal amplifiers (where $\Delta = \sigma = \epsilon = 0$). Then we extend them to non-ideal amplifiers.

A.1 System Model

Let the input signal to the amplifier be

$$v_i(t) = V_i(t)\sin(2\pi f_c t + \theta(t)) \tag{A.1}$$

where $V_i(t)$ is the voltage envelope of the signal, $\theta(t)$ is the phase, and f_c is the carrier frequency. The output of the amplifier is expressed as

$$v_o(t) = V_o(t)\sin\{2\pi f_c t + \theta(t) + \Phi(t)\}. \tag{A.2}$$

The phase shift $\Phi(t)$ of the considered amplifiers is $\pi/2$ (which has no effect on power characteristics), and the maximum input and output voltages of the linear region are

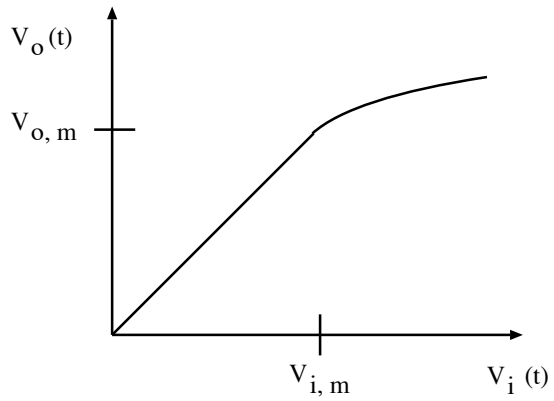

Figure A.1: Input and output RF envelope characteristics.

denoted by $V_{i,m}$ and $V_{o,m}$ as shown in Figure A.1. The normalized input and output envelopes are defined as

$$e(t) = V_i(t)/V_{i,m} \leq 1 \quad \text{(A.3)}$$

$$r(t) = V_o(t)/V_{o,m} \leq 1, \quad \text{(A.4)}$$

respectively. Since $V_i(t)$ and $V_o(t)$ have a linear relationship in the linear region

$$e(t) = r(t) \leq 1. \quad \text{(A.5)}$$

Note that $1/\overline{r^2(t)}$ is the PMEPR, where the overbar indicates averaging over signal envelope variations, i.e. $r(t)$.

A.1.1 Basic Circuit Parameters

A simplified FET (Field Effect Transistor) amplifier circuit is shown in Figure A.2, and the ideal I-V characteristics of the considered FET are shown in Figure A.3. The elements L and C in Figure A.2 represent an inductor and a capacitor, respectively. The inductor is selected so that it approximates an open circuit for the input carrier frequency and a short circuit for dc [90, page 243], that is

$$2\pi f_c L \gg R_L \quad \text{(A.6)}$$

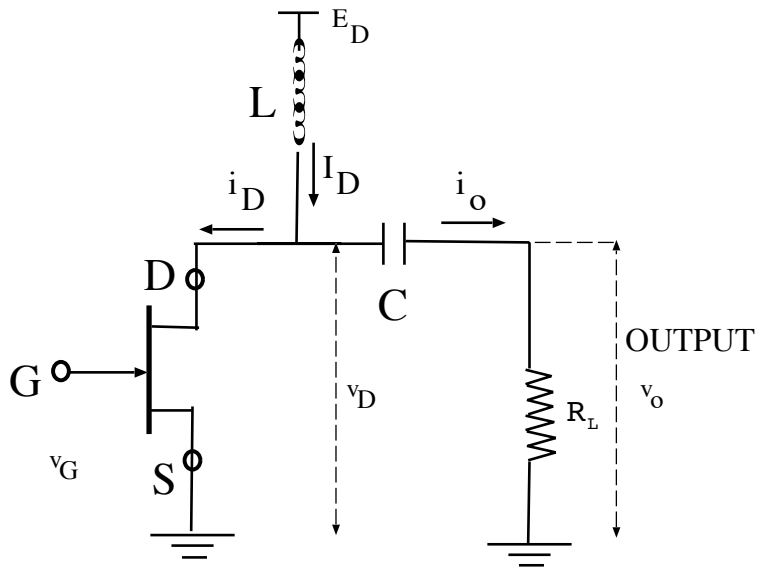

Figure A.2: Simple FET circuit model.

where R_L denotes load resistance. The capacitor C is assumed to be large enough to be a short circuit for ac signals and an open circuit for dc. In other words,

$$i_o = -i_d = -(i_D - I_D) \tag{A.7}$$

$$v_o = v_d = v_D - V_D \tag{A.8}$$

where I_D and V_D denote the dc components of i_D and v_D, respectively.

In Figure A.3, the gate pinch off voltage is denoted by V_p. The maximum allowable drain voltage and current are denoted by V_m and I_m, respectively. We can set the Q-point (dc operation point) by biasing the gate and the drain. The gate and drain biasing voltage are denoted by E_G and E_D, respectively. This biasing determines dc drain current I_D and dc drain voltage V_D. By convention, the AC load line and the bias point $Q(V_D, I_D)$ are chosen in such a way as to maximize the linear output voltage swing $v_o(t)$. Note that the slope of the AC load line is always $-1/R_L$ and the AC load line should cross the Q-point $Q(V_D, I_D)$.

Finally, the RF output power and dc drain power are given by

$$P_o(t) = V_o(t)I_o(t)/2 = V_o^2(t)/(2R_L) \tag{A.9}$$

$$P_D(t) = E_D(t)I_D(t) \tag{A.10}$$

where the output drain current $I_o(t) = V_o(t)/R_L$.

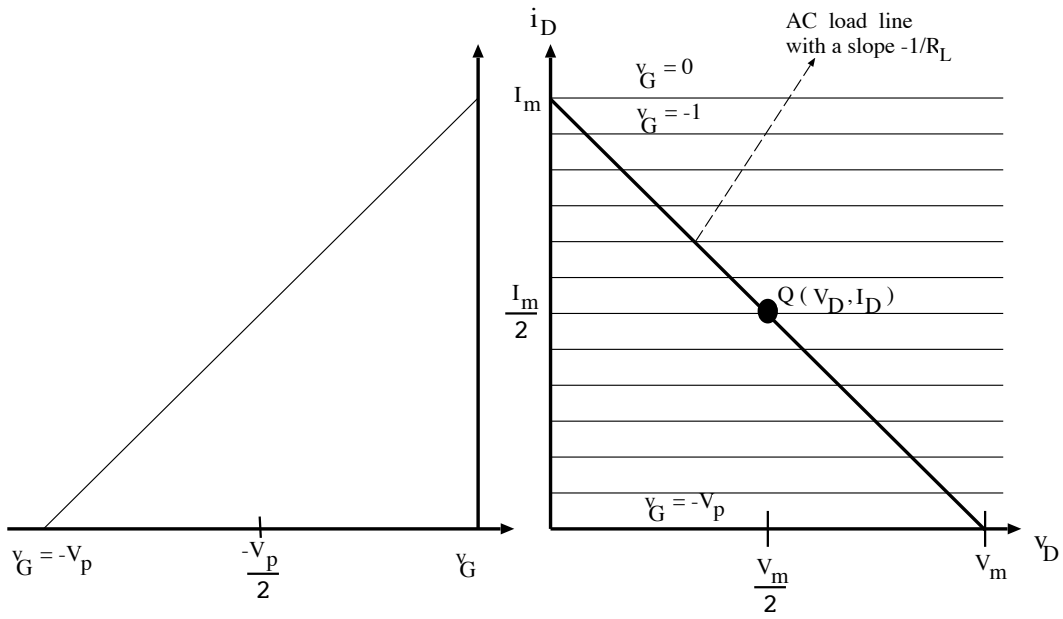

Figure A.3: Ideal FET transistor characteristics.

A.2 Ideal dc bias Controlled Amplifiers

A.2.1 Circuit Parameters

The equivalent circuit for the ideal dc bias controlled amplifier is shown in Figure A.4 and the transistor characteristics are shown in Figure A.5. The drain current i_D is related to the gate voltage v_G by

$$i_D = \frac{I_m}{V_p}(v_G + V_p) \tag{A.11}$$

where the maximum allowable drain current I_m is the drain current when $v_G = 0$. The resistance load R_L is set to

$$R_L = V_m/I_m \tag{A.12}$$

to maximize v_D (a possible swing range of V_o). The dc biases for fixed, single, and dual bias schemes are listed in Table A.1. These biases set the $Q(V_D, I_D)$ and $V_D = E_D$ in the considered amplifier models.

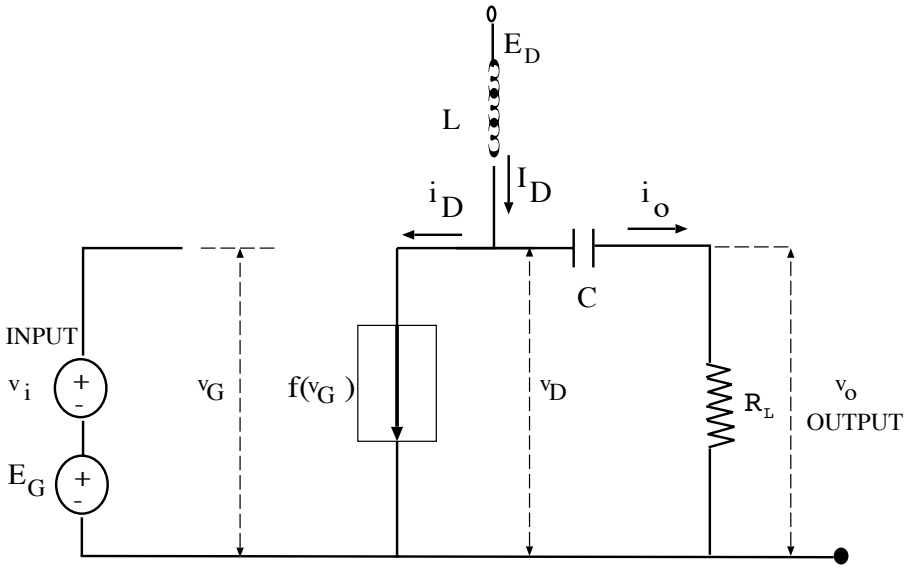

Figure A.4: An ideal FET amplifier equivalent circuit model.

Table A.1: dc bias for different bias schemes.

Bias	fixed	single	dual
E_G	$-V_p/2$	$-V_p/2$ if $V_i(t) > \frac{V_p}{2}$ $-V_p + V_i(t)$ otherwise	$-V_p/2$ if $V_i(t) > \frac{V_p}{2}$ $-V_p + V_i(t)$ otherwise
E_D	$V_m/2$	$V_m/2$	$V_m/2$ if $V_o > \frac{V_m}{2}$ V_o otherwise

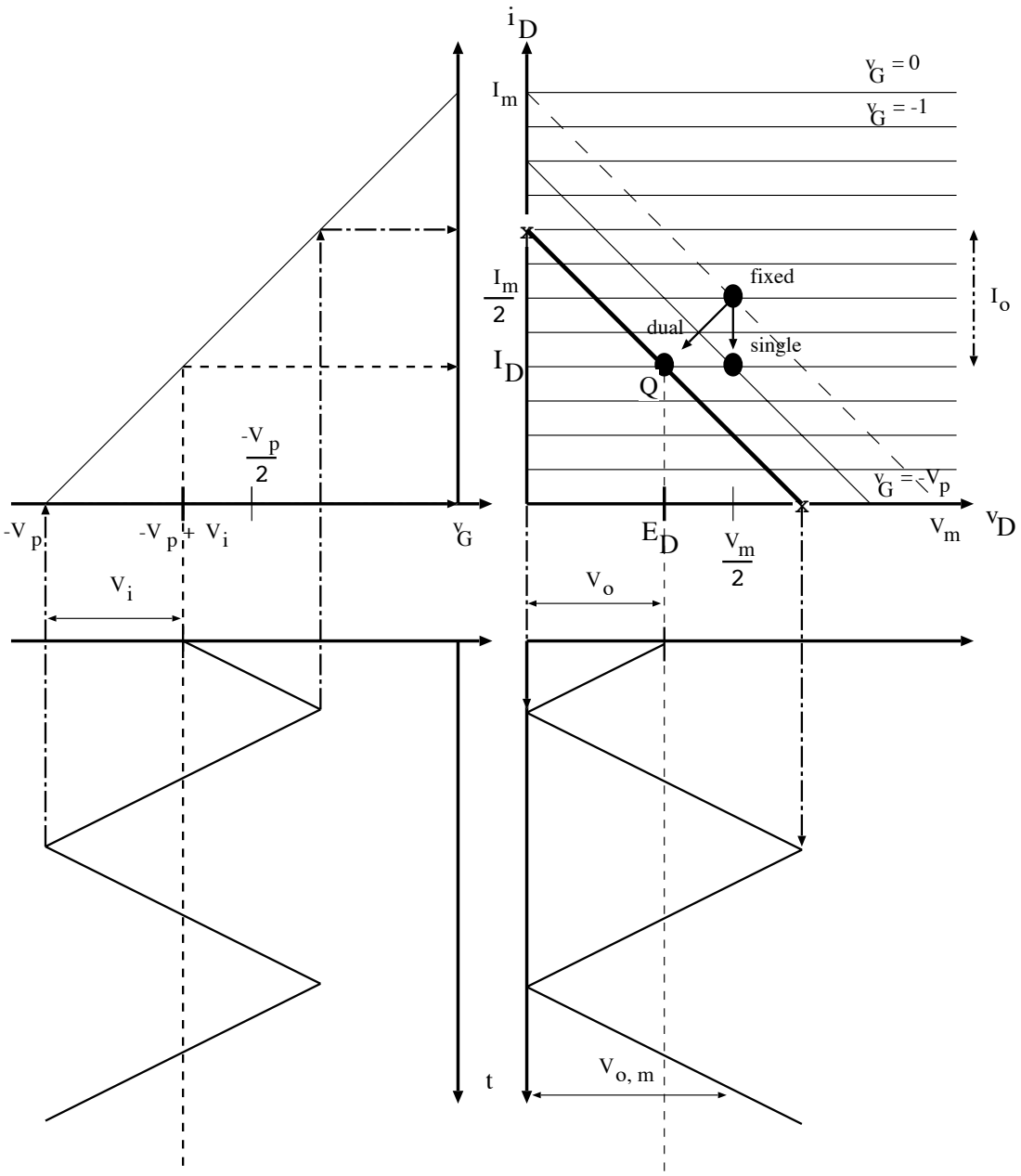

Figure A.5: An ideal FET amplifier characteristics.

A.2.2 Output Power and dc Power Analysis

Since the bias schemes do not affect the amplifier output signal, the RF output power is the same for all bias schemes and is derived as follows

$$P_o(t) = \frac{V_o^2(t)}{2R_L} = \left(\frac{V_o(t)}{V_{o,m}}\right)^2 \left(\frac{V_{o,m}}{2R_L}\right) = r^2(t)\frac{V_m I_m}{8} \tag{A.13}$$

where $V_{o,m} = V_m/2$ (from Figure A.5), and $I_m = V_m/R_L$. The dc power (i.e. drain power) for the dual bias scheme is derived as follows

$$\begin{aligned} P_D(t) &= E_D(t)I_D(t) = (V_o)\left(\frac{V_i(t)I_m}{V_p}\right) \\ &= (V_o)\left(\frac{V_i(t)}{V_p/2}\frac{I_m}{2}\right) = (V_o)\left(\frac{V_o(t)}{V_{o,m}}\frac{I_m}{2}\right) \\ &= \left(r(t)\frac{V_m}{2}\right)\left(r(t)\frac{I_m}{2}\right). \end{aligned} \tag{A.14}$$

Note that dc power in the fixed bias scheme is given by (A.14) with $r(t) = 1$, and the dc power in the single bias scheme is given by (A.14) with $r(t) = 1$ only in the first set of parentheses. Power efficiency (dc conversion efficiency) of the amplifier is defined by

$$\eta_D = \overline{P_o}/\overline{P_D}. \tag{A.15}$$

With a fixed dc bias scheme (conventional class A amplifier), the power efficiency in the case of perfect linear amplification (i.e. $r(t) \leq 1$)

$$\eta_D = \overline{r^2}/2 = \frac{1}{2PMEPR} \tag{A.16}$$

which is an inverse linear function of the peak-to-mean-envelope-power ratio (PMEPR).

A.3 Non-ideal dc bias Controlled Amplifiers

A.3.1 Circuit Parameters

In this section, we consider a more realistic FET amplifier model shown in Figures A.6 and A.7, which includes the following dimensionless parameters [48]:

- Δ (output knee voltage parameter): The i_D vs. v_D characteristic for $V_G = 0$ has a knee at $i_D = I_m$ and $v_D = \Delta V_m$.

- ϵ (output conductance parameter): A constant drain conductance $G_D = \epsilon I_m / V_m$ exists in the region $v_D \geq \Delta V_m$.

- σ (nonlinear soft cut-off/pinch-off parameter at low output current levels): The relation v_G vs. j_D is assumed to be linear only between $v_G = -(1-\epsilon)V_p$ and $v_G = 0$.

The drain current i_D is related to the gate voltage v_G by

$$i_D = j_D + G_D v_D \tag{A.17}$$

where

$$j_D = \frac{J_m}{V_p}(v_G + V_p) \tag{A.18}$$

and J_m is the drain current when $v_G = 0$. In addition,

$$J_m = (1 - \epsilon\Delta) I_m \tag{A.19}$$

from $I_m = J_m + G_D \Delta V_m$. Note that for linear amplification, v_G should be in $[-(1-\epsilon)V_p, 0]$. This clearly shows a reduced linear amplification range.

The load resistance R_L is set to be

$$R_L = \frac{V_m}{I_m} \frac{(1-\Delta)}{(1-\epsilon-\sigma+\Delta\epsilon\sigma)} \tag{A.20}$$

and the dc biases for the fixed, single, and dual bias schemes, which set the Q points, are listed in Table A.2. From the fact that $i_d = -v_d/R_L$ and $i_d = (J_m v_i)/V_p + G_D v_d$, we obtain the following:

$$\begin{aligned} V_o &= \frac{V_m V_i}{V_p} \frac{(1-\Delta)}{(1-\sigma)} \\ \frac{V_o}{V_{o,m}} &= \frac{2V_i}{(1-\sigma)V_p} \\ \frac{2V_i}{V_p} &= (1-\sigma) r(t) \end{aligned} \tag{A.21}$$

which will be used in the following subsection.

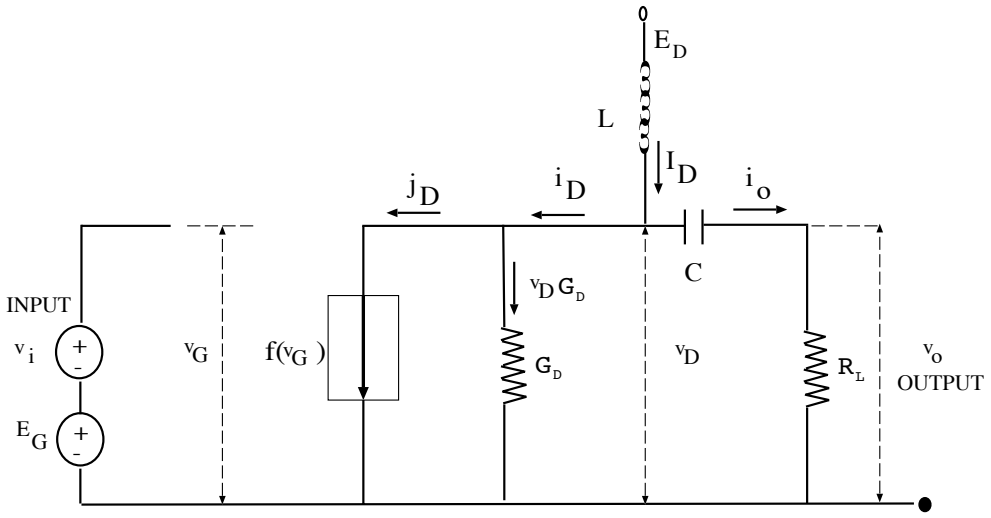

Figure A.6: A non-ideal FET amplifier equivalent circuit model

Table A.2: dc bias for different schemes.

Bias	fixed	single	dual
E_G	$\frac{-V_p(1-\sigma)}{2}$	$-\frac{V_p(1-\sigma)}{2}$ if $V_i(t) > \frac{V_p(1-\sigma)}{2}$ $-V_p(1-\sigma)+V_i(t)$ otherwise	$-\frac{V_p(1-\sigma)}{2}$ if $V_i(t) > \frac{V_p(1-\sigma)}{2}$ $-V_p(1-\sigma)+V_i(t)$ otherwise
E_D	$\frac{V_m(1+\Delta)}{2}$	$V_m(1+\Delta)/2$	$\frac{V_m(1+\Delta)}{2}$ if $V_o > \frac{V_m(1+\Delta)}{2}$ $\Delta V_m + V_o$ otherwise

A.3.2 Output Power and dc Power Analysis

Similar to the derivation of the ideal amplifier characteristics, the RF output power is the same for all bias schemes and is given by

$$\begin{aligned} P_o(t) &= \frac{V_o^2(t)}{2R_L} = \left(\frac{V_o(t)}{V_{o,m}}\right)^2 \left(\frac{V_{o,m}}{2R_L}\right) = r^2(t)\left(\frac{(1-\Delta)V_m}{2}\right)^2 \left(\frac{1}{2R_L}\right) \\ &= r^2(t)\left(\frac{(1-\Delta)^2 V_m^2}{8}\right)\left(\frac{I_m}{V_m}\frac{(1-\epsilon-\sigma-\Delta\epsilon\sigma)}{(1-\Delta)}\right) \\ &= r^2(t)\frac{V_m I_m}{8}(1-\Delta)(1-\epsilon-\sigma+\Delta\epsilon\sigma) \end{aligned} \tag{A.22}$$

where $V_{o,m} = V_m(1-\Delta)/2$ (from Figure A.7) has been used.

In order to derive the dc power of the dual bias scheme, we need to find $E_D(t)$ and $I_D(t)$. The dc drain voltage $E_D(t)$ is obtained as

$$\begin{aligned} E_D(t) &= \Delta V_m + V_o = \Delta V_m + V_{o,m} r(t) \\ &= \Delta V_m + \frac{(1-\Delta)V_m}{2} r(t) = \frac{V_m}{2}[2\Delta + (1-\Delta)r(t)]. \end{aligned} \tag{A.23}$$

The dc drain current $I_D(t)$ can be obtained using (A.17) and (A.19) as follows. With the gate bias $E_G = V_i(t) - V_p(1-\sigma)$ we get

$$j_D = J_m(\sigma + \frac{V_i}{V_p}) + \frac{J_m v_i}{V_p} \tag{A.24}$$

and if we substitute j_D in (A.17) with (A.24),

$$I_D(t) = J_m(\sigma + \frac{V_i}{V_p}) + \epsilon\frac{I_m}{V_m}\frac{V_m}{2}[2\Delta + (1-\Delta)r(t)]. \tag{A.25}$$

With (A.19), $I_D(t)$ becomes

$$I_D(t) = I_m(1-\epsilon\Delta)(\sigma + \frac{V_i}{V_p}) + \frac{I_m}{2}\epsilon[2\Delta + (1-\Delta)r(t)] \tag{A.26}$$

$$= \frac{I_m}{2}\{(1-\epsilon\Delta)(2\sigma + (1-\sigma)r(t)) + \epsilon[2\Delta + (1-\Delta)r(t)]\} \tag{A.27}$$

$$= \frac{I_m}{2}\{2(\sigma(1-\epsilon\Delta) + \epsilon\Delta) + r(t)(1-\sigma-2\epsilon\Delta+\epsilon+\sigma\epsilon\Delta)\} \tag{A.28}$$

where (A.21) is used in going from (A.26) to (A.27). Hence, the dc power of the dual dc bias scheme, $P_D(t) = E_D(t)I_D(t)$, is

$$\frac{V_m I_m}{4}[2\Delta + (1-\Delta)r(t)]\{2(\sigma(1-\epsilon\Delta) + \epsilon\Delta) + r(t)(1-\sigma-2\epsilon\Delta+\epsilon+\sigma\epsilon\Delta). \tag{A.29}$$

Furthermore, by letting, $\frac{V_m}{2}\frac{I_m}{2} = 1$ and $r(t) = e(t)$ in (A.29), the normalized dc power, in (4.11) for $e(t) \leq 1$, is obtained.

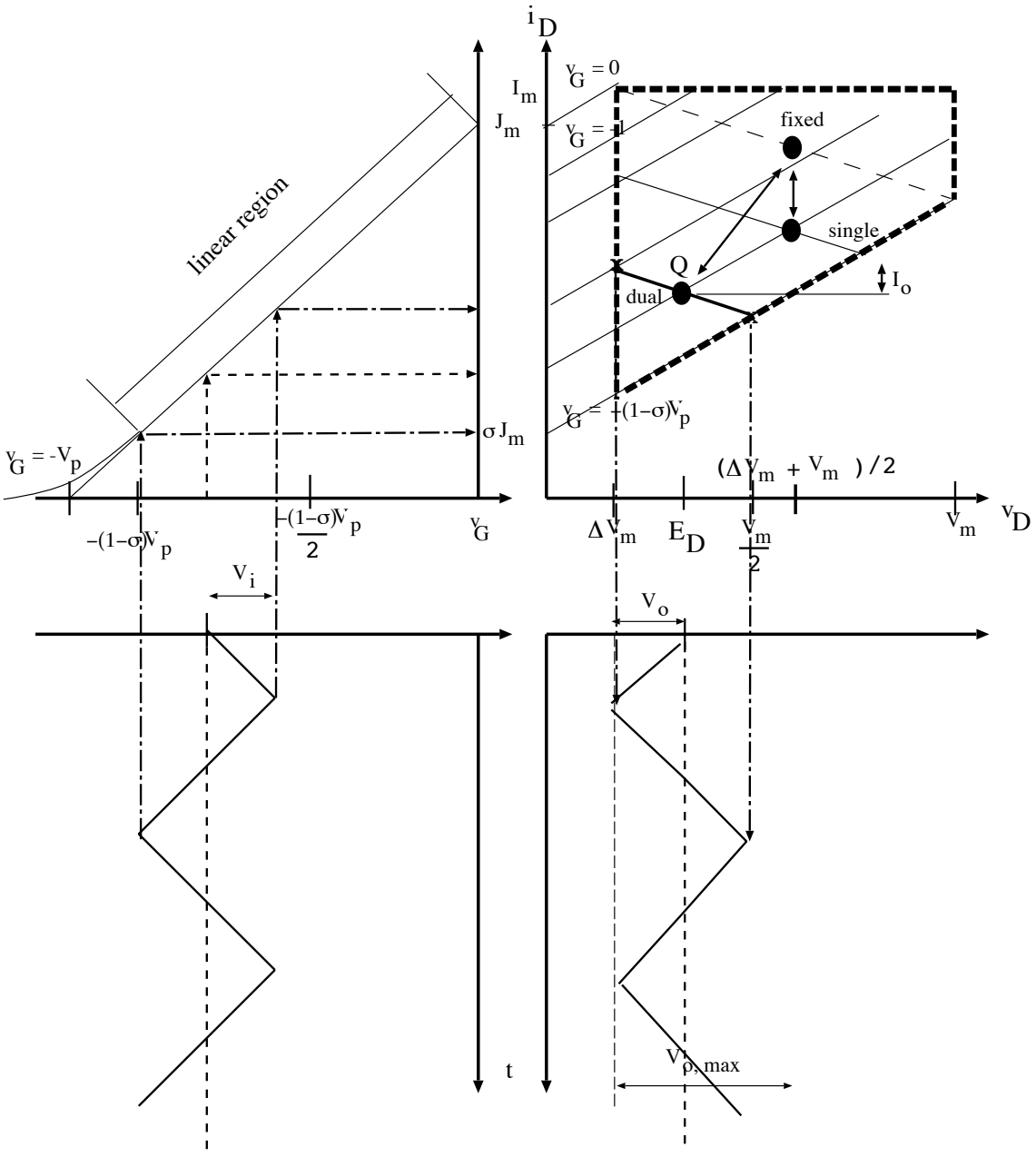

Figure A.7: A non-ideal dual bias FET model.

APPENDIX B

The Lowpass Equivalent Signal Model of (5.1) and Derivation of (5.7)

First, we represent the signal $x(t)$ in (5.1) by its lowpss equivalent signal $x_L(t)$. Then based on this representation, we derive (5.7).

B.1 Lowpass equivalent model of (5.1)

The modulated signal $x(t)$ in (5.1) can be represented by its lowpass equivalent signal $x_L(t)$ as follows:

$$\begin{aligned} x(t) &= \sqrt{2P}\sum_{q=1}^{M} a_q(t)d_q(t)\cos\{(w_c+w_q)t+\theta_q\} \\ &= A(t)\cos\{(w_ct+\phi(t)\} = \mathrm{Re}\{(x_L(t))\,e^{jw_ct}\} \end{aligned} \tag{B.1}$$

where $\mathrm{Re}\{X\}$ denotes the real part of X, and

$$x_L(t) = A(t)e^{j\phi(t)} = \sqrt{2P}\sum_{q=1}^{M} a_q(t)d_q(t)e^{j(w_qt+\theta_q)}. \tag{B.2}$$

The envelope of $x(t)$ is $A(t)=\sqrt{x_c^2(t)+x_s^2(t)}$, and its phase is $\phi(t)=\tan^{-1}(x_s(t)/x_c(t))$, where

$$x_c(t) = \sqrt{2P}\sum_{q=1}^{M} a_q(t)d_q(t)\cos\{w_qt+\theta_q\} \tag{B.3}$$

$$x_s(t) = \sqrt{2P}\sum_{q=1}^{M} a_q(t)d_q(t)\sin\{w_qt+\theta_q\}. \tag{B.4}$$

B.2 Derivation of (5.7)

We can derive $x_n(t)$ in (5.7), where n is odd, as follows:

$$\begin{aligned} x_n(t) &= \alpha_n A^{n-1}(t)A(t)\cos\{w_c t+\phi(t)\} = \alpha_n \mathrm{Re}\left\{A^{n-1}(t)A(t)e^{j(w_c t+\phi(t))}\right\} \\ &= \alpha_n \mathrm{Re}\left\{A^{n-1}(t)A(t)e^{j\phi(t)}e^{jw_c t}\right\} = \alpha_n \mathrm{Re}\left\{A^{n-1}(t)x_L(t)e^{jw_c t}\right\} \\ &= \alpha_n \mathrm{Re}\left\{A^{n-1}(t)\left(\sqrt{2P}\sum_{l_1=1}^{M} a_{l_1}(t)d_{l_1}(t)e^{j(w_{l_1}t+\theta_{l_1})}\right)e^{jw_c t}\right\} \end{aligned} \tag{B.5}$$

where the $(n-1)/2$-th power of $A^2(t)$ is

$$\begin{aligned} A^{n-1}(t) &= \{x_L(t)x_L^*(t)\}^{(n-1)/2} \\ &= \left\{2P\sum_{l_2=1}^{M}\sum_{l_3=1}^{M} a_{l_2}(t)d_{l_2}(t)a_{l_3}(t)d_{l_3}(t)e^{j\{(w_{l_2}-w_{l_3})t+\theta_{l_2}-\theta_{l_3}\}}\right\}^{(n-1)/2} \\ &= (2P)^{(n-1)/2}\sum_{l_2=1}^{M}\sum_{l_3=1}^{M}\cdots\sum_{l_{n-1}=1}^{M}\sum_{l_n=1}^{M} a_{l_2}(t)d_{l_2}(t)a_{l_3}(t)d_{l_3}(t)\cdots a_{l_{n-1}}(t)d_{l_{n-1}}(t) \\ &\quad a_{l_n}(t)d_{l_n}(t)e^{j\{(w_{l_2}-w_{l_3}+\cdots+w_{l_{n-1}}-w_{l_n})t+\theta_{l_2}-\theta_{l_3}+\cdots+\theta_{l_{n-1}}-\theta_{l_n}\}}. \end{aligned} \tag{B.6}$$

Hence, from (B.5) and (B.6),

$$\begin{aligned} x_n(t) &= \alpha_n \mathrm{Re}\left\{(2P)^{\frac{n}{2}}\sum_{l_1=1}^{M}\sum_{l_2=1}^{M}\sum_{l_3=1}^{M}\cdots\sum_{l_{n-1}=1}^{M}\sum_{l_n=1}^{M}\widetilde{a}_n(t)\widetilde{d}_n(t)\right. \\ &\quad \left. e^{j\{(w_c+w_{l_1}+w_{l_2}-w_{l_3}+\cdots+w_{l_{n-1}}-w_{l_n})t+\theta_{l_1}+\theta_{l_2}-\theta_{l_3}+\cdots+\theta_{l_{n-1}}-\theta_{l_n}\}}\right\} \\ &= \alpha_n(\sqrt{2P})^n\sum_{l_1=1}^{M}\sum_{l_2=1}^{M}\cdots\sum_{l_n=1}^{M}\widetilde{a}_n(t)\widetilde{d}_n(t)\cos\{(w_c+w_{j_n})t+\theta_{\hat{j}_n}\} \end{aligned} \tag{B.7}$$

where $w_{j_n} = w_{l_1}+w_{l_2}-w_{l_3}+\cdots+w_{l_{n-1}}-w_{l_n}$, the phase $\theta_{\hat{j}_n} = \theta_{l_1}+\theta_{l_2}-\theta_{l_3}+\cdots+\theta_{l_{n-1}}-\theta_{l_n}$, and

$$\widetilde{a}_n(t) = a_{l_1}(t)\,a_{l_2}(t)\cdots a_{l_n}(t) \tag{B.8}$$

$$\widetilde{d}_n(t) = d_{l_1}(t)\,d_{l_2}(t)\cdots d_{l_n}(t). \tag{B.9}$$

APPENDIX C

Size of the Union of Sets and Lists of $\Lambda_M(n)$

Size of the union of sets is given by [84, page 37],

$$|S_1 \cup S_2 \cup \cdots \cup S_p| = \sum_{i=1}^{p} |S_i| - \sum_{i_1<i_2} |S_{i_1} \cap S_{i_2}| + \cdots +$$
$$(-1)^{r+1} \sum_{i_1<i_2<\cdots<i_r} |S_{i_1} \cap S_{i_2} \cap \cdots \cap S_{i_r}| + \cdots + (-1)^{p+1} |S_{i_1} \cap S_{i_2} \cap \cdots \cap S_{i_p}|.$$

The summation $\sum_{i_1<i_2<\cdots<i_r} |S_{i_1} \cap S_{i_2} \cap \cdots \cap S_{i_r}|$ is taken over all of the $\binom{p}{r}$ possible subsets of size r of the set $1, 2, \ldots, p$.

$\Lambda_M(3) = 2M - 1$, $\Lambda_M(5) = 6M^2 - 9M + 4$, $\Lambda_M(7) = 24M^3 - 72M^2 + 82M - 33$, $\Lambda_M(9) = 120M^4 - 600M^3 + 1250M^2 - 1225M + 456$, and $\Lambda_M(n) \approx M\{(n+1)/2\}$ $\Lambda_M(n-2)$ for large n.

APPENDIX D

$\sum_i |G_{i,q}(n)|^2$ for $n = 3$ and $1 \leq q \leq M$

For $n = 3$, there are 2 different types of groups, based on whether the indices l_1 and l_2 are equal or not. For each group of the first type, which is the case of $l_1 = l_2$, one index vector (l_1, l_2, l_3) itself constitutes a group as shown in the example $(l_1 = 2, l_2 = 2, l_3 = 3)$ in Section 5.3.1. For groups of the other type, $l_1 \neq l_2$, two index vector (l_1, l_2, l_3) and (l_2, l_1, l_3) constitute a same group. Hence, the total variance from the groups in first type is the number of groups $X(M, q)$ in first type and the total variance from the second type is the 4 times the number groups $Y(M, q)$ in the second type. This is because (l_1, l_2, l_3) and (l_2, l_1, l_3) yield the same terms and these terms are added coherently. Then

$$\sum_i |G_{i,q}(3)|^2 = X(M,q) + 4Y(M,q) \tag{D.1}$$

where

$$\begin{aligned} X(M,q) &= \sum_{l_1=1}^{M}\sum_{l_2=1}^{M}\sum_{l_3=1}^{M} \mathrm{I}_{\left\{\{l_1+l_2-l_3=q\}\wedge\{l_3\neq l_1\}\wedge\{l_3\neq l_2\}\wedge\{l_1=l_2\}\right\}} \\ &= \sum_{l_1=1}^{M}\sum_{l_3=1}^{M} \mathrm{I}_{\left\{\{2l_1-l_3=q\}\wedge\{l_3\neq l_1\}\right\}} \\ &= \begin{cases} \frac{M-2}{2} & \text{if } M \text{ is even} \\ \frac{M-2+(-1)^q}{2} & \text{if } M \text{ is odd} \end{cases} \end{aligned} \tag{D.2}$$

and

$$\begin{aligned} Y(M,q) &= \sum_{l_1=1}^{M}\sum_{l_2=l_1+1}^{M}\sum_{l_3=1}^{M} \mathrm{I}_{\left\{\{l_1+l_2-l_3=q\}\wedge\{l_3\neq l_1\}\wedge\{l_3\neq l_2\}\right\}} \\ &= \frac{1}{2}\left(\sum_{l_1=1}^{M}\sum_{l_2=1}^{M}\sum_{l_3=1}^{M} \mathrm{I}_{\left\{\{l_1+l_2-l_3=q\}\wedge\{l_3\neq l_1\}\wedge\{l_3\neq l_2\}\wedge\{l_1\neq l_2\}\right\}}\right) \\ &= \frac{1}{2}\left(\sum_{l_1=1}^{M}\sum_{l_2=1}^{M}\sum_{l_3=1}^{M} \mathrm{I}_{\left\{\{l_1+l_2-l_3=q\}\wedge\{l_3\neq l_1\}\wedge\{l_3\neq l_2\}\right\}} - X(M,q)\right) \quad \text{(D.3)} \end{aligned}$$

where

$$\sum_{l_1=1}^{M}\sum_{l_2=1}^{M}\sum_{l_3=1}^{M} \mathrm{I}_{\left\{\{l_1+l_2-l_3=q\}\wedge\{l_3\neq l_1\}\wedge\{l_3\neq l_2\}\right\}} = (q-1)(M-q) + \frac{(M-2)(M-1)}{2} \quad \text{(D.4)}$$

Since derivation of (D.2) is similar to and easier than that of (D.4), we only derive (D.4). The calculation of (D.4) is the same as finding the number of index vectors (l_1, l_2, l_3) that satisfy the following conditions:

1. $\{1 \le l_1 \le M\}$, $\{1 \le l_2 \le M\}$, and $\{1 \le l_3 \le M\}$
2. $\{l_3 \neq l_1\}$ and $\{l_3 \neq l_2\}$
3. $\{l_1 + l_2 - l_3 = q\}$
4. $\{1 \le q \le M\}$.

From condition 3, for a fixed $l_1 = j$, $l_2 = q - j + l_3$ and from condition 1, $1 \le q - j + l_3 \le M$. Hence,

$$max(1, j - q + 1) \le l_3 \le min(M, M + j - q) \quad \text{(D.5)}$$

but note that $l_3 \neq j$ from condition 2, and $q \neq j$ from conditions 2 and 3. Hence, for $j < q$, l_3 can be $1, 2, \ldots, j-1, j+1, \ldots, M+j-q-1, M+j-q$ and for $j > q$, l_3 can be $j-q+1, j-q+2, \ldots, j-1, j+1, \ldots, M-1, M$. It follows that for each value of $l_1 = j < q$ there are $M + j - q - 1$ possible values of (l_2, l_3) and $l_1 = j > q$, there are $M - j + q - 1$ possible values of (l_2, l_3). Thus, the number of possible index vector (l_1, l_2, l_3)'s is

$$\sum_{j=1}^{q-1}\{M + j - q - 1\} + \sum_{j=q+1}^{M}\{M - j + q - 1\} = (q-1)(M-q) + \frac{(M-2)(M-1)}{2}$$

which is desired from (D.3). Thus, from (D.2), (D.3), and (D.4), we obtain (D.1).

APPENDIX E

Derivation of (5.28)

Since $\bar{\gamma}_q = (1+\varrho_q)(H^{(1)})^2 PT_s/N_0$,

$$\bar{\gamma} \;=\; \frac{1}{M}\sum_{q=1}^{M}\bar{\gamma}_q \;=\; (H^{(1)})^2\frac{PT_s}{N_0}(1+\bar{\varrho}). \tag{E.1}$$

The equality in (5.28) can be derived as follows:

$$\begin{aligned}
\mathrm{SNR}(\beta_q) &= \frac{2\beta_q^2(H^{(1)})^2\frac{PT_s^2}{4}}{\frac{N_0T_s}{4}+\frac{\beta_q^2PT_s^2}{4N}\{(\widetilde{H}_q^{(n)})^2\}}\left(\frac{\frac{4}{N_0T_s}}{\frac{4}{N_0T_s}}\right) && \text{(E.2)}\\
&= \frac{2\beta_q^2(H^{(1)})^2\frac{PT_s}{N_0}}{1+\frac{\beta_q^2PT_s}{NN_0}\{(\widetilde{H}_q^{(n)})^2\}} && \text{(E.3)}\\
&= \frac{2\beta_q^2(H^{(1)})^2\frac{PT_s}{N_0}}{1+\frac{\beta_q^2}{N}\frac{(H^{(1)})^2PT_s}{N_0}\{\frac{(\widetilde{H}_q^{(n)})^2}{(H^{(1)})^2}\}} && \text{(E.4)}\\
&= \frac{2\beta_q^2\ \{\bar{\gamma}/(1+\bar{\varrho})\}}{1+\frac{\beta_q^2}{N}\{\bar{\gamma}/(1+\bar{\varrho})\}\varrho_q}\left(\frac{1+\bar{\varrho}}{1+\bar{\varrho}}\right) && \text{(E.5)}\\
&= \frac{2\bar{\gamma}\beta_q^2}{1+\bar{\varrho}+\bar{\gamma}\beta_q^2\frac{\varrho_q}{N}} && \text{(E.6)}
\end{aligned}$$

where (E.1) is used in (E.4) to (E.5).

BIBLIOGRAPHY

BIBLIOGRAPHY

[1] L. E. Larson, "Radio frequency integrated circuit technology for low-power wireless communications," *IEEE Personal Commun.*, vol. 5, pp. 11–19, June 1998.

[2] J. A. C. Bingham, "Multicarrier modulation for data transmission: An idea whose time has come," in *IEEE Commun. Mag.*, pp. 5–14. May 1990.

[3] W. Y. Zou and Y. Wu, "COFDM: an overview," *IEEE Trans. Broadcasting*, vol. 41, no. 1, pp. 1–8, Mar. 1995.

[4] J. S. Kenney and A. Leke, "Power amplifier spectral regrowth for digital cellular and PCS application," *Microwave Journal*, pp. 74–92, Oct. 1995.

[5] S. L. Miller and R. J. O'Dea, "Peak power and bandwidth efficient linear modulation," *IEEE Trans. Commun.*, vol. 46, no. 12, pp. 1639–1648, Dec. 1998.

[6] M. L. Doelz, E. T. Heald, and D. L. Martin, "Binary data transmission techniques for linear systems," *Proc. IRE*, vol. 45, pp. 656–661, May 1957.

[7] B. R. Salzberg, "Performance of efficient parallel data transmission systems," *IEEE Trans. Commun.*, vol. COM-15, no. 5, pp. 805–811, Dec. 1967.

[8] S. B. Weinstein and Paul M. Ebert, "Data transmission by frequency-division multiplexing using the discrete Fourier transform," *IEEE Trans. Commun.*, vol. COM-19, no. 5, pp. 628–634, Oct. 1971.

[9] B. Hirosaki, "An orthogonally multiplexed QAM system using the discrete Fourier transform," *IEEE Trans. Commun.*, vol. COM-29, no. 7, pp. 982–989, July 1981.

[10] J.R. L. J. Cimini, "Analysis and simulation of a digital channel using orthogonal frequency division multiplexing," *IEEE Trans. Commun.*, vol. COM-33, no. 7, pp. 665–675, July 1985.

[11] B. Hirosaki and S. Hasegawa, "Advanced groupband data modem using orthogonally multiplexed QAM technique," *IEEE Trans. Commun.*, vol. COM-34, no. 6, pp. 587–592, June 1986.

[12] I. Kalet, "The multitone channel," *IEEE Trans. Commun.*, vol. 37, no. 2, pp. 119–124, Feb. 1989.

[13] E. F. Casas and C. Leung, "OFDM for data communication over mobile radio FM channels–part I: Analysis and experimental results," *IEEE Trans. Commun.*, vol. 39, no. 5, pp. 783–793, May 1991.

[14] E. F. Casas and C. Leung, "OFDM for data communication over mobile radio FM channels–part II: Performance improvement," *IEEE Trans. Commun.*, vol. 40, no. 4, pp. 680–683, Apr. 1992.

[15] A. Ruiz, J. M. Cioffi, and S. Kasturia, "Discrete multiple tone modulation with coset coding for the spectrally shaped channel," *IEEE Trans. Commun.*, vol. 40, no. 6, pp. 1012–1029, June 1992.

[16] M. Ho, J. M. Cioffi, and J. A. C. Bingham, "Discrete multitone echo cancellation," *IEEE Trans. Commun.*, vol. 44, no. 7, pp. 817–825, July 1996.

[17] European Telecommunication Standards Institute, "Radio broadcasting systems; digital audio broadcasting (DAB) to mobile, portable and fixed receivers," ETSI std. ETS 300 401, Feb. 1995.

[18] American National Standards Institute, "Network and customer installation interface –asymmetrical digital subscriber line (ADSL) metallic interface," ANSI std. T1E1, Aug. 1995.

[19] European Telecommunication Standards Institute, "Digital broadcasting systems for television, sound and data services; frame structure, channel coding and modulation for digital terrestrial television," ETSI std. ETS 300 744, 1996.

[20] H. Takanashi and R. van Nee, "Merged physical layer specification for the 5 GHz band," IEEE P802.11-98/72-r1, Mar. 1998.

[21] R. van Nee, "A new OFDM standard for high rate wireless LAN in the 5 GHZ band," in *Proc. of the IEEE Vehicular Technology Conference*, 1999, pp. 258–262.

[22] S. Muneta, Y. Matsumoto, N. Mochizuki, and M. Umehira, "A new frequency-domain link adaptation scheme for broadband OFDM systems," in *Proc. of the IEEE Vehicular Technology Conference*, 1999, pp. 253–257.

[23] S. Kondo and L. B. Milstein, "Performance of multicarrier DS CDMA systems," *IEEE Trans. Commun.*, vol. 44, no. 2, pp. 238–246, Feb. 1996.

[24] A. Chouly, A. Brajal, and S. Jourdan, "Orthogonal multicarrier techniques applied to direct sequence spread spectrum CDMA systems," in *Proc. of the IEEE Global Telecommunications Conference*, 1993, pp. 1723–1728.

[25] Q. Chen, E. S. Sousa, and S. Pasupathy, "Multi-carrier DS-CDMA with adaptive sub-carrier hopping for fading channels," in *Proc. of the IEEE International Symposium on Personal, Indoor and Mobile Radio Communications*, 1995, pp. 76–80.

[26] S. Kondo and L. B. Milstein, "On the use of multicarrier direct sequence spread spectrum systems," in *Proc. of the IEEE Vehicular Technology Conference*, 1993, pp. 52–56.

[27] E.A. Sourour and M. Nakagawa, "Performance of orthogonal multi-carrier CDMA in a multipath fading channel," *IEEE Trans. Commun.*, vol. 44, no. 3, pp. 356–367, Mar. 1996.

[28] F. Classen and H. Meyr, "Frequency synchronization algorithms for OFDM systems suitable for communication over frequency selective fading channels," in *Proc. of the IEEE Vehicular Technology Conference*, 1994, pp. 1655–1659.

[29] F. Daffara and O. Adami, "New frequency detector for orthogonal multicarrier transmission technique," in *Proc. of the IEEE Vehicular Technology Conference*, 1995, pp. 804–809.

[30] F. Daffara and O. Adami, "Novel carrier recovery technique for orthogonal multicarrier systems," in *European Trans. Telecommunications*, 1996, pp. 323–334.

[31] L. Tomba and W. A. Krzymien, "Effect of carrier phase noise and frequency offset on the performance on multicarrier CDMA systems," in *Proc. of the IEEE International Conference on Communications*, 1996, pp. 1513–1517.

[32] P. Schafer and M. Nakagawa, "Direct-sequence multi-carrier CDMA parallel acquisition in a multipath fading channel," in *Proc. of the IEEE International Conference on Communications*, 1996, pp. 1503–1507.

[33] X. Li and L. J. Jr. Cimini, "Effects of clipping and filtering on the performance of OFDM," in *Proc. of the IEEE Vehicular Technology Conference*, 1997, pp. 1634–1638.

[34] T. A. Wilkinson and A. E. Jones, "Minimization of the peak to mean envelope power ratio of multicarrier transmission schemes by block coding," in *Proc. of the IEEE Vehicular Technology Conference*, 1995, vol. 2, pp. 825–829.

[35] H. Ochiai and H. Imai, "Block coding scheme based on complementary sequences for multicarrier signals," *IEICE Trans. Fundamentals of Electronics, Communications and Computer Sciences*, vol. E80-A, no. 11, pp. 2136–2143, Nov. 1997.

[36] H. Ochiai and H. Imai, "Performance of block codes with peak power reduction for indoor multicarrier systems," in *Proc. of the IEEE Vehicular Technology Conference*, 1998, pp. 338–342.

[37] S. Shepherd, J. Orriss, and S. Barton, "Asymptotic limits in peak envelope power reduction by redundant coding in orthogonal frequency-division multiplex modulation," *IEEE Trans. Commun.*, vol. 46, no. 1, pp. 5–10, Jan. 1998.

[38] A. E. Jones and T. A. Wilkinson, "Performance of reed-muller codes and a maximum-likelihood decoding algorithm for OFDM," *IEEE Trans. Commun.*, vol. 47, no. 7, pp. 949–952, July 1999.

[39] D. J. A. and J. Jonathan, "Peak-to-mean power control in OFDM, Golay complementary sequences, and Reed-Muller codes," *IEEE Trans. Inform. Theory*, vol. IT-45, no. 7, pp. 2397–2417, Nov. 1999.

[40] G. Karam and H. Sari, "A data predistortion technique with memory for QAM radio systems," *IEEE Trans. Commun.*, vol. 39, no. 2, pp. 336–343, Feb. 1991.

[41] A. N. D'Andrea, V. Lotici, and R. Reggiannini, "RF power amplifier linearization through amplitude and phase predistortion," *IEEE Trans. Commun.*, vol. 44, no. 11, pp. 1477–1484, Nov. 1996.

[42] J. K. Cavers, "Adaptation behavior of a feedforward amplifier linearizer," *IEEE Trans. Veh. Technol.*, vol. 44, no. 1, pp. 31–39, Feb. 1995.

[43] W. G. Jeon, K. H. Chang, and Y. S. Cho, "An adaptive data predistorter for compensation of nonlinear distortion in OFDM systems," *IEEE Trans. Commun.*, vol. 45, no. 10, pp. 1167–1171, Oct. 1997.

[44] K. Yang, J. R. East, and G. I. Haddad, "High-efficiency class-A power amplifiers with a dual-bias-control scheme," in *IEEE Trans. Microwave Theory and Techniques*, Aug. 1999, pp. 1426–1432.

[45] G. Hanington, P. F. Chen, V. Radisic, T. Itoh, and P. M. Asbeck, "Microwave power amplifier efficiency improvement with a 10MHz HBT dc-dc converter," in *IEEE Int. Microwave Symp. Dig.*, 1998, pp. 589–592.

[46] S. Bouthillette and A. Platzker, "High-efficiency L-band variable output power amplifiers for use in communication systems," in *IEEE Int. Microwave Symp. Dig.*, 1996, pp. 563–566.

[47] C. Buoli, A. Abbiati, and D. Riccardi, "Microwave power amplifier with envelope controlled drain power supply," in *25th Proc. Euro. Microwave Conf.*, 1995, pp. 31–35.

[48] A. A. M. Saleh and D. C. Cox, "Improving the power-added efficiency of FET amplifiers operating with varying-envelope signals," *IEEE Trans. Microwave Theory and Techniques*, vol. 31, no. 1, pp. 51–56, Jan. 1983.

[49] A. Brajal, A. Chouly, and K. Fazel, "TCM schemes with predistortion techniques on nonlinear channels," in *Proc. of the IEEE International Conference on Communications*, 1992, pp. 633–637.

[50] A. Brajal and A. Chouly, "Compensation of nonlinear distortion for orthogonal multicarrier schemes using predistortion," in *Proc. of the IEEE GLOBECOM*, 1994, pp. 1909–1914.

[51] G. Santella and F. Mazzenga, "A hybrid analytical-simulation procedures for performance evaluation in M-QAM-OFDM schemes in presence of nonlinear distortions," *IEEE Trans. Veh. Technol.*, vol. 47, no. 1, pp. 142–151, Feb. 1998.

[52] M. T.Le and L. Thibault, "Performance evaluation of COFDM for digital audio broadcasting part II: Effects of HPA nonlinearities," *IEEE Trans. Broadcasting*, vol. 44, no. 2, pp. 165–171, June 1998.

[53] M. C. Jeruchim, P. Balaban, and K. S. Shanmugan, *Simulations of Communication Systems*, Plenum, 1992.

[54] E. Bogenfeld, R. Valentin, K. Metzger, and W. Sauer-Greff, "Influence of nonlinear HPA on trellis-coded OFDM for terrestrial broadcasting of digital HDTV," in *Proc. of the IEEE GLOBECOM*, 1993, pp. 1443–1438.

[55] S. Merchan, A. Garcia Armada, and J.L. Garcia, "OFDM performance in amplifier nonlinearity," *IEEE Trans. Broadcasting*, vol. 44, no. 1, pp. 106–114, Mar. 1998.

[56] K. W. Schneider and W. H. Tranter, "Efficient simulation of multicarrier digital communication systems in nonlinear channel environments," *IEEE J. Select Areas Commun*, vol. 11, no. 3, pp. 328–339, Apr. 1993.

[57] E. A. Sourour, "The effects of non-linearity on the performance of multi-carrier CDMA system," in *Proc. of the IEEE Vehicular Technology Conference*, 1996, pp. 1853–1857.

[58] A. J. Viterbi, A. M. Viterbi, and E. Zehavi, "Performance of power-controlled wideband terrestrial digital communication," *IEEE Trans. Commun.*, vol. 41, no. 4, pp. 559–569, Apr. 1993.

[59] R.J. Westcott, "Investigation of multiple FM/FDM carriers thorough a satellite TWT operating near saturation," *Proceedings of IEE*, pp. 726–740, June 1967.

[60] J. S. Lee, "Signal-to-crosstalk power ratio in smoothly limited multichannel FDM signals," *IEEE Trans. Commun.*, vol. COM-16, no. 1, pp. 63–67, Feb. 1968.

[61] F. E. Bond and H. F. Meyer, "Intermodulation effects in limiter amplifier repeaters," *IEEE Trans. Commun.*, vol. COM-18, no. 2, pp. 127–135, Apr. 1970.

[62] O. Shimbo, "Effects of intermodulation, AM-PM conversion, and additive noise in multicarrier TWT systems," *Proceedings of the IEEE*, vol. 59, no. 2, pp. 230–238, Feb. 1971.

[63] N. M. Blachman, "Band-pass nonlinearities," *IEEE Trans. Inform. Theory*, vol. IT-10, no. 2, pp. 162–164, Apr. 1964.

[64] N. M. Blachman, "Detectors, bandpass nonlinearities, and their optimization: Inversion of the Chebyshev transform," *IEEE Trans. Inform. Theory*, vol. IT-17, no. 4, pp. 398–404, July 1971.

[65] A. R. Kaye, D.A. George, and M. J. Eric, "Analysis and compensation of bandpass nonlinearities for communications," *IEEE Trans. Commun.*, vol. COM-20, pp. 965–972, Oct. 1972.

[66] S. Benedetto, E. Biglieri, and R. Daffara, "Modeling and performance evaluation of nonlinear satellite links–a Volterra series approach," *IEEE Trans. Aerospace and Electronics System*, vol. AES-15, no. 4, pp. 494–507, July 1979.

[67] A. A. M. Saleh, "Frequency-independent and frequency-dependent nonlinear models of TWT amplifiers," *IEEE Trans. Commun.*, vol. COM-29, no. 11, pp. 1715–1720, Nov. 1981.

[68] R. Blum and M. C. Jeruchim, "Modeling nonlinear amplifiers for communication simulation," in *Proc. of the IEEE International Conference on Communications*, 1989, pp. 1468–1472.

[69] J. B. Minkoff, "Wideband operation of nonlinear solid state power amplifiers—comparision of calculations and measurements," *AT & T Bell Labs Tech. Journal*, vol. 63, no. 2, pp. 231–248, 1984.

[70] A. J. Cann, "Nonlinearity model with variable knee sharpness," *IEEE Trans. Aerospace and Electronics System*, vol. 16, no. 6, pp. 874–877, Nov. 1980.

[71] J. Boccuzzi, "Performance evaluation of non-linear transmit power amplifiers for North American digital cellular portables," *IEEE Trans. Veh. Technol.*, vol. 44, no. 2, pp. 220–228, May 1995.

[72] P.A. Bello, "Characterization of randomly time-variant linear channels," *IEEE Trans. Commun.*, vol. CS-11, pp. 360–393, Dec. 1963.

[73] J. G Proakis, *Digital communications*, McGraw-Hill, 1995.

[74] S. Shamai E. Biglieri, J. Proakis, "Fading channels: Information-theoretic and communications aspects," *IEEE Trans. Inform. Theory*, vol. 44, no. 6, pp. 652–667, Oct. 1998.

[75] S. Sampei, *Applications of Digital Wireless Techniques to Global Wireless Communications*, Prentice Hall, 1997.

[76] K. Pahlavan and A. H. Levesque, *Wireless Information Networks*, John Wiley & Sons, 1995.

[77] E. H. Dinan and B. Jabbari, "Spreading code for direct sequence CDMA and wideband CDMA celluar networks," in *IEEE Commun. Mag.*, pp. 48–54. Sept. 1998.

[78] B. Sklar, *Digital Communications*, Prentice Hall, 1988.

[79] S. Hara and R. Prasad, "Overview of multicarrier CDMA," in *IEEE Commun. Mag.*, pp. 126–133. Dec. 1997.

[80] K. Chen and S. Wu, "A programmable architecture fo OFDM-CDMA," in *IEEE Commun. Mag.*, pp. 76–82. Nov. 1999.

[81] GSM Recommendation 05.05, "Radio transmission and reception," ETSI/PT 12, Jan. 1991.

[82] E. Biglieri, G. Caire, and G. Taricco, "Coding and modulation under power constraints," *IEEE Personal Commun.*, vol. 5, pp. 32–39, June 1998.

[83] J. F. Sevic and J. Staudinger, "Simulation of adjacent-channel power for digital wireless communication systems," *Microwave Journal*, pp. 66–80, Oct. 1996.

[84] S. Ross, *A First Course in Probability*, Prentice Hall, fourth edition, 1994.

[85] S. Lin and Jr. D. J. Cotello, *Error Control Coding: Fundamentals and Applications*, Prentice-Hall, 1983.

[86] J. Conan, "The weight spectra of some short low-rate convolutional codes," *IEEE Trans. Commun.*, vol. COM-32, no. 9, pp. 1050–1053, Sept. 1984.

[87] J.W. Craig, "A new, simple, and exact result for calculating the probability of error for two-dimensional signal constellation," in *Proc. of IEEE Military Communications Conference (MILCOM)*, 1991, pp. 571–575.

[88] M. K. Simon and D. Divsalar, "Some new twists to problems involving the Gaussian probability integral," *IEEE Trans. Commun.*, vol. 46, no. 2, pp. 200–210, Feb. 1998.

[89] S. Moshavi, "Multi-user detection for DS-CDMA communications," in *IEEE Commun. Mag.*, pp. 124–136. Oct. 1996.

[90] C. J. Savant, M. S. Roden, and G. L. Carpenter, *Electronic Design: Circuits and Systems*, The Benjamin/Cummings Publishing Company, Inc., second edition, 1991.